26697

National Library of Canada

Bibliothèque nationale du Canada

CANADIAN THESES ON MICROFICHE

THÈSES CANADIENNES SUR MICROFICHE

NAME OF AUTHOR/*NOM DE L'AUTEUR* John Wallace ANDREW

TITLE OF THESIS/*TITRE DE LA THÈSE* An Assessment of Some Approximations in the Dynamical Theory of Electron Diffraction

UNIVERSITY/*UNIVERSITÉ* Univ of Alberta

DEGREE FOR WHICH THESIS WAS PRESENTED/ *GRADE POUR LEQUEL CETTE THÈSE FUT PRÉSENTÉE* Ph. D

YEAR THIS DEGREE CONFERRED/*ANNÉE D'OBTENTION DE CE GRADE* 1975

NAME OF SUPERVISOR/*NOM DU DIRECTEUR DE THÈSE* Prof. S. S. Sheinin

Permission is hereby granted to the NATIONAL LIBRARY OF CANADA to microfilm this thesis and to lend or sell copies of the film.

The author reserves other publication rights, and neither the thesis nor extensive extracts from it may be printed or otherwise reproduced without the author's written permission.

L'autorisation est, par la présente, accordée à la BIBLIOTHÈQUE NATIONALE DU CANADA de microfilmer cette thèse et de prêter ou de vendre des exemplaires du film.

L'auteur se réserve les autres droits de publication; ni la thèse ni de longs extraits de celle-ci ne doivent être imprimés ou autrement reproduits sans l'autorisation écrite de l'auteur.

DATED/*DATÉ* October 8, 1975 SIGNED/*SIGNÉ* John W. Andrew

PERMANENT ADDRESS/*RÉSIDENCE FIXE* East Royalty R.R. #3
Charlottetown P.E.I.
Canada C1A 7J7

NL-91 (3-74)

THE UNIVERSITY OF ALBERTA

AN ASSESSMENT OF SOME APPROXIMATIONS IN THE DYNAMICAL THEORY OF ELECTRON DIFFRACTION

by

JOHN WALLACE ANDREW ©

A THESIS

SUBMITTED TO THE FACULTY OF GRADUATE STUDIES AND RESEARCH
IN PARTIAL FULFILLMENT OF THE REQUIREMENTS FOR THE DEGREE
OF DOCTOR OF PHILOSOPHY

IN

SOLID STATE PHYSICS

DEPARTMENT OF PHYSICS

EDMONTON, ALBERTA

FALL, 1975

THE UNIVERSITY OF ALBERTA

FACULTY OF GRADUATE STUDIES AND RESEARCH

The undersigned certify that they have read, and recommend to the Faculty of Graduate Studies and Research, for acceptance, a thesis entitled "An Assessment of Some Approximations in the Dynamical Theory of Electron Diffraction", submitted by John Wallace Andrew in partial fulfillment of the requirements for the degree of Doctor of Philosophy in Solid State Physics.

Supervisor

Michael L. Wayman

J M Cowley
External Examiner

Date: October 2, 1975

ABSTRACT

An assessment of some approximations in the dynamical theory of electron diffraction has been carried out. The approximations which have been considered are firstly, the s-value approximation for calculating the diagonal elements of the $\underline{A}$ matrix, secondly, the kinematical approximation, and thirdly, the approximations which can be used to take the imaginary part of the lattice potential into account when absorption is considered.

The s-value approximation has been found to be a reasonable approximation under the diffraction conditions which were considered.

The kinematical approximation has been assessed for large deviations of the first order reflection g from the Bragg condition by comparing the kinematical theory to the many-beam theory. It has been found that the kinematical theory is not as good an approximation as comparison with the two-beam theory had indicated. In addition, it has been found that the kinematical theory is a poor approximation when the deviation parameter, s_h, of a non-systematic reflection is equal to zero or s_g. It has also been found that the kinematical theory becomes a poorer approximation as atomic number or accelerating voltage is increased or if a lower order systematic row is considered.

In order to assess the approximations for taking absorption into account, a general formulation of the dynamical theory of electron diffraction including absorption has been developed. This theory is based on generalized perturbation theory. It has been shown that the introduction of the imaginary potential leads to a mixing of the unperturbed Bloch waves characteristic of the system without absorption. The assumptions involving the importance of Bloch wave mixing which are required to reduce the exact theory to the low order perturbation theories previously published in the literature have been examined. This is of interest since an understanding of these assumptions provides a physical basis for comparing these theories as well as giving the insight required to develop new approximations. The details of a new approximate theory, referred to as the sub-matrix method, have also been given. Numerical calculations have been presented which show that it is important to take the mixing of Bloch waves into account in high atomic number materials or when quasi-degeneracy or degeneracy of the kinetic energies of the unperturbed Bloch waves is obtained. A comparison of the approximate and exact methods for taking absorption into account has been carried out and it has been found that the sub-matrix approach has a number of advantages over other approximate methods. Firstly, it is applicable under conditions which lead to either non-degenerate, quasi-degenerate or degenerate Bloch waves. As well, the method can give very close agreement with the exact theory while at the same time providing computational advantages.

As an illustration of a phenomenon where Bloch wave mixing is important, the critical voltage effect has been examined. It has been shown that it is necessary to take Bloch wave mixing into account in order to obtain a physical understanding of the contrast mechanism involved. For small deviations from the exact second order Bragg condition, this mechanism has been found to be different from the standard theory mechanism.

ACKNOWLEDGMENTS

I would like especially to thank my supervisor, Professor S.S. Sheinin, whose continued assistance and advice have influenced every aspect of this thesis. I am also grateful to Drs. P.S. Turner, C.D. Cann, K.Z. Botros, and H.J. Kreuzer for many helpful discussions, and to Mr. J.C. Brunel for his assistance in the laboratory.

I would like to express my appreciation to Mrs. Mary Yiu for typing the manuscript.

Financial assistance from the National Research Council of Canada, the University of Alberta, and the Department of Physics is gratefully acknowledged.

Finally, I would like to thank my wife Christine, my daughter Melissa, and my parents, who have actively encouraged and supported my efforts in every way.

TABLE OF CONTENTS

CHAPTER PAGE

1 THE HISTORY OF ELECTRON DIFFRACTION THEORY AND INTRODUCTION TO THE PRESENT STUDY 1

1.1 Introduction 1

1.2 Historical Introduction to the Theory of Electron Diffraction 2

1.3 Introduction to the Present Study 7

1.3.1 An Examination of the Approximations Involved in the Many-Beam, Two-Beam and Kinematical Theories 10

1.3.2 An Examination of the Approximations Which Can be Used to Take the Imaginary Part of the Lattice Potential into Account 14

2 ASPECTS OF THE DYNAMICAL THEORY OF ELECTRON DIFFRACTION 18

2.1 Basic Outline of the Dynamical Theory 18

2.1.1 The Solution of the Schrodinger Wave Equation 18

2.1.2 The Calculation of Diffracted Beam Intensities in a Perfect Crystal 27

2.2 Effects of Inelastic Scattering 29

2.2.1 Inelastic Scattering Processes 30

2.2.2 Extension of Bethe's Theory to Include Inelastic Scattering Processes 33

2.2.3 Anomalous Absorption Effects 38

CHAPTER PAGE

2.3 Relativistic Corrections to the Dynamical Theory 40

3 APPROXIMATIONS INVOLVED IN THE MANY-BEAM, TWO-BEAM AND KINEMATICAL THEORIES 42

3.1 Introduction 42

3.2 The Many-Beam Dynamical Theory 43

3.2.1 The Systematic Case 44

3.2.2 The Non-Systematic Case 46

3.2.3 The Diffracted Beam Intensity in the Many-Beam Theory 48

3.3 The Two-Beam Theory 55

3.4 The Kinematical Theory 59

4 COMPUTATIONAL METHODS 67

4.1 Introduction 67

4.2 Methods Used to Specify the Crystal Orientation 67

4.3 The Calculation of the Diagonal Elements of the $\underline{A}$ Matrix 69

4.3.1 The s-Value Method 71

4.3.2 The t-Value Method 74

4.3.3 The Exact Method 75

4.3.4 A Comparison of the s-Value, t-Value and Exact Methods 77

4.4 The Calculation of the Off-Diagonal Elements of the $\underline{A}$ Matrix 81

4.5 The Calculation of the $\underline{A}'$ Matrix 82

4.6 Matrix Diagonalization and the Calculation of Diffracted Beam Intensity 85

CHAPTER PAGE

5 A COMPARISON OF THE KINEMATICAL, TWO-BEAM AND MANY-BEAM THEORIES 87

5.1 Introduction 87

5.2 A Comparison of the Kinematical, Two-Beam and Many-Beam Theories in the Systematic Case for Large Values of δ. 89

5.2.1 A Comparison of the Kinematical and Two-Beam Extinction Distances with the Many-Beam Average Extinction Distance 90

5.2.2 The Variation with Thickness of the Many-Beam Extinction Distance 95

5.3 Analysis of the Results for the Systematic Case 97

5.3.1 An Analysis of the Results for Values of δ where no Systematic Reflection is Close to its Bragg Condition 99

5.3.1(a) Numerical analysis of average extinction distance results 99

5.3.1(b) Numerical analysis of the variation in extinction distance results 105

5.3.1(c) Analytical examination of the primary and secondary Bloch waves 106

5.3.1(d) Analytical methods for comparing the kinematical extinction distance and the many-beam average extinction distance 111

5.3.2 Analysis of the Results for Orientations where a High Order Systematic Reflection is Close to its Bragg Condition 114

CHAPTER PAGE

5.3.2(a) Numerical approach 114

5.3.2(b) Analytical approach 119

5.4 The Effect of Non-Systematic Reflections on Many-Beam Effects 120

5.4.1 The Results of the Calculations which Included Non-Systematic Reflections 121

5.4.2 An Analysis of the Results for the Non-Systematic Case 124

5.5 The Effect of Atomic Number, Accelerating Voltage, and the Order of the Systematic Row on Many-Beam Effects 126

5.5.1 The Effect of Atomic Number on Many-Beam Effects 128

5.5.2 The Effect of Changes in the Accelerating Voltage on Many-Beam Effects 131

5.5.3 The Effect of the Order of the Systematic Row on Many-Beam Effects 137

5.6 Summary and Conclusions 140

6 EXACT AND APPROXIMATE METHODS FOR TAKING ABSORPTION INTO ACCOUNT IN THE DYNAMICAL THEORY OF ELECTRON DIFFRACTION 143

6.1 Introduction 143

6.2 The Solution of the Equations of the Dynamical Theory Including Absorption Using Generalized Perturbation Theory 147

6.3 Calculation of Diffracted Beam Intensities 153

6.4 Some Properties of the $q^{(ij)}$ Elements of the $\underline{B}$ Matrix 155

CHAPTER PAGE

6.5 The Relationship Between the Exact Approach and the Low Order Perturbation Theory Approaches 164

6.5.1 The First Order Approximation to the Solution of the Perturbed Equation 166

6.5.2 The Second Order Approximation to the Solution of the Perturbed Equation 167

6.6 The Sub-Matrix Approach 172

6.7 A Criterion for Determining which Bloch Wave Mixing Terms are Important in the Sub-Matrix Approach 176

6.8 Summary 178

7 THE IMPORTANCE OF BLOCH WAVE MIXING IN CALCULATIONS OF DIFFRACTED BEAM INTENSITY 180

7.1 Introduction 180

7.2 The Effect of Atomic Number on the Importance of Bloch Wave Mixing 180

7.3 The Effect of Quasi-Degenerate Diffraction Conditions on the Importance of Bloch Wave Mixing 187

7.3.1 Anomalous Absorption Effects in Diffracted Beam Intensity Profiles 187

7.3.2 The Effect of Bloch Wave Mixing on Rocking Curves 190

7.4 Discussion 196

7.5 A Comparison of Approximate and Exact Methods for Taking Absorption into Account 198

CHAPTER PAGE

8 THE IMPORTANCE OF BLOCH WAVE MIXING IN THE CRITICAL VOLTAGE EFFECT 204

8.1 Introduction 204

8.2 A Review of the Critical Voltage Effect 204

8.3 Critical Voltage Effects for Small Departures from the Exact Second Order Bragg Condition 211

8.3.1 An Examination of the Critical Voltage Intensity Minimum at Small Departures from $\delta = 2.0$ 212

8.3.1 (a) An examination of the critical voltage intensity minimum in molybdenum 213

8.3.1 (b) An examination of the critical voltage intensity minimum in copper 218

8.3.2 The Standard Theory Mechanism for the Critical Voltage Effect 220

8.3.3 The Sub-Matrix Mechanism for the Critical Voltage Effect 227

8.3.3 (a) The sub-matrix mechanism for $\delta = 2.003$ 229

8.3.3 (b) The sub-matrix mechanism for $\delta < 2.003$ 232

8.3.3 (c) The sub-matrix mechanism for $\delta > 2.003$ 236

8.4 The Critical Voltage Effect in Materials of Differing Atomic Number 237

8.5 Summary and Conclusions 243

CHAPTER PAGE

9 SUMMARY AND SUGGESTIONS FOR FURTHER WORK 245

9.1 Summary 245

9.2 Suggestions for Further Work 246

REFERENCES 459

APPENDIX A Approximate Methods for Calculating the Eigenvalues and Normalized Eigenvectors of a Symmetric Matrix 255

APPENDIX B Typical Values for the Elements in the $\underline{C}$ Matrix of Table 2 and for the Bloch Wave Excitation Amplitudes $C_o^{(h)} C_g^{(h)}$ 262

APPENDIX C Typical Values for the Second Order Correction Terms in Equation 5.2 265

LIST OF TABLES

TABLE PAGE

1 The magnitudes of the Bloch wave excitation amplitudes $C_o^{(i)}C_g^{(i)}$ for the many-beam calculation discussed in the text. 100

2 The first order approximation to the many-beam eigenvector matrix $\underline{C}$. 108

3 Typical Bloch wave excitation amplitudes for values of δ close to the Bragg condition of a high order systematic reflection. 115

4 A comparison of many-beam effects in materials of high and low atomic number. 130

5 The effect of changes in the accelerating voltage on many-beam effects in molybdenum. 134

6 The effect of changes in the accelerating voltage on many-beam effects in molybdenum when the terms U_h are not relativistically corrected. 136

7 A comparison of many-beam effects for high and low order systematic rows. 139

8 The first four rows and columns of typical $\underline{B}$ matrices for a thirteen beam calculation in gold and aluminum. 181

9 The average percentage difference in the intensities for gold and aluminum found using the standard and exact theories. 185

10 Parameters indicating the effect of Bloch wave mixing on the standard theory excitation amplitudes $C_o^{(i)}C_h^{(i)}$ in gold. 199

B-1 Typical values for the elements of the $\underline{C}$ matrix of Table 2 and for the Bloch wave excitation amplitudes $C_o^{(h)}C_g^{(h)}$. 263

C-1 Typical values for the second order corrections to the eigenvalues $\gamma^{(o)}$ and $\gamma^{(g)}$ of equation 5.2. 266

LIST OF FIGURES

FIGURE		PAGE
1	The method used in this thesis to indicate the deviation of the systematic reflections from their Bragg conditions.	12
2	The dispersion surface and the Ewald sphere construction for high energy electrons.	22
3	Ewald sphere construction showing reflections in different Laue zones.	24
4	The variation of diffracted beam intensity with depth in the presence of (a) no absorption (b) normal absorption and (c) anomalous absorption.	39
5	An experimental diffraction pattern obtained under systematic diffraction conditions in molybdenum.	45
6	A portion of a typical diffraction pattern in the non-systematic case.	47
7	A many-beam dispersion surface plot for the (110) systematic row in molybdenum at 100 kV.	50
8	A diffracted beam intensity profile typical of the case where there are two primary Bloch waves and other secondary Bloch waves present.	52
9	A diffracted beam intensity profile typical of the case where there are three or more primary Bloch waves present.	54
10	A two-beam dispersion surface plot for the (110) systematic row in molybdenum at 100 kV.	58
11	A typical two-beam intensity profile showing a constant peak to peak spacing.	60
12	A geometrical construction showing that the distance d between the two K spheres centered at o and g is equal to s_g.	61

FIGURE PAGE

13 The intersection of the Ewald sphere with the zero order Laue zone. 70

14 The dispersion surface and Ewald sphere construction for calculating the diagonal elements of the $\underline{A}$ matrix. 72

15 A comparison of the diffracted beam intensities found in thick crystals using the t-method, s-method, and exact method. 78

16 Values of U_g as a function of g for 100 kV electrons in aluminum and gold (FCC crystal structure) and in molybdenum (BCC crystal structure). 83

17 Values of U_g'/U_g for 100 kV electrons obtained from the data presented by Humphreys and Hirsch (1968). 84

18 Typical (110) dark field intensity profiles in molybdenum: (a) $\delta = 3.5$, and (b) $\delta = 4.99$. 91

19 The kinematical and two-beam extinction distances and the many-beam average extinction distance for the (110) dark field intensity in molybdenum. The many-beam average extinction distance was obtained for a thickness range of 0 to 1000 Å. 93

20 The kinematical and two-beam extinction distances and the many-beam average extinction distance for the (110) dark field intensity in molybdenum. The many-beam average extinction distance was obtained for a thickness range of 0 to 1500 Å. 94

21 The variation with thickness in the many-beam extinction distance for the (110) dark field intensity in molybdenum. The accelerating voltage used was 100 kV and a crystal thickness range of 0 to 1000 Å was considered. 96

FIGURE PAGE

22 The variation with thickness in the many-beam extinction distance for the (110) dark field intensity in molybdenum. A crystal thickness range of 0 to 1500 Å was considered. 98

23 The K-sphere scheme for labelling the branches of the dispersion surface. 102

24 A part of the many-beam dispersion surface for the systematic case. 104

25 The conditions under which the s-values of two different systematic reflections are equal. 109

26 A geometrical construction showing that, for large δ and a low order reflection h, the values s_h and $s_h - s_g$ increase with increasing δ. 113

27 A plot of a portion of the many-beam dispersion surface in the systematic case when the reflection 5g is close to its Bragg condition. 117

28 A diffraction pattern indicating the crystal orientations considered in the calculations which took non-systematic reflections into account. 122

29 The percentage variation in extinction distance for the (110) intensity in molybdenum when non-systematic reflections are taken into account. 123

30 The Ewald sphere construction for deviation parameters $\delta = y/g$ and $\delta = -y/g$ which are equal in magnitude but opposite in sign. 158

31 The Ewald sphere construction for deviation parameters $\delta = y/g$ and $\delta = (y+2\ell)/g$ where $\vec{\ell}$ is a reciprocal lattice vector. 162

32 Typical values of $|q^{(ij)}|$ in gold as a function of the deviation parameter δ. 165

FIGURE PAGE

33 The exact theory and standard theory second order dark field intensity profiles for gold at $\delta = 1.8$. 186

34 The second order dark field intensity for the (110) systematic row in molybdenum at the critical voltage of 74 kV and for $\delta = 2.004$. 188

35 Second order dark field rocking curves for molybdenum close to $\delta = 2.0$ obtained using the standard and exact theories. The accelerating voltage was 74 kV (the critical voltage). 191

36 Bright field rocking curves for molybdenum close to the symmetry position ($\delta = 0.0$) obtained using the standard and exact theories. The accelerating voltage was 74 kV (the critical voltage). 193

37 Second order dark field rocking curves for molybdenum close to $\delta = 2.0$ obtained using the standard and exact theories. The accelerating voltage was 100 kV. 195

38 Second order dark field rocking curves for molybdenum close to $\delta = 2.0$ obtained using the standard, second order, submatrix, and exact theories. The accelerating voltage was 74 kV (the critical voltage). 203

39 (a) The eigenvalues, and (b) the excitation amplitudes for Bloch waves two and three close to the critical voltage in copper for $\delta = 2.0$. 208

40 The critical voltage intensity minimum for the (222) intensity in copper. 210

41 The variation of the (220) intensity in molybdenum as a function of accelerating voltage for $\delta = 2.001$. 215

42 The variation of the (222) intensity in copper as a function of accelerating voltage for $\delta = 2.002$. 219

FIGURE PAGE

43 The variation of the (222) intensity in copper as a function of accelerating voltage for $\delta = 2.02$. 221

44 (a): A plot of $C_o^{(i)}C_{2g}^{(i)}$ (i = 2,3) as a function of accelerating voltage at the exact Bragg condition of the reflection 2g; (b) and (c): Plots of $C_o^{(i)}C_{2g}^{(i)}$ (i = 2,3) in the complex plane for voltages below and above the critical voltage. 223

45 (a): A plot of $C_o^{(i)}C_{2g}^{(i)}$ (i = 2,3) as a function of accelerating voltage for $\delta = 2.002$; (b), (c), and (d): Plots of $C_o^{(i)}C_{2g}^{(i)}$ (i = 2,3) in the complex plane for voltages below, at, and above the critical voltage. 225

46 The excitation amplitudes $X^{(n)}C_{2g}^{\prime(n)}$ of perturbed Bloch waves two and three plotted in the complex plane for $\delta = 2.003$. 230

47 The excitation amplitudes $X^{(2)}C_{2g}^{\prime(2)}$ and $X^{(3)}C_{2g}^{\prime(3)}$ for $\delta = 2.002$. 233

48 The excitation amplitudes for Bloch waves two and three for (a) $\delta = 2.0017$, (b) $\delta = 2.001$, and (c) $\delta = 2.0$. 235

49 The excitation amplitudes $X^{(n)}C_{2g}^{\prime(n)}$ of perturbed Bloch waves two and three plotted in the complex plane for $\delta = 2.02$. 238

50 The critical voltage intensity minima obtained for the sub-matrix and exact theories in gold. 241

CHAPTER 1

THE HISTORY OF ELECTRON DIFFRACTION THEORY AND INTRODUCTION TO THE PRESENT STUDY

1.1 Introduction

The electron microscope is an important tool in the study of the structure of materials. In order for the microscopist to interpret the experimental micrographs obtained from his instrument, it is necessary that reference be made to some theory which relates image contrast to specimen structure. In some cases, such as in the interpretation of micrographs of biological specimens, useful information can be obtained by using the mass thickness method for interpreting image contrast. This method assumes that the intensity reaching a particular area of the micrograph is proportional to the product of the mass times the thickness in the corresponding area of the specimen. The interpretation of electron micrographs of crystalline materials, however, requires the use of a more complicated theory which takes the diffraction of electrons into account. In this case, useful information can usually only be obtained by comparing experimental micrographs to the results of theoretical calculations based on electron diffraction theory.

In using electron diffraction theory in practice, approximations of various kinds must be made. The validity of some of these approximations will be examined in this thesis.

1.2 Historical Introduction to the Theory of Electron Diffraction

The phenomenon of electron diffraction was first discovered experimentally by Davisson and Germer (1927) and almost simultaneously by Thomson and Reid (1927). These authors confirmed the de Broglie postulate of wave particle duality in the case of electrons (de Broglie, 1924) and provided the basis for the development of the electron microscope. In the year following these first experimental discoveries of electron diffraction, Bethe (1928) published a quantum mechanical theory describing the interaction of a high energy electron with a periodic crystal potential. This theory, known as Bethe's formulation of the dynamical theory of electron diffraction, now plays a very important role in the analysis of electron diffraction effects.

Initially, however, after the development of the electron microscope by Knoll and Ruska (1932), the interpretation of the images from crystalline specimens was carried out in terms of the simpler kinematical theory of electron diffraction. This theory is similar to the kinematical theory of X-ray diffraction which had been used successfully to explain many aspects of the interaction of X-rays and crystals. However, in the case of electrons, the kinematical assumptions of single scattering and of negligible diffracted beam intensity in comparison to that of the directly transmitted beam are not usually justified. It is not surprising, therefore, that a number of authors (for example, Blackman, 1939; von Borries and Ruska, 1940; Heidenreich, 1942; Hillier and Baker, 1942; Boersch, 1942, 1943; Kinder, 1943; Heidenreich and Sturkey, 1945) reported experimental results which could only be partially explained in terms of the kinematical theory. As a result, there was a renewed interest in Bethe's dynamical theory.

In Bethe's theory any number of strong diffracted beams could, in principle, be taken into account. In practice, however, it was found that analytical expressions for the intensity of the different diffracted beams could be obtained easily only for the case where two reflections, the directly transmitted beam and one diffracted beam, were taken into account. These analytical solutions gave good agreement with experiment in strong beam imaging situations where only one low order reflection was close to its Bragg condition. As a result, the use of this two-beam approximation of the dynamical theory became widespread.

In order to take the effects of additional weak beams into account and yet retain the simplicity of the two beam analytical solutions, it is possible to use Bethe's second approximation (see for example, Bethe, 1928; MacGillavry, 1940; Kato, 1952; Pinsker, 1953). In this approximation, the effects of additional weak beams are included by adding correction terms to the lattice potentials corresponding to the two strong beams considered. As would be expected, however, Bethe's second approximation was found to be inadequate when three or more strong beams were present, and interest therefore turned to theories which could take the dynamical interactions of many beams into account.

There were two principal approaches which were taken in the late 1950's for calculating intensities in a many-beam situation. The first was quantum mechanical in nature while the second involved the use of optical models to obtain expressions for the diffracted beam intensity. Although Fujiwara (1959) showed that the Schrodinger wave equation could be solved by the method of higher order Born approximation, the quantum mechanical approach which was generally adopted was Bethe's approach. In order to make Bethe's approach more suitable for many-beam numerical calculations, an eigenvalue formulation of this theory was developed (see Niehrs, 1959; Fujimoto, 1959; Howie and Whelan, 1960). The eigenvalue formulation of Bethe's theory has gained wide acceptance for calculating many-beam effects and is the method used in this thesis. Methods based on obtaining the eigenvalues and eigenvectors by approximate methods have also been published by Gevers (1970) and Serneels and Gevers (1973A). In these methods, the diffracted beams are classified into strong and weak beams. The eigenvalue equation is then solved using partition theory. In applying this theory, it is assumed that the strong beams interact dynamically and the weak beams kinematically. The latter method, termed a kinematical approach by Gevers, should not be confused with the kinematical theory discussed in this thesis.

The second of the two principal approaches which were developed for taking the dynamical interaction of many strong beams into account involves the use of optical models to obtain expressions for the diffracted beam intensity. Examples of this approach are the Cowlie-Moodie (1957) theory, which was developed from scattering principles in light optics, and the Howie-Whelan (1961) differential equation approach, which was based on the plane wave reflection approach of Darwin (1914). These methods have been justified by showing that they are equivalent to the more basic quantum mechanical approach (Fujiwara, 1959; Hirsch et al.,1965; Goodman and Moodie, 1974). The relationships between the different many-beam dynamical theories have been summarized by Goodman and Moodie (1974).

It can be seen from this brief historical sketch of the development of electron diffraction theory that the kinematical, the two-beam, and the many-beam theories came into use as theories were required to better describe the interaction of the fast electron with the crystal. Although the many-beam theories have proven to be very useful for calculating diffracted beam intensities, these theories are numerical in form and results are generally forthcoming only with the aid of a computer. For this reason, the two-beam dynamical and kinematical theories have not fallen into disuse. Rather, they have remained as important qualitative aids for giving insight into diffraction phenomena. These theories are also used in a more quantitative sense under diffraction conditions where they are thought to be good approximations. The two-beam and kinematical theories are therefore discussed at length in the textbooks of electron diffraction (see for example Pinsker, 1953; Heidenreich, 1964; Hirsch et al., 1965; Amelinckx et al., 1970) and have been used extensively in the literature. Recently, for example, the kinematical, and the two-beam and many-beam dynamical theories have been used by Cockayne (1972) in the analysis of his weak-beam results. Under weak-beam diffraction conditions, the intensity of the diffracted beam being imaged is small and the approximations of the kinematic theory are more likely to apply.

1.3 Introduction to the Present Study

In introducing the research to be carried out in this thesis, it is first convenient to discuss some of the basic concepts involved in Bethe's approach to the dynamical theory of electron diffraction. (The details of Bethe's approach will be considered in Chapters 2 and 3.) Bethe's approach is a quantum mechanical approach in which the interaction of the fast electrons with the crystal is described by the Schrodinger wave equation. The wave function solutions to this equation are Bloch waves of the form

$$|b^{(i)}> = \sum_g C_g^{(i)} \exp(2\pi i(\vec{k}^{(i)} + \vec{g})\cdot\vec{r}) \qquad (1.1)$$

where $\vec{g}$ is a reciprocal lattice vector, $\vec{k}^{(i)}$ is the

Bloch wave vector and $C_g^{(i)}$ is the amplitude of the Bloch wave in the direction $\vec{k}^{(i)}+\vec{g}$. In solving the Schrodinger equation, the lattice potential is also expressed as a Fourier series. If only the elastic scattering of electrons is considered, then this potential is real and can be written

$$V(\vec{r}) = \sum_g V_g \exp(2\pi i\vec{g}\cdot\vec{r}) \qquad (1.2)$$

where V_g is the Fourier coefficient of the lattice potential. However, inelastic scattering processes also occur. Some of these electrons will be scattered outside the objective aperture and therefore do not contribute to the image. These electrons are effectively absorbed and it is in this context that the term absorption is used in this thesis. As will be shown in Section 2.2, absorption can be taken into account in the dynamical theory by the introduction of an imaginary part to the lattice potential. The lattice potential is then considered to be complex and can be written

$$V(\vec{r}) + iV'(\vec{r}) = \sum_g (V_g + iV_g')\exp(2\pi i\vec{g}\cdot\vec{r}) \ . \qquad (1.3)$$

The expression for the Bloch wave amplitude in equation 1.1 involves the sum over an infinite number of reciprocal lattice vectors $\vec{g}$. However, when this

Bloch wave function is incorporated into Bethe's theory, an infinite set of equations results (see Chapter 2). In order to obtain numerical solutions, this infinite set of equations must be reduced to a finite set by taking only a finite number of reciprocal lattice points into account. Since every point in the reciprocal lattice corresponds to a possible reflection from the real lattice, this means that the number of diffracted beams taken into account must be finite. By reducing the number of beams considered, the many-beam and two-beam dynamical theories can be developed. If only the directly transmitted beam and one diffracted beam of small intensity are considered, then the kinematical theory can be obtained. These theories will be considered in the first part of this thesis (see Section 1.3.1).

Another important aspect of the dynamical theory is the manner in which the imaginary Fourier coefficient iV'_g of equation 1.3 is incorporated into the theory. The method widely adopted in the literature is based on the fact that V'_g is generally much smaller than V_g. This permits the imaginary potential to be taken into account by using first order perturbation theory for the non-degenerate state. (This method is referred to as the standard method in the literature.) In the second part of this thesis, the validity of this method is examined and an alternate method is developed (see Section 1.3.2).

1.3.1 An Examination of the Approximations Involved in the Many-Beam, Two-Beam and Kinematical Theories

There are a number of approximations which can be used in taking the different diffracted beams into account. The first is the many-beam theory, which takes a finite number N of the beams into account. The actual number of beams included is generally determined by using a criterion to order the different diffracted beams according to their effect on the intensity. Beams are then included in order of their decreasing importance until the inclusion of additional beams does not result in any significant change in the diffracted beam intensity. In the many-beam formulation of the dynamical theory, ten to one hundred beams are generally required and the theory is usually numerical in form. Because all the important diffracted beams are included in a properly executed many-beam calculation, the approximations involved in developing the theory are very small. Accordingly, the many-beam theory has been found to be in good agreement with experiment under all diffraction conditions and has become the established method for interpreting experimental results (see for example, Cann and Sheinin, 1974A, 1974B; Sheinin and Botros, 1971; Ayroles, Mazel and Ajustron, 1973).

The second approximation obtained by taking only a finite number of diffracted beams into account is the two-beam theory. The theory considers only the directly transmitted beam, o, and one diffracted beam, g. This approximation results in expressions for the diffracted beam intensity which are analytical in form. The two-beam theory is often a questionable approximation, however, since higher order reflections of the type ... -2g, -g, 2g, 3g, ... are always excited when the reflection g is excited. (These reflections are referred to as systematic reflections.) The effects of these systematic reflections have been studied by a number of authors. For example, Sheinin (1967) found in examining the (110) dark field intensity in molybdenum that the two-beam theory was a good approximation for crystal orientations approximately between $\delta \doteq 0.0$ and $\delta = 2.4$. (In this thesis, the deviation of the systematic reflections from their Bragg conditions will be indicated by a deviation parameter δ. See Fig. 1). For values of δ approximately between 2.4 and 3.2, Sheinin found that the two-beam theory was a very poor approximation. For values of $\delta > 3.2$, the agreement between the two-beam theory and experimental results improved.

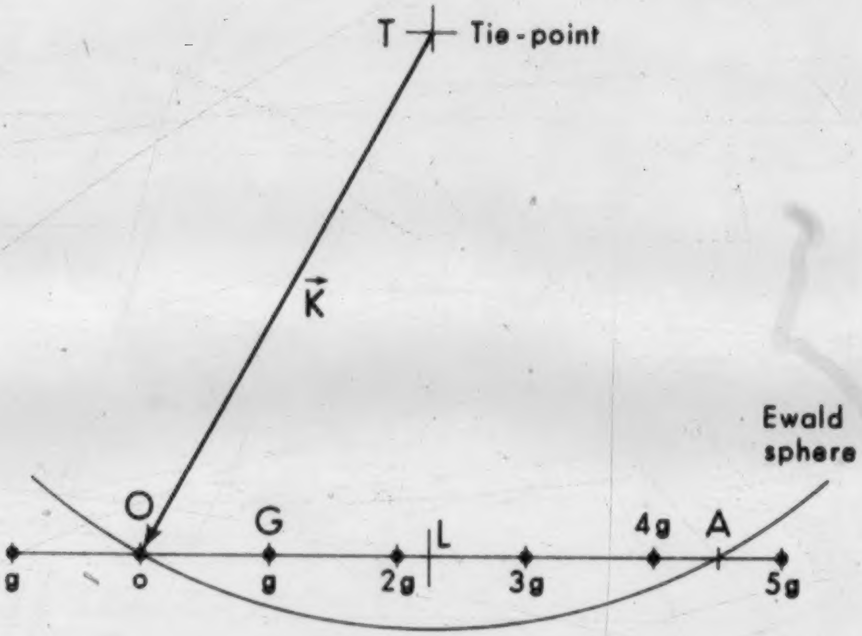

Fig. 1. The method used in this thesis to indicate the deviation of the systematic reflections from their Bragg conditions. The deviation of these reflections from their Bragg conditions is indicated by a deviation parameter δ which is obtained by dividing the distance OA by the distance OG. For example, in the above figure $\delta = 4.5$. If $\delta = n$ where n is a positive or negative integer or zero, then the reflection ng is in its exact Bragg condition. The point L is the perpendicular projection of the tie-point T onto the systematic row.

The third theory which will be considered is the kinematical theory. In this theory no further assumptions about the number of important diffracted beams are made. Rather, it is assumed that the intensity of the one diffracted beam taken into account is small compared to the directly transmitted beam. As will be shown in Chapter 3, the kinematical theory is analytical in form and can be derived from the two-beam theory if certain approximations are made about the size of the Fourier coefficient V_g. Because the intensity of the diffracted beam is assumed to be small, it has been found (except for very thin crystals) that the kinematical theory is a poor approximation for the reflection g close to its Bragg condition, i.e. for $\delta \approx 1.0$. However, the kinematical theory has been assumed to be a good approximation, even for thick crystals, if the reflection g is far from its Bragg condition (see for example, Whelan, 1970; Gevers, 1970) because the intensity of the diffracted beam will then be small compared with the directly transmitted beam. This assumption has been justified by the fact that the two theories become equivalent for large deviations of the reflection g from its Bragg condition, i.e. for $\delta >> 1.0$. It has therefore become widely accepted in the literature that the kinematical theory is valid for values of the deviation parameter $\delta >> 1.0$.

Although there is good agreement between the kinematical and two-beam theories for $\delta >> 1.0$, it is important to note that the kinematical theory still takes only two beams into account. However, it is possible that other beams will also be important and should be included. In order to properly assess the kinematical theory for $\delta >> 1.0$, it is therefore not sufficient to compare the kinematical and two-beam theories as has been the practice in the past. Rather, it is necessary to compare the kinematical theory to the more correct many-beam theory. Such a comparison has not yet been presented in the literature. A comparison of the kinematical, two-beam and many-beam theories for large values of δ will therefore be carried out in the first part of this thesis.

1.3.2 An Examination of the Approximations Which Can be Used to Take the Imaginary Part of the Lattice Potential into Account

There are two approaches which have been adopted in the literature to the solution of the Schrodinger wave equation including the imaginary potential $iV'(\vec{r})$. The first assumes that the imaginary part is much smaller than the real part. Low order perturbation theory is then used to calculate corrections to the Bloch wave functions found using the real potential. The standard method has been to use first order perturbation theory for the non-degenerate state (Hirsch et al., 1965). The use of this theory has been brought into question, however, when the imaginary potential becomes large, as in high atomic number materials (Sheinin and Andrew, 1974), or when the assumption of non-degeneracy does not apply. Under certain diffraction conditions this second assumption is questionable, as for example, near critical voltage diffraction conditions (Andrew and Sheinin, 1974A) or when a non-systematic reflection is excited (Cann and Sheinin, 1974A, 1974B). Although higher order perturbation theories have been developed (Serneels and Gevers, 1972, 1973B) and the theory has been modified to properly take into account Bloch waves which are precisely degenerate (Sheinin and Cann, 1973; Serneels and Gevers, 1973B), this perturbation approach is incomplete in that no method is available to handle quasi-degenerate Bloch waves. (In this thesis the term Bloch wave degeneracy will be taken to mean an equality in the kinetic energies of the Bloch waves, while quasi-degeneracy will be taken to mean nearly degenerate Bloch waves or close branches of the dispersion surface.)

The second and alternative approach is to solve the Schrodinger wave equation including the complex potential without making any approximations about the size of the perturbation or about how close the kinetic energies of the Bloch waves are to one another (Hewat reported by Lally et al., 1972; Thomas, 1972; Andrew and Sheinin, 1974A). However, this method, referred to as the exact method in this thesis, does not give any insight into the interaction between Bloch waves which results from the introduction of the complex lattice potential. Furthermore, the relationships between the exact method and the perturbation approaches are not evident.

Because of the inadequacies of the two available approaches, a study is undertaken in the second part of this thesis of the approximations which can be used to take the imaginary part of the periodic lattice potential into account. In this research, generalized perturbation theory is used to develop a general formulation of the dynamical theory of electron diffraction including absorption. This new formulation of the theory is very useful since it provides a physical basis for comparing the diffraction conditions under which the various low order perturbation approximations are applicable as well as giving the insight required to develop new approximations. The details of a new approximation, referred to as the sub-matrix method, will be presented. This approach has a number of advantages over other approximate methods. Firstly, it is applicable under conditions which lead to either non-degenerate, quasi-degenerate or degenerate Bloch waves. As well, the method can give very close agreement with the exact theory while at the same time providing advantages from a computational point of view.

In order to illustrate the usefulness of the new theory, it is then applied to the situations where the standard theory does not apply, namely for high atomic number materials and for diffraction conditions which lead to degenerate or quasi-degenerate Bloch waves. Because of the ability of the new theory to handle quasi-degenerate and degenerate states, this theory is also used in a study of the mechanism leading to the reduction of the second order dark field intensity which is associated with the critical voltage effect.

CHAPTER 2

ASPECTS OF THE DYNAMICAL THEORY OF ELECTRON DIFFRACTION

2.1 Basic Outline of the Dynamical Theory

2.1.1 The Solution of the Schrodinger Wave Equation

The dynamical theory of electron diffraction, proposed by Bethe (1928), starts with the Schrodinger wave equation for an electron in a crystal potential $V(\vec{r})$. This equation can be written as

$$\nabla^2\psi(\vec{r}) + \frac{8\pi^2 m_o e}{h^2}(E + V(\vec{r}))\psi(\vec{r}) = 0 \qquad (2.1)$$

where $\psi(\vec{r})$ is the wave function of the electron, and E is the potential through which the electron was accelerated before entering the crystal. The quantities m_o and e denote the rest mass of the electron and the electronic charge respectively, and h is Planck's constant. Since the crystal potential, $V(\vec{r})$, is periodic in nature, it can be expressed as a Fourier series of the form

$$V(\vec{r}) = \sum_g V_g \exp(2\pi i\vec{g}\cdot\vec{r}) = \frac{h^2}{2me}\sum_g U_g \exp(2\pi i\vec{g}\cdot\vec{r}) \qquad (2.2)$$

where the summation is over all reciprocal lattice vector $\vec{g}$ and $V_g = (h^2/(2me))U_g$ is the g^{th} Fourier coefficient of the lattice potential. If only elastic scattering is considered, the crystal potential is real, $V(\vec{r}) = V^*(\vec{r})$, and therefore

$$U_g = U^*_{-g} \quad . \tag{2.3}$$

In addition, if the crystal is centrosymmetric, which is the case for the crystals considered in this thesis, then an origin can be chosen such that $V(\vec{r}) = V(-\vec{r})$. In this case, it can be seen from equations 2.2 and 2.3 that

$$U_g = U_{-g} = U^*_g \tag{2.4}$$

and the U_g's are all real.

In the case of electrons with energies of the order of those used in the electron microscope, $E \gg V(\vec{r})$ and the Schrodinger equation can be solved using the nearly free electron approximation. The solutions outside the crystal, where $V(\vec{r}) = 0$, are plane waves of the form

$$\psi(\vec{r}) = \exp(2\pi i\vec{\chi}\cdot\vec{r}) \tag{2.5}$$

where the magnitude of the wave vector $\vec{\chi}$ is given by

$$\chi = \left(\frac{2meE}{h^2}\right)^{\frac{1}{2}} \quad . \tag{2.6}$$

In the crystal, the effect of the lattice potential, $V(\vec{r})$, results in solutions to the Schrodinger equation which are Bloch waves, that is plane waves modulated by a function which has the periodicity of the lattice. Accordingly, solutions to equation 2.1 are of the form

$$\psi(\vec{r}) = |b^{(i)}(\vec{k}^{(i)},\vec{r})> = \sum_{g} C_{g}^{(i)}(\vec{k}^{(i)})\exp\{2\pi i(\vec{k}^{(i)}+\vec{g})\cdot\vec{r}\} \tag{2.7}$$

where $\vec{k}^{(i)}$ is the Bloch wave vector and $C_{g}^{(i)}(\vec{k}^{(i)})$ is the amplitude of the Bloch wave in the direction $\vec{k}^{(i)}+\vec{g}$. If equations 2.2 and 2.7 are substituted into the Schrodinger equation 2.1, the following expression is obtained:

$$\sum_{g}[\{-(\vec{k}^{(i)}+\vec{g})^{2}+\chi^{2}+U_{o}\}C_{g}^{(i)}(\vec{k}^{(i)}) + \sum_{g}{}' C_{g-h}^{(i)}(\vec{k}^{(i)})U_{h}] \times \exp\{2\pi i(\vec{k}^{(i)}+\vec{g})\cdot\vec{r}\} = 0 \tag{2.8}$$

where the prime on the second summation indicates that the term h = 0 is excluded. Since each of the terms involving $\exp\{2\pi i(\vec{k}^{(i)}+\vec{g})\cdot\vec{r}\}$ is linearly independent, the coefficients of these terms must all be identically equal to zero. This condition results in a set of equations of the form

$$(K^{2} - (\vec{k}_{g}^{(i)})^{2})C_{g}^{(i)}(\vec{k}^{(i)}) + \sum_{h}{}' U_{h}C_{g-h}^{(i)}(\vec{k}^{(i)}) = 0 \tag{2.9}$$

where

$$K^{2} = \chi^{2} + U_{o} \tag{2.10}$$

and

$$\vec{k}_g^{(i)} = \vec{k}^{(i)} + \vec{g} \ . \qquad (2.11)$$

The quantity K is the magnitude of the electron wave vector in the crystal after correction for the wavelength change due to the mean crystal potential U_o.

The homogeneous set of equations 2.9 gives the general relationships between the amplitudes $C_g^{(i)}(\vec{k}^{(i)})$, the Fourier coefficients U_g, and the Bloch wave vectors $\vec{k}^{(i)}$. This equation will have solutions only if the determinant formed by the coefficients vanishes, i.e.

$$\begin{vmatrix} K^2-(\vec{k}_o^{(i)})^2 & U_{-g} & \cdots \\ U_g & K^2-(\vec{k}_g^{(i)})^2 & \cdots \\ \cdots & \cdots & \cdots \end{vmatrix} = 0 \ . \qquad (2.12)$$

It can be seen from equations 2.10 and 2.6 that this condition relates the Bloch wave vector $\vec{k}_g^{(i)}$ to the energy eE. The locus of the end points of the wave vectors $\vec{k}_g^{(i)}$ satisfying this relation traces out branches of a surface of constant energy eE in $\vec{k}$ space which is known as the dispersion surface. For this reason, equation 2.9 is known as Bethe's dispersion equation.

The method which will be adopted in this thesis to solve Bethe's equation 2.9 is based on the eigenvalue method. The manner in which the eigenvalue equation is derived can be understood by considering Fig. 2.

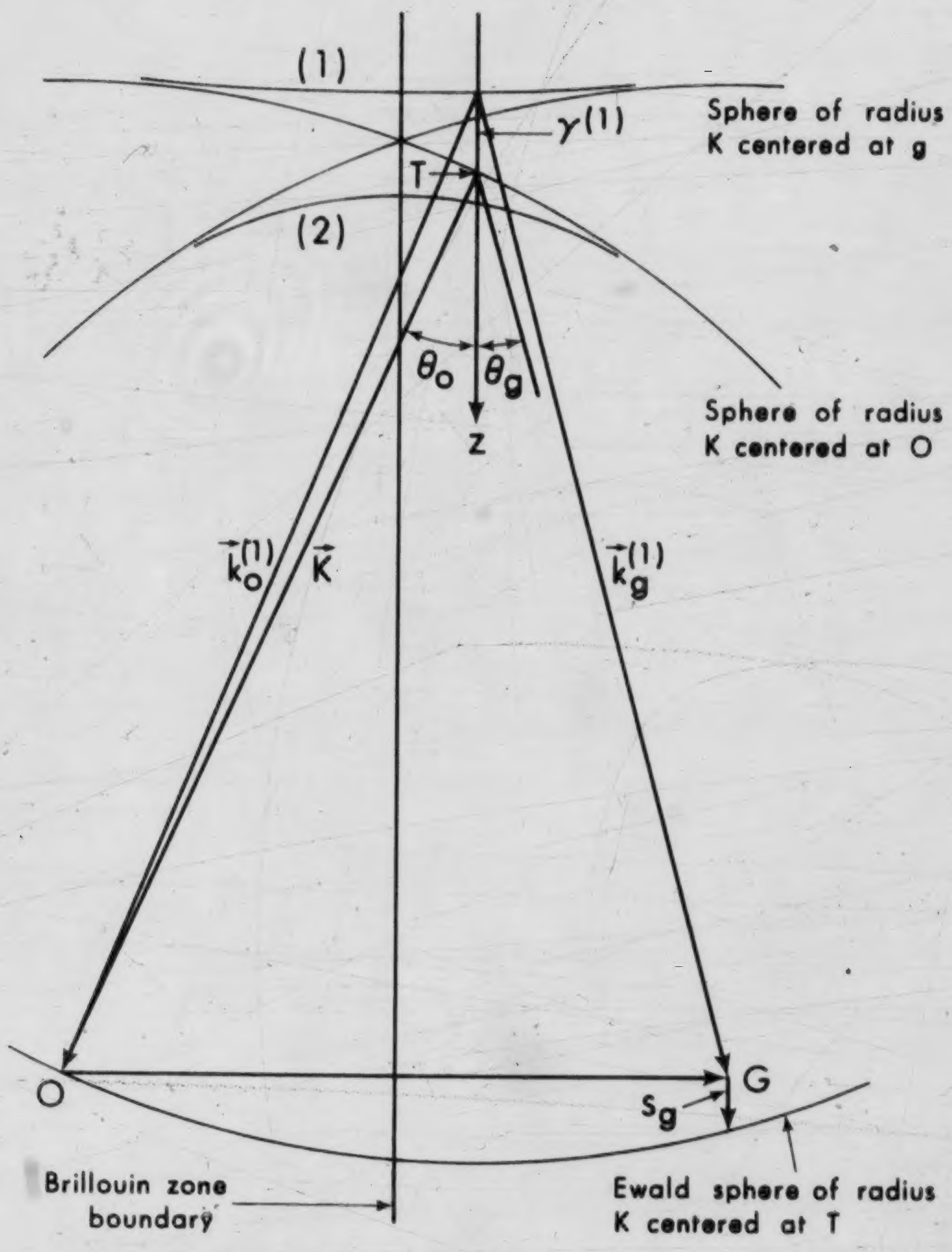

Fig. 2. The dispersion surface and the Ewald sphere construction for high energy electrons.

In this figure the incident wave vector, after allowing for the effect of refraction, is given by $\vec{K}$. For simplicity only the two reciprocal lattice points, o and g, and the two dispersion surfaces, (1) and (2), have been included. In order to determine the allowed Bloch wave vectors $\vec{k}_o^{(i)}$ within the crystal, it is necessary to apply the boundary conditions at the top surface of the crystal. In order for the wave functions to join smoothly at the boundary, it is necessary that the wave function and its derivative normal to the surface should be continuous at the surface. The fact that these conditions must hold at any point on the surface requires that the wave vectors $\vec{k}_o^{(i)}$ have the same tangential components along the surface as $\vec{K}$. Generally, reflected waves from the surface can be ignored up to angles of incidence of approximately 80° (see Hirsch et al., 1965) because of the large difference between the energy of the incident electron and the lattice potential.

In order to apply the above boundary conditions, it is necessary to consider the inclination of the crystal surface with respect to the incident beam. In order to simplify this process, it will be assumed in this thesis that the symmetrical Laue case holds. In the symmetrical Laue case, the different Laue zones (see Fig. 3) are assumed to be parallel to the crystal

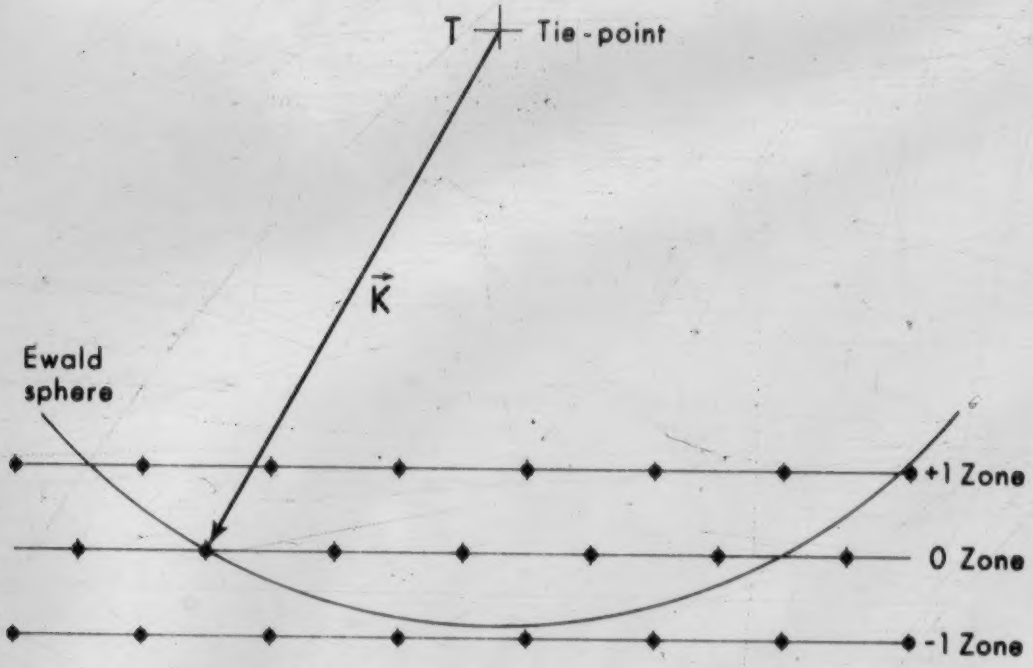

Fig. 3. Ewald sphere construction showing reflections in different Laue zones. Because $|\vec{K}|$ is much greater than the reciprocal lattice spacing, the Laue zones are nearly perpendicular to the incident beam.

surface. For the small Bragg angles found in high energy electron diffraction, this means that the crystal surface is assumed to be nearly perpendicular to the incident beam. It has been shown by Whelan and Hirsch (1957) that this symmetrical Laue approximation is a good approximation in the two-beam case for angles of incidence up to approximately 70° to 80°. Spencer and Humphreys (1971) have noted that in nearly all cases, the symmetrical Laue approximation is a good one, but that there are cases where it is not, as for example in the description of scanning electron microscope channeling patterns from a tilted specimen.

The boundary conditions can now be applied in Fig. 2 by drawing, through point T, a line perpendicular to the crystal surface. The points where this line intersects the branches of the dispersion surface are termed wave points and determine the allowed Bloch wave vectors within the crystal. In the symmetrical Laue case for the reflection g, this line will be parallel to the Brillouin zone boundary as shown. Now let $\gamma^{(i)}$ be the distance of a possible wave point from T and let s_g be the distance of the reciprocal lattice point g from the Ewald sphere, measured in the z direction (normal to g). For small $\gamma^{(i)}$ and s_g, it can be seen from Fig. 2 that

$$\begin{aligned} K^2 - (\vec{k}_g^{(i)}) &\approx K^2 - (K - s_g \cos\theta_g + \gamma^{(i)} \cos\theta_g)^2 \\ &= K^2 - (K + (\gamma^{(i)} - s_g) \cos\theta_g)^2 \qquad (2.13) \\ &= -2K(\gamma^{(i)} - s_g) \cos\theta_g \left[1 + \frac{(\gamma^{(i)} - s_g)}{2K} \cos\theta_g\right] . \end{aligned}$$

If it is assumed that $K \gg g$ and $K \gg (\gamma^{(i)} - s_g)$ then

$$\cos\theta_g \approx 1 \qquad (2.14)$$

and $$\frac{(\gamma^{(i)} - s_g)}{2K} \approx 0 \quad . \qquad (2.15)$$

Equation 2.13 then reduces to

$$K^2 - (\vec{k}_g^{(i)})^2 \approx -2K(\gamma^{(i)} - s_g) \qquad (2.16)$$

and Bethe's equation 2.9 can be written in the eigenvalue form

$$\underline{\underline{A}}\underline{C}^{(i)} = \gamma^{(i)} \underline{C}^{(i)} \quad . \qquad (2.17)$$

Here $\underline{C}^{(i)}$ is a column vector whose elements $C_g^{(i)}$ are the components of the Bloch wave of equation 2.7 and $\underline{A}$ is a matrix with elements $A_{oo} = 0$, $A_{gg} = s_g$, and $A_{gh} = U_{g-h}/(2K)$ where $g \neq h$. The eigenvalue $\gamma^{(i)}$ is related to the z component of the Bloch wave vector $\vec{k}_o^{(i)}$ through the relation

$$(k_o^{(i)})_z = K_z + \gamma^{(i)} \quad . \qquad (2.18)$$

In order to be able to refer to the different Bloch waves present, it is convenient to label the Bloch waves and their corresponding dispersion surfaces in accordance with some accepted convention. The method generally adopted in the literature is to use the integer labels i = 1,2,3,... in order of the decreasing values of $(k_o^{(i)})_z$ (Humphreys and Fisher, 1971).

The formulation of the dynamical theory just presented has been expressed in terms of the eigenvalues and eigenvectors of an infinite $\underline{A}$ matrix. The application of the theory in practice, however, clearly will require that this matrix be finite. The approximations which are involved in reducing the matrix to a finite size will be considered in the next chapter. In the remainder of this chapter, the methods which can be used to calculate the diffracted beam intensity, and to take inelastic scattering and relativistic effects into account will be considered.

2.1.2 The Calculation of Diffracted Beam Intensities in a Perfect Crystal

The total wave function $\psi(\vec{r})$ of the high energy electron in the crystal can be written as a linear combination of all the Bloch waves excited, i.e.

$$\psi(\vec{r}) = \sum_i X^{(i)} |b^{(i)}\rangle = \sum_i X^{(i)} \sum_g C_g^{(i)} \exp(2\pi i(\vec{k}^{(i)}+\vec{g})\cdot\vec{r}) \; . \tag{2.19}$$

The coefficients $X^{(i)}$ in this expression are known as excitation coefficients and determine the extent to which the associated Bloch wave is excited in the crystal. In order to calculate the intensity I_g of a directly transmitted or diffracted beam g, equation 2.19 is sorted into components in the directions of these beams. If these components are then multiplied by the phase term $\exp(-2\pi i\vec{K}\cdot\vec{r})$, then the intensity of beam g at a depth z in the crystal is found to be

$$I_g(z) = |\Phi_g(z)|^2 = |\sum_i X^{(i)}C_g^{(i)} \exp(2\pi i\gamma^{(i)}z)|^2 \qquad (2.20)$$

where $\Phi_g(z)$ is the amplitude of the beam g.

The excitation coefficients required in equation 2.20 can be calculated from the boundary conditions at the top surface of the crystal, i.e.

$$\Phi_0(0) = 1\ , \qquad \Phi_g(0) = 0 \qquad (g \neq 0)\ . \qquad (2.21)$$

Equation 2.20 together with 2.21 gives

$$\underline{C}\underline{X} = \underline{u} \qquad (2.22)$$

where $\underline{C}$ is a matrix having the elements $C_g^{(i)}$ in the g^{th} row and i^{th} column, $\underline{X}$ is a column vector containing the excitation coefficients $X^{(i)}$ in the i^{th} row, and $\underline{u}$ is a column vector containing the diffracted beam amplitudes 1,0,0,... of equation 2.21. The excitation coefficients

$X^{(i)}$, required in equation 2.20, can then be found by obtaining numerical solutions to the nonhomogeneous set of linear equations 2.22. The effort required to solve this set of equations can be greatly reduced, however, by noting that the $\underline{A}$ matrix of equation 2.17 is real and symmetric. Hence the matrix $\underline{C}$ of normalized eigenvectors is orthogonal and $\underline{C}^{-1} = \underline{C}^T$, the transpose of $\underline{C}$. If equation 2.22 is multiplied from the left by $\underline{C}^{-1}$, then

$$\underline{X} = \underline{C}^T \underline{u} \tag{2.23}$$

and it can immediately be seen that the excitation coefficients $X^{(i)}$ are given by the elements in the first row of $\underline{C}$, i.e.

$$X^{(i)} = C_o^{(i)} \ . \tag{2.24}$$

The expression for the diffracted beam intensity therefore becomes

$$I_g(z) = |\phi_g(z)|^2 = |\sum_i C_o^{(i)} C_g^{(i)} \exp(2\pi i\gamma^{(i)} z)|^2 \ . \tag{2.25}$$

2.2 Effects of Inelastic Scattering

The high energy electrons incident on the crystal can undergo both elastic and inelastic scattering. The dynamical theory as formulated by Bethe takes only elastic scattering into account. It has been found, however, that the inelastic scattering of electrons outside of the objective aperture leads to the very important anomalous absorption effect. This section will consider the important types of inelastic scattering processes and the modification which is usually made in Bethe's theory to take these processes into account. This will be followed by a discussion of the anomalous absorption effect.

2.2.1 Inelastic Scattering Processes

The high energy electrons travelling through the crystal can be involved in several different inelastic scattering processes. The three most important of these processes are plasmon scattering, short range single electron scattering, and phonon or thermal diffuse scattering.

Plasmon scattering results from the long range Coulomb interaction between the high energy electron and the conduction electron gas as a whole. The incident electron loses energy by exciting long wavelength density oscillations, called plasma oscillations or plasmons, in the electron gas. These oscillations have a characteristic frequency ω_p and an excitation energy $\hbar\omega_p$ which is usually in the range of 3 eV to 30 eV. The mean free paths for plasmon excitation lie typically in the range of 1000 - 5000 Å (Pines, 1963), so that in many cases almost all the electrons emerging from the crystal have lost energy by this method. Because the plasmon wavelength is long compared to the lattice spacing (i.e. the wave vector $q << g$), it is not expected that Bragg reflection would occur during plasmon excitation (Howie, 1963, 1970). Only small angle scattering is therefore expected and most electrons suffering plasmon losses will pass through the objective aperture (see also Heidenreich, 1964).

In addition to the long range Coulomb interaction just discussed, the incident electrons can interact at short range with the individual electrons in the crystal. Most of the electrons inelastically scattered by single electron excitation are thought to scatter through angles less than a Bragg angle (Hirsch et al., 1965). Although it is possible for some of these inelastically scattered electrons to pass through the objective aperture, most of the inelastically scattered electrons contributing to the image are thought to have been scattered by plasma excitation (Howie, 1970).

The third of the important energy loss processes is phonon or thermal diffuse scattering, which involves the scattering of Bloch waves by thermal vibrations. In the treatment of this scattering process, the scattered intensity can be divided into two parts (see for example Hall and Hirsch, 1965). The first term is the Bragg scattered term. This term is found to be equal to exp(-2M) times the intensity Bragg scattered by a static lattice. Here M is the Debye temperature factor given by $M = Bg^2$, and $B = 8\pi^2\overline{u^2}$ where $\overline{u^2}$ is the mean square displacement of the atoms in a direction perpendicular to the Bragg planes. The Bragg scattered term is taken into account in the dynamical theory by multiplying the Fourier coefficients of the lattice potential by the Debye-Waller correction factor $\exp(-B|g^2|/4)$. The second term is called the diffuse scattering term. This term is taken into account in the calculation of the imaginary part iU'_g of the lattice potential (see Section 2.2.2). The energy changes involved in thermal diffuse scattering are small ($\Delta E \approx k_B T = 0.025$ at room temperature) and the scattering has been found to be greatest at moderate angles of the order of 10° (Howie, 1970). The contribution of thermal diffuse scattering is of prime importance to electron absorption since most electrons suffering this type of loss will not enter the objective aperture and are therefore considered to be absorbed. Since thermal diffuse scattering is a function of the thermal motion of the crystal, it is not surprising that it has been found to decrease with decreasing temperature (Steeds and Valdrè, 1968; Howie and Valdrè, 1964).

It should be noted that, for crystals of the thickness commonly examined in the electron microscope, nearly all the electrons are expected to have undergone inelastic scattering. This point is of interest since good agreement with experiment can be found by using diffraction theories which assume that none of the electrons reaching the image have been inelastically scattered. This apparent contradiction has been resolved by Howie (1963) who showed that the phase relationships among elastically scattered Bloch waves are the same as among Bloch waves which have been inelastically scattered through small angles. Thus, the inelastically scattered electrons give the same image contrast as those undergoing only elastic scattering. This was first shown experimentally by Kamiya and Uyeda (1961), who displaced the objective aperture in a manner such that only inelastically scattered electrons contributed to the image. The resulting images were very similar to those obtained with elastically scattered electrons.

2.2.2 Extension of Bethe's Theory to Include Inelastic Scattering Processes

In Bethe's original formulation of the dynamical theory, the depletion of the elastically scattered beams by inelastic scattering processes is not taken into account. In order to include these inelastic scattering effects, Molière (1939) introduced the phenomenological concept of a complex lattice potential. If a small imaginary component $iV'(\vec{r})$ is added to the real potential $V(\vec{r})$, then the total crystal potential becomes

$$V(\vec{r}) + iV'(\vec{r}) = \frac{h^2}{2me} \sum_g (U_g + iU'_g)\exp(2\pi i\vec{g}\cdot\vec{r}) \quad . \qquad (2.26)$$

The addition of this imaginary component leads to imaginary components in the Bloch wave vector $\vec{k}^{(i)}$ of equation 2.7 and in the eigenvalue $\gamma^{(i)}$ of equation 2.25. It will be shown below that this leads to the attenuation of the diffracted beams with thickness and, in this manner, accounts for the loss of electrons from the beam by inelastic scattering.

The addition of an imaginary component to the lattice potential was substantiated theoretically by Yoshioka (1957). Rather than solve the Schrodinger equation using a static potential $V(\vec{r})$ as Bethe had done, Yoshioka used a potential which was able to take inelastic scattering effects into account. He showed that these additional interactions give rise to an additional complex term in the Fourier potential. The real part of this additional term is small and is usually neglected, while the imaginary part is more important and represents absorption effects associated with inelastic scattering. The contributions of the various inelastic scattering processes to the imaginary potential have been calculated by several authors (Heidenreich, 1962; Whelan, 1965A, 1965B; Hall and Hirsch, 1965; Humphreys and Hirsch, 1968; Radi, 1970). These calculations have indicated that the principal contribution to the inelastic scattering of electrons outside the objective aperture arises from thermal diffuse scattering. (A review of Yoshioka's theory and an assessment of the importance of the different inelastic scattering processes are given by Kambe and Molière (1970).)

There are several approaches which can be taken in order to take the imaginary part of the periodic lattice potential into account. Since these approaches will be discussed in detail in the second part of the thesis, only one approach, which has been widely adopted in the literature, will be introduced in this section. This standard method assumes that the $V'(\vec{r}) << V(\vec{r})$, and takes $iV'(\vec{r})$ into account by using the methods of first order perturbation theory for the non-degenerate state. The effect of the perturbation $iV'(\vec{r})$ is to change the energy of the Bloch wave by an amount $e\Delta E$ given by

$$e\Delta E = -i\int \langle b^{(i)}|V'(\vec{r})|b^{(i)}\rangle d\tau \;. \tag{2.27}$$

This energy change can be related to a change $\Delta k_z^{(i)}$ in the z-component of the Bloch wave vector, i.e.

$$\Delta k_z^{(i)} = -\frac{me}{h^2K}\Delta E \tag{2.28}$$

$$= -iq^{(i)}$$

where $q^{(i)}$ is the absorption coefficient of Bloch wave $|b^{(i)}\rangle$. This coefficient can be calculated from the integral in equation 2.27 to be

$$q^{(i)} = \frac{1}{2K}\sum_g \sum_h C_g^{(i)} C_h^{(i)} U'_{g-h} \;. \tag{2.29a}$$

In matrix form this equation becomes

$$q^{(i)} = (\underline{C}^{(i)})^T \underline{A}' \,\underline{C}^{(i)} \tag{2.29b}$$

where $\underline{A}'$ is a matrix containing the elements $U'_{g-h}/2K$ in the g^{th} row and h^{th} column. It can be seen from the definition of $\gamma^{(i)}$ in equation 2.18 that this change $iq^{(i)}$ in $k_z^{(i)}$ will produce a similar change in $\gamma^{(i)}$. Accordingly, when the effects of inelastic scattering are included in the dynamical theory, the expression for the diffracted beam intensity given in equation 2.25 becomes

$$I_g(z) = |\phi_g(z)|^2 = \left|\sum_i C_0^{(i)} C_g^{(i)} \exp\{2\pi i(\gamma^{(i)} + iq^{(i)})z\}\right|^2 \;. \tag{2.30}$$

By examining this relation it can be seen that the diffracted beam intensity is effectively attenuated or absorbed with depth in the crystal due to the presence of the $\exp(-2\pi q^{(i)}z)$ terms.

Calculations of the Bloch wave absorption parameters indicate that some Bloch waves are more highly absorbed than others. This observation has been explained by several authors (for example, Hashimoto, Howie, and Whelan, 1962; Howie, 1966) in terms of channeling of Bloch waves. In general, the intensity $\langle b^{(i)}|b^{(i)}\rangle$ of a Bloch wave as it propagates through the crystal is not evenly distributed, but instead, is localized or channeled into certain regions of the crystal either at or between the atomic planes. On the other hand, scattering processes such as thermal diffuse scattering occur with a relatively higher probability near the atomic positions than in other regions of the crystal. Accordingly, Bloch waves whose intensity is concentrated at the atomic planes will be more highly absorbed and therefore have larger absorption coefficients than Bloch waves whose intensity is concentrated between the atomic planes. The fact that different Bloch waves generally have different absorption coefficients leads to the anomalous absorption effect which is considered in the next section.

2.2.3 Anomalous Absorption Effects

The principal reason for including inelastic scattering in calculations of diffracted beam intensity is to take anomalous absorption into account. In order to illustrate this effect, it is first convenient to examine the variation of the diffracted beam intensity with thickness in a perfect wedge-shaped crystal. Consider first a situation where absorption is neglected and where there are only two Bloch waves with large excitation amplitudes $C_o^{(i)} C_g^{(i)}$. In this case, intensity I_g is found to vary sinusoidally with crystal thickness as shown in Fig. 4(a). Fig. 4(b) shows the same situation except that both important Bloch waves have been assumed to have equal absorption coefficients. It can be seen in Fig. 4(b) that the mean intensity decreases with increasing thickness but the sinusoidal variations are still present. This is termed normal absorption and simply decreases the scale of intensity of the fringes in thick regions of the crystal. The visibility or contrast of the fringes, as measured by $(I_{max}-I_{min})/(I_{max}+I_{min})$, is not changed. Fig. 4(c) on the other hand shows the intensity profile obtained when one Bloch wave is absorbed much more strongly than the other. This profile illustrates the effect of anomalous absorption in a wedge-shaped crystal. In thicker

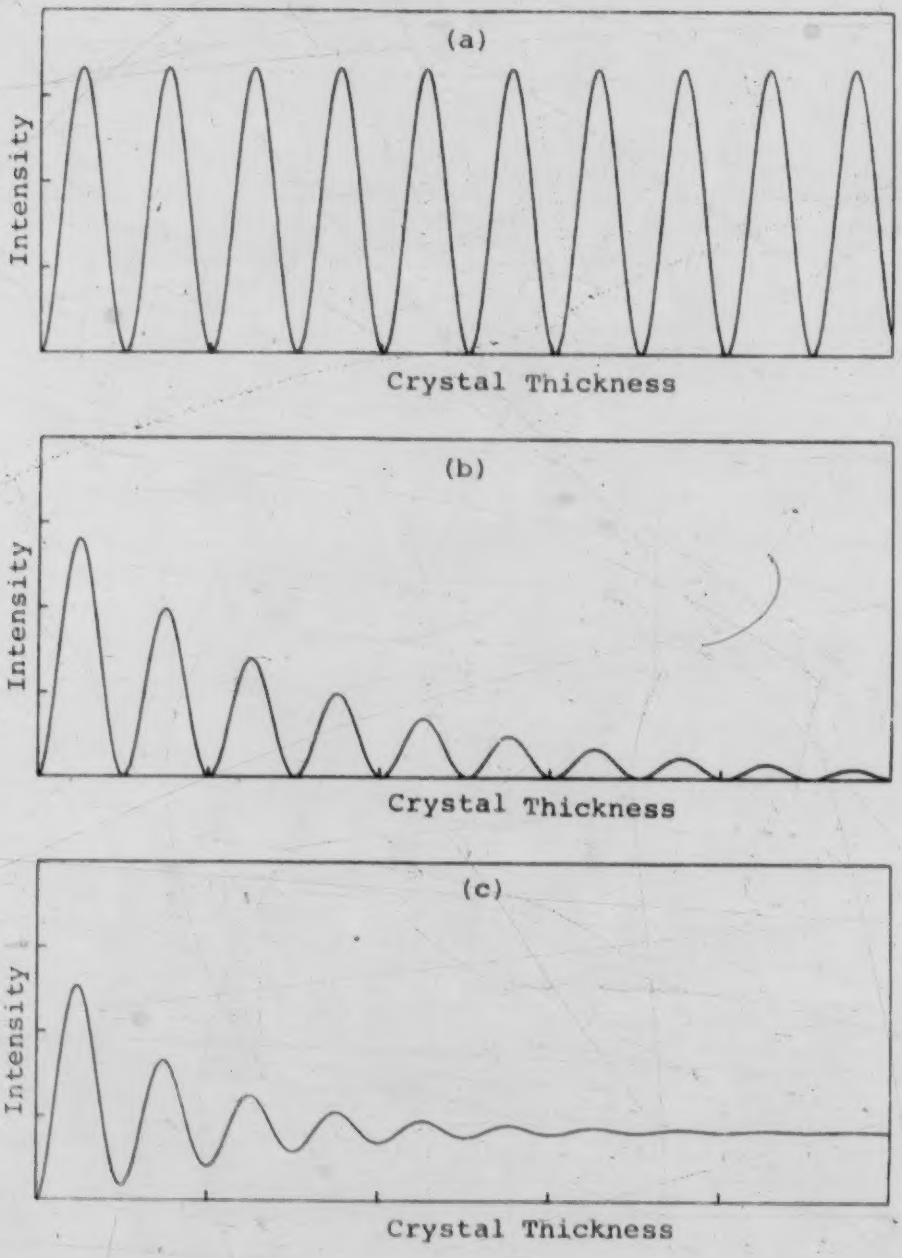

Fig. 4. The variation of diffracted beam intensity with thickness in the presence of (a) no absorption (b) normal absorption and (c) anomalous absorption.

regions, the intensity variations have essentially disappeared due to the strong attenuation of one of the Bloch waves. However, considerable diffracted beam intensity is still present due to the weakly absorbed beam. Besides having an important effect on intensity profiles in perfect crystals, anomalous absorption has also been found to lead to important effects in the images of crystal defects.

2.3 Relativistic Corrections to the Dynamical Theory

Since the velocity of the imaging electrons in the electron microscope is approaching the speed of light, it is necessary to take relativistic effects into account in the dynamical theory. These effects have been considered by Fujiwara (1962), who developed a relativistic dynamical electron diffraction theory using the Dirac wave equation. His results showed that the non-relativistic theory developed using the Schrodinger wave equation can be corrected for relativistic effects by employing two simple substitutions. These consist of replacing the non-relativistic wavelength by a relativistically corrected one and multiplying the Fourier coefficient terms, U_g, by a relativistic mass correction term

$$\beta = (1 - \frac{v^2}{c^2})^{-\frac{1}{2}} \quad . \qquad (2.31)$$

Here v and c are the velocities of the electrons and light respectively. The validity of these corrections has been confirmed experimentally by Hashimoto (1964), Dupouy et al. (1965) and Goringe et al. (1966).

CHAPTER 3

APPROXIMATIONS INVOLVED IN THE MANY-BEAM, TWO-BEAM AND KINEMATICAL THEORIES

3.1 Introduction

The dynamical theory was formulated in the last chapter in terms of the eigenvalues and eigenvectors of an infinite matrix

$$\underline{A} = \begin{pmatrix} 0 & \frac{U_{-g}}{2K} & \frac{U_{-h}}{2K} & \cdots \\ \frac{U_g}{2K} & s_g & \frac{U_{g-h}}{2K} & \cdots \\ \frac{U_h}{2K} & \frac{U_{h-g}}{2K} & s_h & \cdots \\ \cdots & \cdots & \cdots & \cdots \end{pmatrix} . \tag{3.1}$$

This matrix is infinite because an infinite number of diffracted beams were taken into account in the Bloch wave function of equation 2.7. In order to carry out calculations using this theory, it is necessary to approximate this infinite matrix by a matrix of finite size. This is accomplished in the dynamical theory by assuming that only a finite number of diffracted beams are important and need to be taken into account. In this way, the many-beam and two-beam dynamical theories can be developed. These two theories and the reduction of the two-beam theory to the kinematical theory will be considered in this chapter.

3.2 The Many-Beam Dynamical Theory

In the many-beam dynamical theory the number of diffracted beams included is reduced to a finite number N. The question which immediately arises is which diffracted beams are of sufficient importance to be taken into account. This is an important question because the computing time required to diagonalize the $\underline{A}$ matrix increases as the square of the number of reflections included. The problem is generally solved by deriving some criterion for indicating the relative importance of the different reflections. Reflections are then included in order of their decreasing importance until a point is reached where additional reflections make no significant change in the diffracted beam intensity. Since the diffracted beam intensity has converged in this manner, the many-beam theory can be considered to be an exact theory because no significant approximations are made by neglecting the remaining beams.

The effect of a particular diffracted beam on the diffracted beam intensity is found to vary with crystal orientation. For this reason, the question of which beams to include can be conveniently divided into two situations: the systematic case and the non-systematic case. These two cases will be considered in this section and typical many-beam intensity profiles will then be discussed.

3.2.1 The Systematic Case

When a high energy electron beam is incident on a crystal, it is generally found that a number of different sets of lattice planes are close to satisfying their Bragg conditions. It is possible, however, to orient the crystal so that the only important diffracted beams result from different order Bragg reflections from the one set of planes. This situation is termed the systematic case. An example of a diffraction pattern obtained under systematic diffraction conditions is shown in Fig. 5. The row of reflections is called the systematic row and the reflections are termed systematic reflections.

In the systematic case, the reflections are generally included by first including those reflections which are on or inside the Ewald sphere (see Fig. 5). Additional reflections are then included in pairs, one from each end of the row already included, until additional beams do not result in any significant

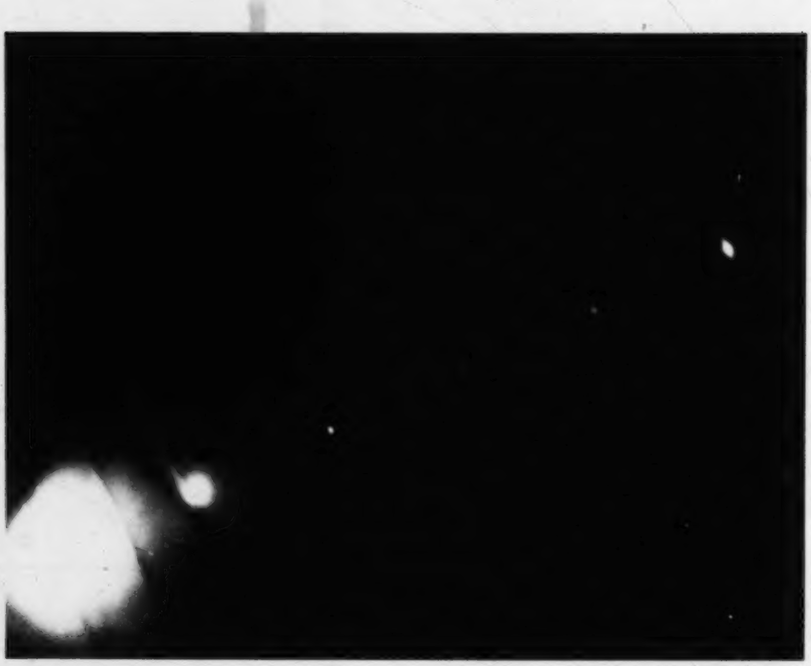

Fig. 5. An experimental diffraction pattern obtained under systematic diffraction conditions in molybdenum. The micrograph shows, from left to right, the reflections (000) through (550) of the (110) systematic row. The reflection (550) is in its Bragg condition and the reflections (000) through (550) are either on or inside the Ewald sphere. The higher order systematic reflections lying to the right and left of the portion of the diffraction pattern shown are outside the Ewald sphere.

change in the diffracted beam intensity. The justification for this procedure is based on the fact that the effect of a systematic reflection h is found to decrease both with the increasing order (i.e. increasing magnitude of the reciprocal lattice vector $\vec{h}$) and increasing deviation from the Bragg condition. Generally ten to twenty reflections are required in a many-beam calculation for the systematic case.

3.2.2 The Non-Systematic Case

The second of the two situations which can occur in determining which beams to include in a many-beam calculation is termed the non-systematic case. In this more complicated situation, the crystal is assumed to be at an orientation where a number of lattice planes are close to satisfying their Bragg conditions and, therefore, a large number of diffracted beams are important. A typical diffraction pattern for the non-systematic case is shown in Fig. 6. In such a pattern, one row of reflections is considered to be the systematic row while those beams which are not colinear with this row are termed the non-systematic reflections (Hoerni, 1956).

In the non-systematic case, all of the important reflections will not necessarily lie in the same plane

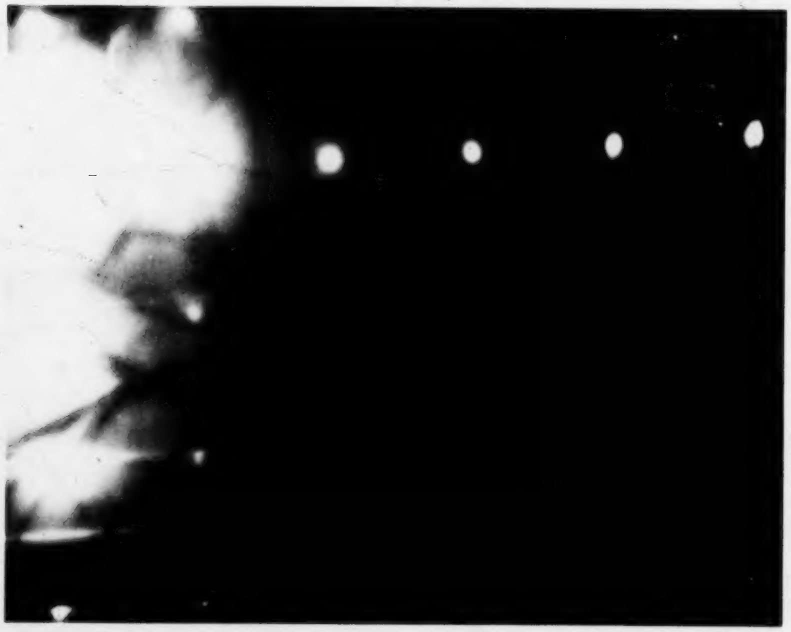

Fig. 6. A portion of a typical diffraction pattern in the non-systematic case. Many diffracted beams are important and must be taken into account in calculating the $\underline{A}$ matrix of the dynamical theory.

or zone. The criterion for ordering reflections which was used in the systematic case is therefore not applicable. This is because the question arises of whether or not a low order reflection far from its Bragg condition is more important than a high order reflection which is in another zone and close to its Bragg condition. Cann (1973) has studied this problem and has developed a criterion based on Bethe's second order approximation (Bethe, 1928). In Cann's theory, the effect of a reflection h on the diffracted beam intensity of reflection g, where s_g is small, is given by

$$\varepsilon_h = \frac{U_{g-h}U_{-h}}{2KU_g s_h} \quad . \qquad (3.2)$$

By using this criterion, reflections can be included in order of decreasing ε_h until additional beams do not result in any significant change in the diffracted beam intensity. Generally thirty to one hundred reflections are required.

3.2.3 The Diffracted Beam Intensity in the Many-Beam Theory

The expression for the diffracted beam intensity in the many-beam theory follows directly from the intensity expression derived in Section 2.3 where an infinite number of diffracted beams were considered. When only

N reflections are considered, only N Bloch waves are excited in the crystal and equation 2.30 for the diffracted beam intensity becomes

$$I_g(z) = |\phi_g(z)|^2 = \left| \sum_{i=1}^{N} C_o^{(i)} C_g^{(i)} \exp(2\pi i(\gamma^{(i)} + iq^{(i)} z)) \right|^2 . \tag{3.3}$$

The form of the diffracted beam intensity profile calculated from this equation can be conveniently examined with reference to a plot of the dispersion surface in the many-beam case. The first seven branches of a dispersion surface calculated by taking thirteen systematic reflections into account are shown in Fig.7. There is one Bloch wave associated with each branch of the dispersion surface, and, in general, each of these Bloch waves has a different value of $\gamma^{(i)}$. It is therefore apparent from the intensity expression 3.3 that the beating between the g^{th} components of these Bloch waves can lead to a diffracted beam intensity profile which is a complicated function of crystal thickness.

It is important to note, however, that it is not the number of Bloch waves, but rather the number of important Bloch waves, which is most significant in determining the form of the intensity profile. The only Bloch waves which will have a large effect on the

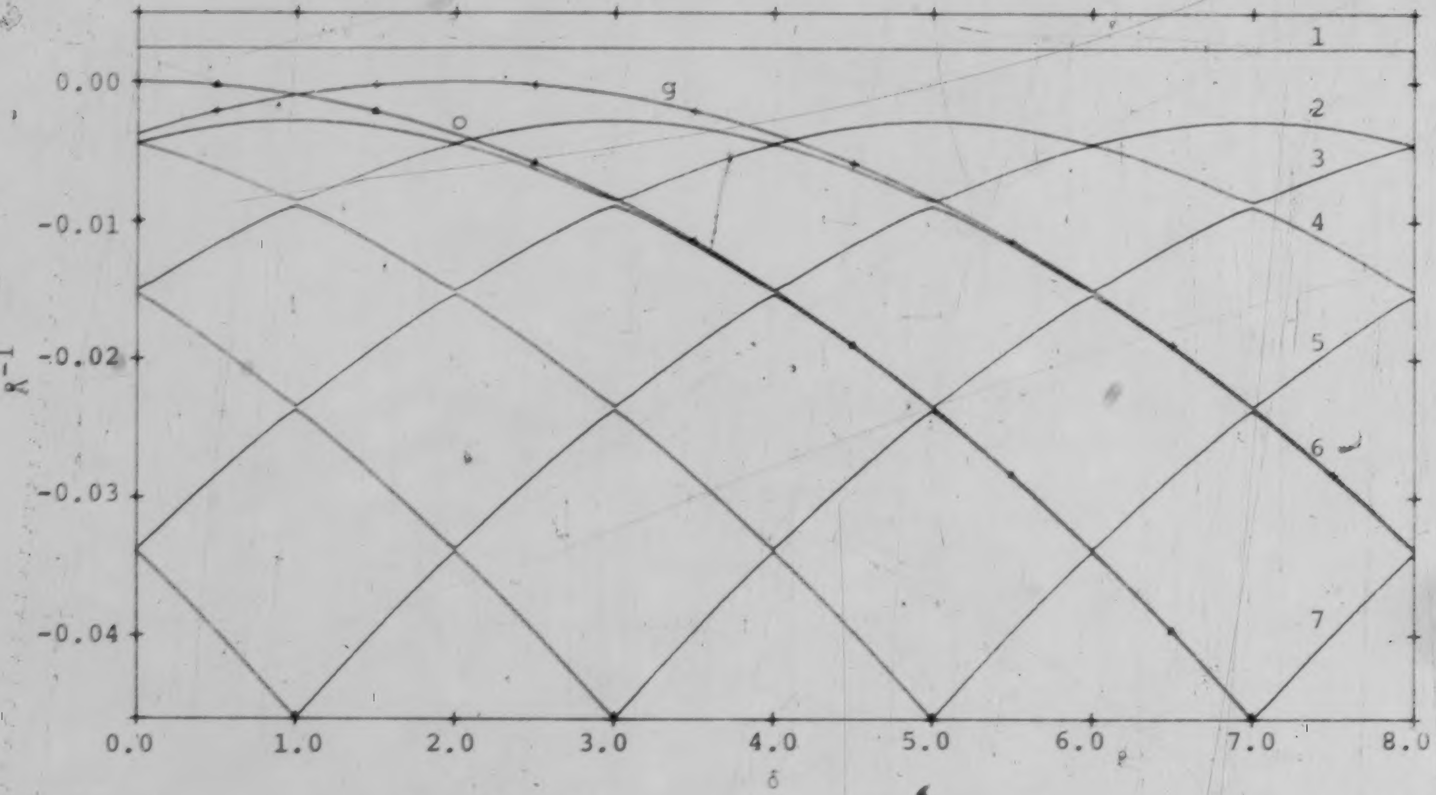

Fig. 7. A many-beam dispersion surface plot for the (110) systematic row in molybdenum at 100 kV. The branches of the dispersion surface are numbered according to decreasing kinetic energy. The circles of radius K about the reciprocal lattice points (000) and (110) have been drawn and are denoted by o and g respectively.

diffracted beam intensity at thickness z will be those for which the terms $C_o^{(i)}C_g^{(i)}\exp(-2\pi q^{(i)}z)$ are large. There are two situations which generally occur. In the first case, the terms $C_o^{(i)}C_g^{(i)}\exp(-2\pi q^{(i)}z)$ for two of the Bloch waves are significantly larger than the corresponding terms for the other Bloch waves. These two Bloch waves, termed primary Bloch waves in this thesis, have a significantly larger effect on the diffracted beam intensity than other Bloch waves. The form of the intensity profile for this situation is shown in Fig. 8. The beating between the two primary Bloch waves leads to the large variation in diffracted beam intensity with thickness. The spacing between the intensity peaks is approximately given by $1/|\gamma^{(i)}-\gamma^{(j)}|$, which is the reciprocal of the difference between the z components of the wave vectors of the two primary Bloch waves. Other Bloch waves, however, can have some effect. If the effect is small, they introduce a variation in the peak to peak spacing as shown in Fig.8. The Bloch waves causing this variation will be termed secondary Bloch waves in this thesis.

The second profile form which is commonly found in a many-beam calculation occurs when one or more of the secondary Bloch waves has such a large term $C_o^{(i)}C_g^{(i)}\exp(-2\pi q^{(i)}z)$ that it can be classified as a primary Bloch wave. When this occurs, there will be

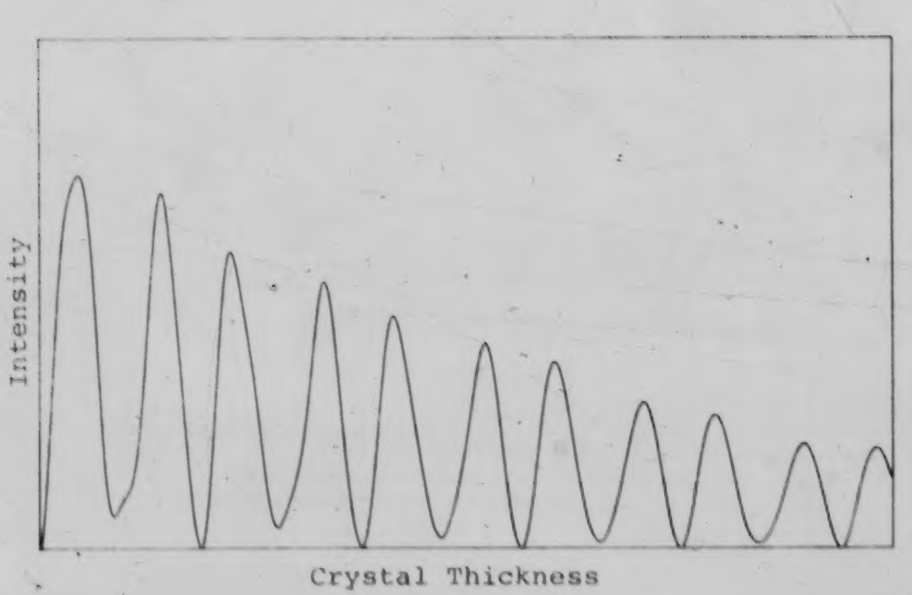

Fig. 8. A diffracted beam intensity profile typical of the case where there are two primary Bloch waves and other secondary Bloch waves present.

three or more primary Bloch waves. A typical profile for this case is shown in Fig. 9. If more than two different wave vectors $(k_o^{(i)})_z$ are involved, then the beating between the three or more primary Bloch waves leads to an intensity profile which exhibits a much larger variation in peak to peak spacing with thickness than occurs when there are only two primary Bloch waves. Profiles of this second type will be referred to in this thesis as complex profiles.

In order to indicate the manner in which the diffracted beam intensity varies with crystal thickness, it is convenient to introduce the terms extinction distance, average extinction distance, and variation in extinction distance. The extinction distance is defined in this thesis to be the peak to peak spacing in plots of the diffracted beam intensity versus crystal thickness. (It should be noted that this definition differs from that used by some authors who define the extinction distance to be the constant U_g/K.) The average extinction distance is the average peak to peak spacing over some specified range of crystal thickness. The third parameter, the variation in extinction distance, is defined to be the difference between the largest and smallest values of the extinction distance over a specified thickness range, expressed as a

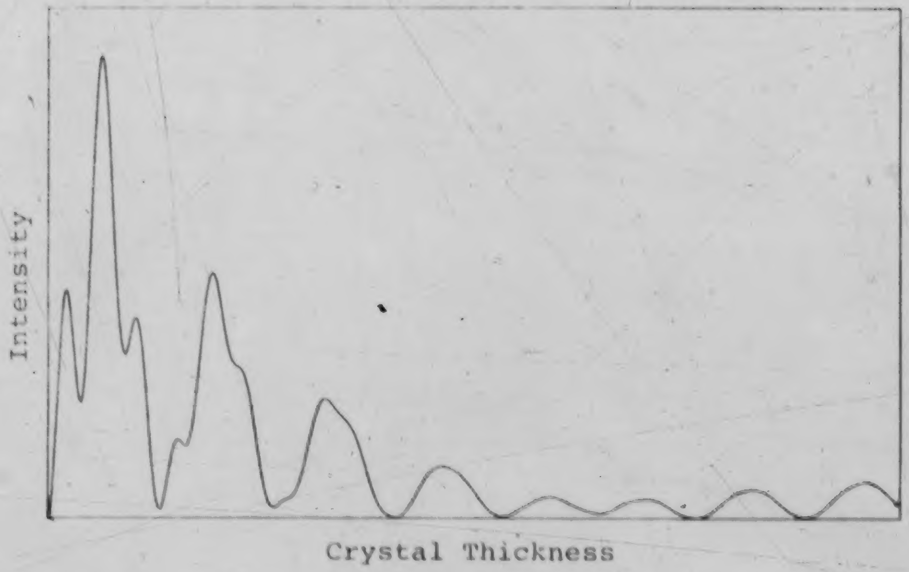

Fig. 9. A diffracted beam intensity profile typical of the case where there are three or more primary Bloch waves present.

percentage of the average extinction distance. By using these three terms it is possible to convey some indication of the manner in which an intensity profile varies with thickness. In Fig. 9 for example, the percent variation is large (~100%). This indicates that the intensity profile is complex and that more than two primary Bloch waves are present. The percent variation for the profile in Fig. 8, where there are two primary and other secondary Bloch waves, is much smaller (~20%). In the two-beam theory considered in the following section, only two Bloch waves are present and the percentage variation will be found to be zero.

3.3 The Two-Beam Theory

The number of diffracted beams included in the many-beam theory generally leads to a large $\underline{A}$ matrix which can only be diagonalized numerically. In order to facilitate examining the dependence of the diffracted beam intensity on the $\underline{A}$ matrix elements, it is of interest to reduce the $\underline{A}$ matrix to a size which can be diagonalized analytically. Fukuhara (1966) has shown that, for certain specific crystal orientations, it is possible to develop analytical expressions when as many as twelve beams are included. Simple eigenvalue and eigenvector expressions, valid for all crystal orientations, can only be found, however, for the case where two reflections are included. In this two-beam theory, the directly transmitted beam and the diffracted beam g are included and the eigenvalue equation 2.17 becomes

$$\begin{pmatrix} 0-\gamma^{(n)} & \frac{U_g}{2K} \\ \frac{U_g}{2K} & s_g-\gamma^{(n)} \end{pmatrix} \begin{pmatrix} C_o^{(n)} \\ C_g^{(n)} \end{pmatrix} = 0 \ . \qquad (3.4)$$

The eigenvalues of this equation can be found by requiring that the determinant of the left hand matrix be zero. This leads to eigenvalues given by

$$\gamma^{(1)} = \frac{1}{2}\left(s_g - \sqrt{s_g^2 + U_g^2/K^2}\right)$$

$$(3.5)$$

and $$\gamma^{(2)} = \frac{1}{2}\left(s_g + \sqrt{s_g^2 + U_g^2/K^2}\right) \ .$$

By substituting each of these eigenvalues back into equation 3.4, the matrix $\underline{C}$ of normalized eigenvectors can be written

$$\underline{C} = \begin{bmatrix} \frac{1}{N} & \frac{(1+\omega^2)^{\frac{1}{2}} - \omega}{N} \\ \frac{\omega - (1+\omega^2)^{\frac{1}{2}}}{N} & \frac{1}{N} \end{bmatrix} \ . \qquad (3.6)$$

where

$$\omega = s_g K/U_g \qquad (3.7)$$

and the normalization factor

$$N = (1 + (\omega - (\omega^2+1)^{\frac{1}{2}})^2)^{\frac{1}{2}} \ . \tag{3.8}$$

This matrix can then be reduced to

$$\underline{C} = \begin{bmatrix} \cos(\beta/2) & \sin(\beta/2) \\ -\sin(\beta/2) & \cos(\beta/2) \end{bmatrix} \tag{3.9}$$

by making the additional substitution

$$\omega = \cot \beta \ . \tag{3.10}$$

If these analytical expressions for the two-beam eigenvalues and eigenvectors are now substituted into the many-beam intensity expression 3.3, then the intensity of the diffracted beam g, neglecting absorption, can be shown to be

$$I_g = \frac{U_g^2}{K^2 s_{eff}} \sin^2(\pi s_{eff} z) \tag{3.11a}$$

where

$$s_{eff} = (s_g^2 + U_g^2/K^2)^{\frac{1}{2}} \ . \tag{3.11b}$$

The form of the two-beam intensity profile can conveniently be examined with reference to the dispersion surface plot of Fig. 10. Since only two refections have been included in the $\underline{A}$ matrix, there are only two branches of the dispersion surface, each branch being

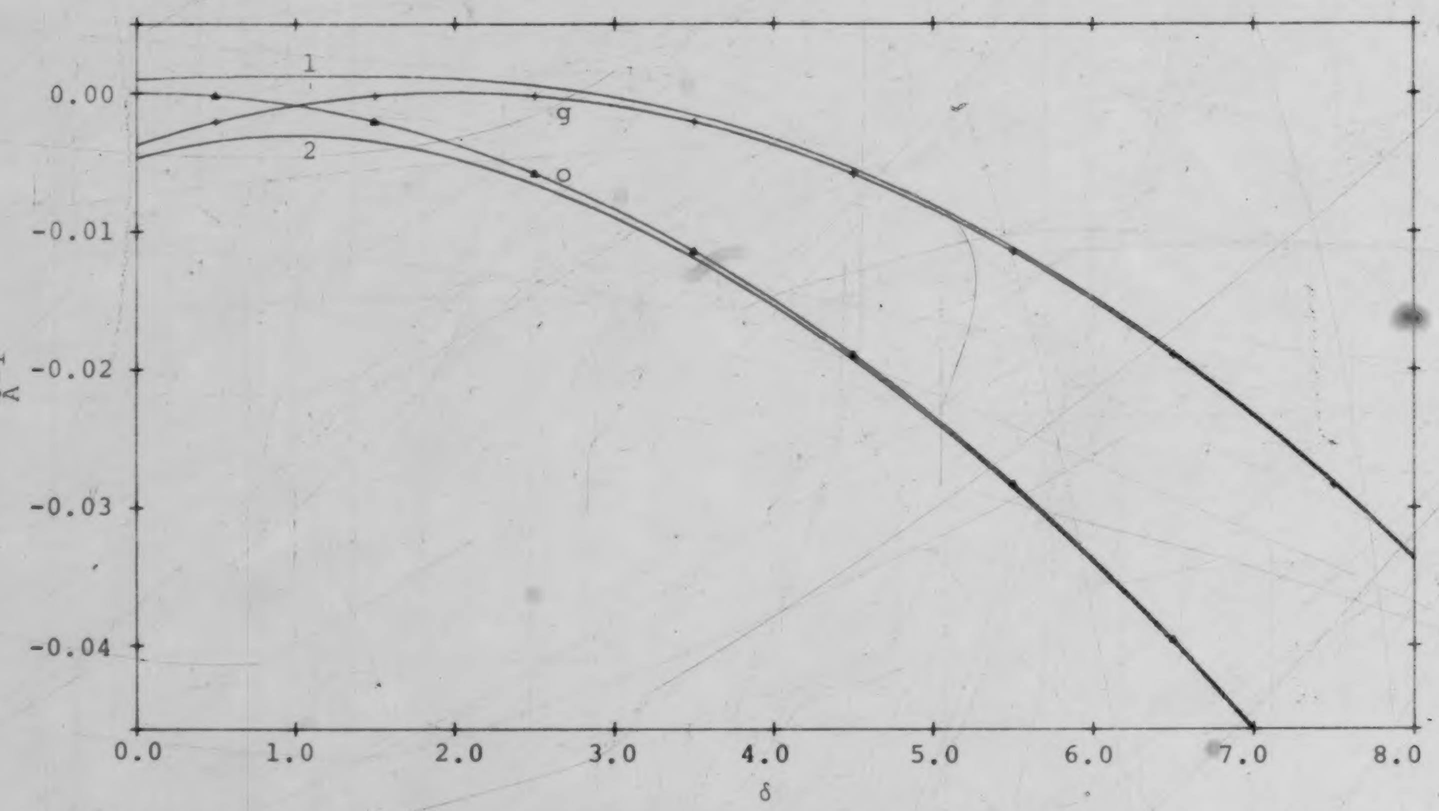

Fig.10. A two-beam dispersion surface plot for the (110) systematic row in molybdenum at 100 kV. The branches of the dispersion surface have been numbered according to decreasing kinetic energy. The circles of radius K about the reciprocal lattice points (000) and (110) have also been drawn and are denoted by o and g respectively.

associated with one of the two Bloch waves present. The beating between the g^{th} components of these two Bloch waves leads to an intensity profile in which the extinction distance is constant as shown in Fig.11. The extinction distance in the two-beam theory is equal to the reciprocal of the spacing between the dispersion surfaces and can be calculated analytically to be

$$\zeta_{2B} = \frac{1}{\gamma^{(1)} - \gamma^{(2)}} = \frac{1}{(s_g^2 + \frac{U_g^2}{K^2})} = \frac{1}{s_{eff}} \quad .. \qquad (3.12)$$

When s_g is zero (i.e., $\delta = 1.0$), this extinction distance is equal to U_g/K, while for large s_g (i.e. large δ), ζ_{2B} approaches $1/s_g$. This latter property is apparent from the dispersion surface plot of Fig. 10. since the distance s_g can be seen from Fig. 12 to be equal to the distance between the spheres of radius K centered on o and g.

3.4 The Kinematical Theory

The kinematical treatment is the simplest approach to the problem of calculating the diffracted beam intensity but it involves two rather drastic assumptions. These assumptions are:

(1) An electron can only be scattered once; and

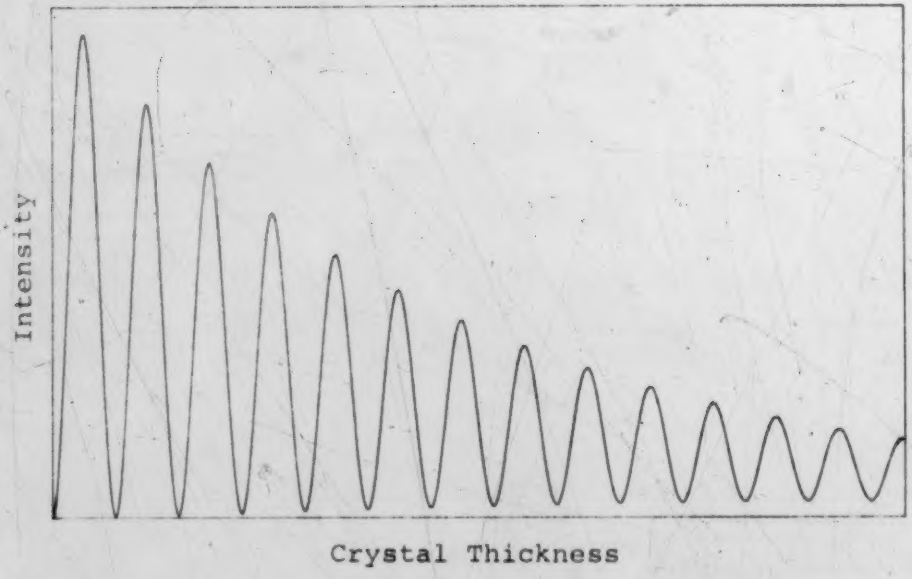

Fig. 11. A typical two-beam intensity profile showing a constant peak to peak spacing.

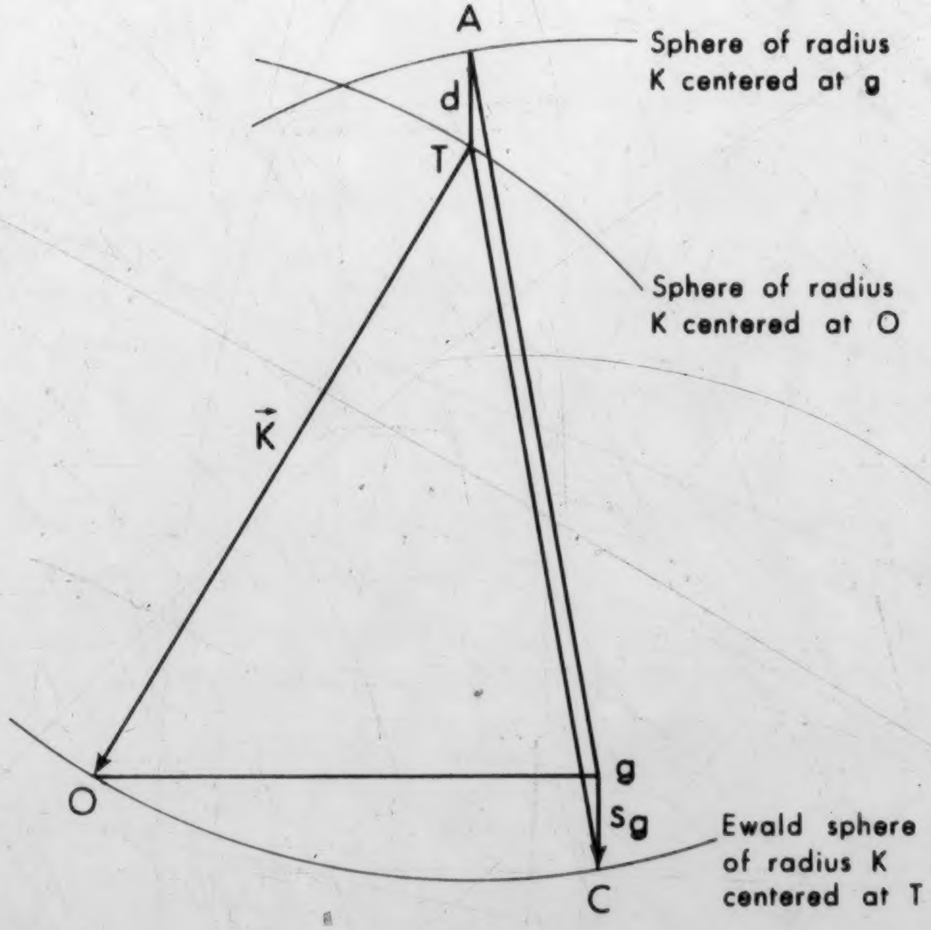
A
d
T
Sphere of radius K centered at g
Sphere of radius K centered at O
$\vec{K}$
O
g
s_g
C
Ewald sphere of radius K centered at T

Fig.12. A geometrical construction showing that the distance d between the two K spheres centered at o and g is equal to s_g. Since d is parallel to s_g and TC = Ag = K, ATCg can be shown to be a parallelogram and s_g = d.

(2) The depletion of the incident beam, as it progresses through the crystal, can be ignored.

The kinematical theory is usually derived in one of two ways. The first is the geometrical method (see for example, Hirsch et al., 1965) in which the scattering by each individual scattering center on the lattice is considered. In this method, which is analogous to the X-ray case, the scattered intensity is calculated by taking the phase relationships between waves from different scattering centers into account. The second approach is a quantum mechanical approach in which the first order Born approximation is used to solve the Schrodinger wave equation 2.1. A good description of this second approach is given, for example, by Vainshtein (1964) and also by Gevers (1970).

The approach to be taken here, however, will be to examine the approximations which can be made in order to reduce the very nearly exact many-beam theory to the kinematical theory. The approximations which are required have previously been given by Serneels and Gevers (1972). These approximations are first, to reduce the many-beam $\underline{A}$ matrix to a two-beam matrix, and second, to calculate the eigenvalues and eigenvectors of this two-beam matrix correct to first order. However, their approach is very involved and therefore a simpler approach has been adopted in this thesis. In the approach used here, the eigenvalues and eigenvectors of the two-beam $\underline{A}$ matrix will be calculated correct to first order by employing the approximate methods of matrix diagonalization presented in Appendix A.

If the procedure given in Appendix A is used to diagonalize the two-beam matrix

$$\underline{A} = \begin{pmatrix} 0 & \frac{U_g}{2K} \\ \frac{U_g}{2K} & s_g \end{pmatrix} \qquad (3.13)$$

then the first order eigenvalues can be found from equation A.2 to be

$$\gamma^{(1)} = 0 \quad \text{and} \quad \gamma^{(2)} = s_g \ . \qquad (3.14)$$

Similarly, the matrix of eigenvectors, correct to first order, can be found from equations A.9 and A.12 to be

$$\underline{C} = \begin{pmatrix} 1 & \frac{U_g}{2Ks_g} \\ \frac{-U_g}{2Ks_g} & 1 \end{pmatrix} \ . \qquad (3.15)$$

If these first-order expressions for the eigenvectors and eigenvalues are substituted into the many-beam intensity expression 3.3, then, neglecting absorption, the intensity of the diffracted beam becomes

$$I_g = \left(\frac{U_g}{Ks_g}\right)^2 \sin^2(-\pi(\gamma^{(1)}-\gamma^{(2)})z)$$

$$= \left(\frac{U_g}{Ks_g}\right)^2 \sin^2(\pi s_g z) \quad . \tag{3.16}$$

This expression is the kinematical expression for the diffracted beam intensity.

The kinematical theory will be a good approximation to the many-beam theory if two conditions are satisfied. Firstly, the effects of systematic reflections other than o and g and of non-systematic reflections must be small, and secondly, the first order eigenvalues and eigenvectors must be good approximations to the two-beam eigenvalues and eigenvectors. The conditions under which this second approximation holds can be examined by considering the approximations used to diagonalize the two-beam $\underset{\sim}{A}$ matrix. The first order approximation $(\gamma^{(1)}-\gamma^{(2)})=-s_g$ used in the intensity expression 3.16 will be a good approximation if the difference between $-s_g$ and $(\gamma^{(1)}-\gamma^{(2)})$ to second order is small. It can be seen from the eigenvalue expression A.14 in Appendix A that, correct to second order,

$$(\gamma^{(1)}-\gamma^{(2)}) \approx - s_g - \frac{2}{s_g}\left(\frac{U_g}{2K}\right)^2 . \qquad (3.17)$$

Accordingly, the first order eigenvalue difference will be a good approximation if

$$|s_g| >> \left|\frac{U_g}{2K}\right| . \qquad (3.18)$$

This same approximation is also used in calculating the orthogonal matrix of first order eigenvectors in equation 3.15. The kinematical theory can therefore be seen to be a good approximation providing only two beams are important and providing the inequality 3.18 holds.

The form of the kinematical theory intensity profile can be seen by examining the intensity expression 3.16. The diffracted beam intensity will vary sinusoidally with thickness with a constant extinction distance of $1/s_g$. The way in which the kinematical extinction distance varies with the deviation parameter δ can be examined by referring to the kinematical dispersion surface which is obtained from the kinematical eigenvalues 0 and s_g. Since it was shown in Fig. 12 that the distance d between spheres of radius K centered on the reciprocal lattice points o and g is simply s_g, the branches of the kinematical dispersion surface can be represented by these spheres. These spheres are indicated on the two-beam dispersion surface plot of Fig. 10. Since the kinematical extinction distance is $1/s_g$, the extinction distance can be seen to be infinite for $\delta = 1.0$ ($s_g = 0$) and to approach the two-beam extinction distance with increasing δ (increasing s_g).

CHAPTER 4

COMPUTATIONAL METHODS

4.1 Introduction

The research presented in this thesis relies extensively on numerical calculations based on the theory presented in the last two chapters. It is therefore important to indicate the procedure used to calculate and diagonalize the $\underline{\Lambda}$ matrix (see equation 2.17, Section 2.1.1) and to calculate the diffracted beam intensity and extinction distance. These procedures will be discussed in this chapter.

4.2 Methods Used to Specify the Crystal Orientation

In order to carry out calculations using the dynamical theory, it is first necessary to obtain the elements s_h on the diagonal of the $\underline{\Lambda}$ matrix (see equation 2.17, Section 2.1.1). It can be seen from Fig. 2, page 22, that the values of these elements depend on the coordinates of the tie-point, i.e. the center of the Ewald sphere. This in turn depends on orientation of the crystal with respect to the incident electron beam. In the research carried out for this thesis, two different methods were used to specify the crystal orientation. In the first method, developed by Cann (1973), an initial crystal orientation was obtained by specifying two reflections which were in their Bragg conditions. This information was then used to calculate the coordinates of the tie-point. The orientation for which the calculation was to be performed was then obtained by changing the direction of the wave vector $\vec{K}$ where $\vec{K}$ is the vector from the tie-point to the origin of the reciprocal lattice. In this manner, new coordinates for the tie-point were obtained. These coordinates were then used to calculate the s-values. In using this method it was found, however, that significant numerical error could arise in the numerical procedure used to calculate the coordinates of the tie-point. As a result, it was very difficult to specify that a particular reflection was in its exact Bragg condition. This was required, for example, in order to obtain dispersion surface shapes accurately and to carry out the critical voltage calculations discussed in Chapter 8.

In order to overcome the problems associated with Cann's method, a second method was developed for specifying the crystal orientation. In this method, referred to in this thesis as the tie-point method, the crystal orientation is specified by the coordinates of the point L which is the perpendicular projection of the tie-point onto the zero order Laue plane (see

Fig. 13). The s-values are then obtained from the coordinates of point L (see Section 4.3). This method was found to be very accurate because no numerical error was involved in specifying the coordinates of the point L.

It should be noted that, if only systematic reflections are considered, complete specification of the crystal orientation is not required. In the systematic case, the deviation of the reflections from their Bragg conditions can be specified by the perpendicular projection of the tie-point onto the systematic row (see Fig. 1, page 12). As indicated in Fig. 1, these deviations will be indicated in this thesis by the parameter δ.

4.3 The Calculation of the Diagonal Elements of the $\underline{A}$ Matrix

Once the crystal orientation has been specified, the orientation dependent diagonal elements of the $\underline{A}$ matrix can then be calculated. The procedure used to calculate these elements when the position of the Ewald sphere is specified using Cann's method has already been documented (Cann 1973) and will not be discussed again here. It is of interest in this thesis, however, to consider in detail the methods which can be used to

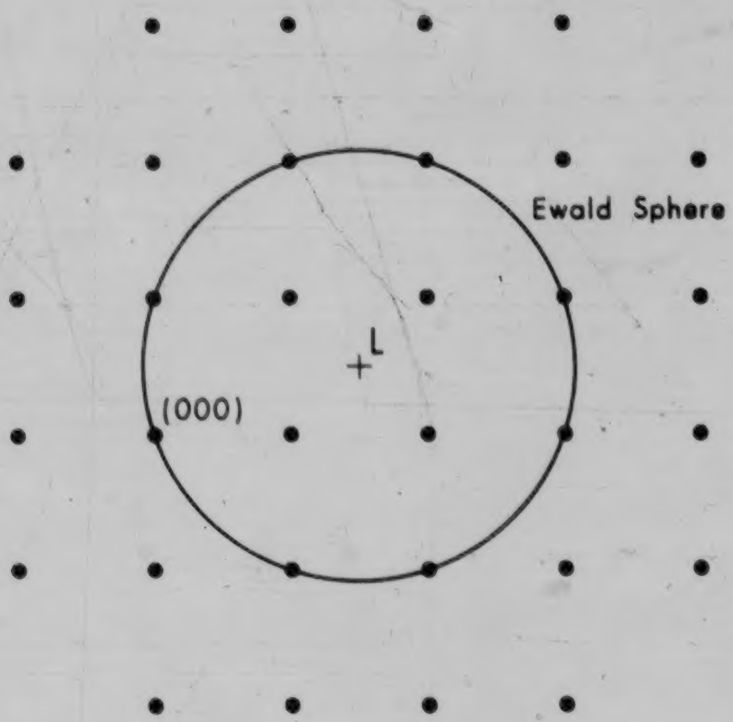

Fig. 13. The intersection of the Ewald sphere with the zero order Laue zone. The crystal orientation is specified in the tie-point method by the point L which is the perpendicular projection of the center of the Ewald sphere (tie-point) onto the zero order Laue plane.

calculate the diagonal elements when the position of the Ewald sphere is specified using the tie-point method. Three possible methods, termed the s-value, t-value, and exact methods will be considered and compared in this section.

4.3.1 The s-Value Method

When the $\underline{A}$ matrix is derived by using the methods discussed in Section 2.1.1, then the elements on the diagonal of the $\underline{A}$ matrix are termed s-values. The s-value for a particular reflection h is defined to be the distance in the z direction from the reciprocal lattice point h to the Ewald sphere. When the position of the Ewald sphere is specified using the tie-point method, then these s-values can be calculated with the aid of Fig. 14. In this figure, the z-axis has been taken to be perpendicular to the crystal surface and the symmetrical Laue case has been assumed. The point L is the projection of the tie-point T onto the zero order Laue plane. It can be seen that the s_h value for some reflection to the n^{th} Laue zone is

$$\begin{aligned} s_h &= LN - \rho_h = TN - TL - \rho_h \\ &= (K^2 - \tau_h^2)^{\frac{1}{2}} - (K^2 - \tau_o^2)^{\frac{1}{2}} - \rho_h \qquad (4.1) \end{aligned}$$

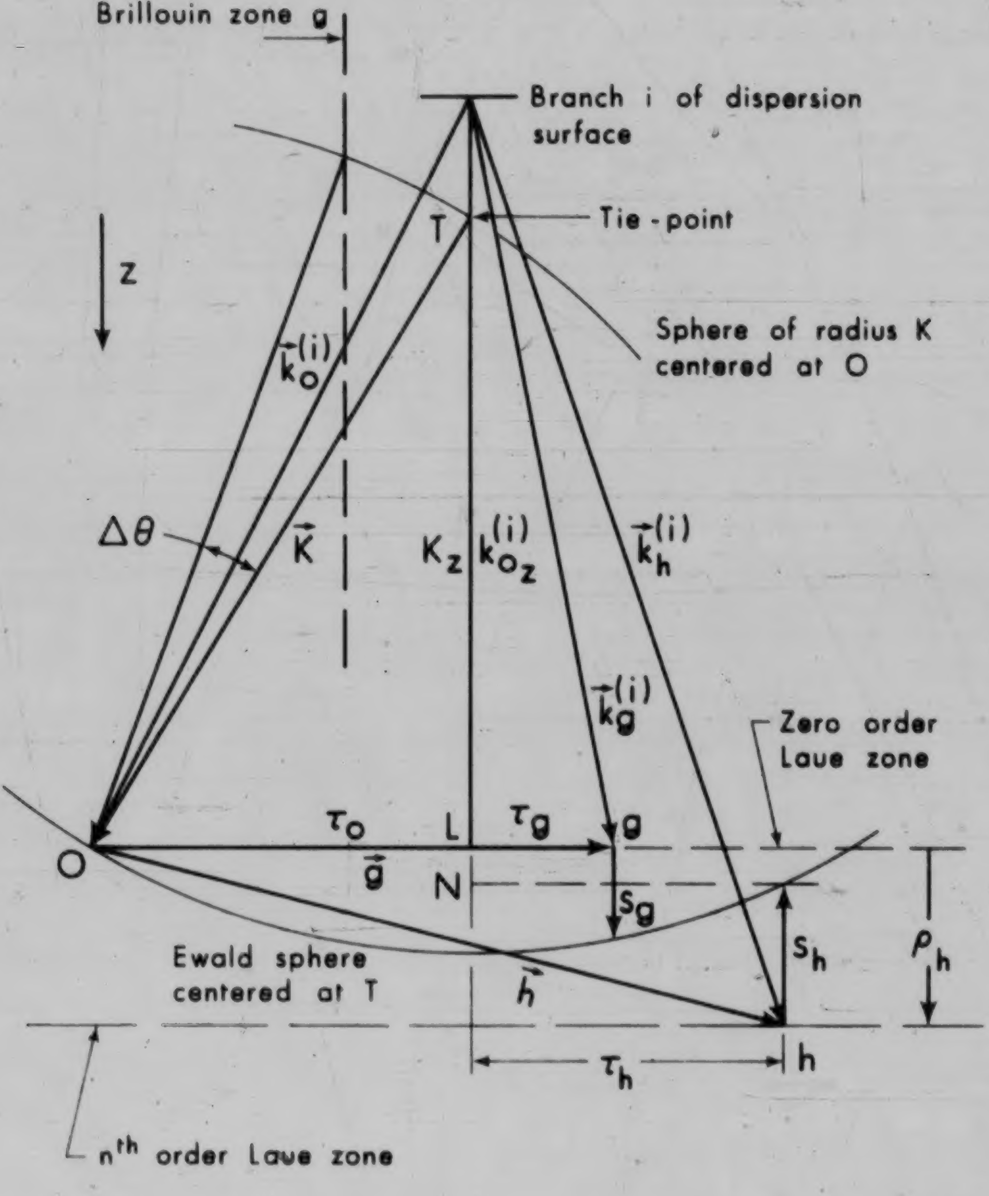

Fig.14. The dispersion surface and Ewald sphere construction for calculating the diagonal elements of the $\underline{A}$ matrix.

where ρ_h is the distance measured in the z direction from the zero order Laue zone to the n^{th} order Laue zone. Although this expression for s_h is analytically correct, significant numerical error can arise when the two large square root terms are nearly equal. Under these conditions, increased numerical accuracy can be obtained by using a Taylor series to expand the square root terms. If terms correct to second order are retained, then s_h becomes

$$s_h = \frac{1}{2K} (\tau_o^2 - \tau_h^2) + \frac{1}{8K^3} (\tau_h^4 - \tau_o^4) - \rho_h \ . \tag{4.2}$$

This method of calculating the diagonal elements of the $\underline{A}$ matrix (i.e., equation 4.1, and for small s_h, equation 4.2) will be referred to as the s-value method.

It is of interest to note that if only the first order term of equation 4.2 is retained, then the s-values for reflections g in the zero order zone become

$$\begin{aligned} s_g &= \frac{1}{2K} (\tau_o^2 - \tau_g^2) && \text{(4.3a)} \\ &= \frac{1}{2K} (\tau_o + \tau_g)(\tau_o - \tau_g) \\ &= \frac{1}{2K} g(\tau_o + \tau_o - \tau_o - \tau_g) \\ &= \frac{1}{K} g(\tau_o - g/2) \\ & g \Delta 0 && \text{(4.3b)} \end{aligned}$$

where $\Delta\theta$ is defined in Fig. 14. This first order approximation is used by many authors (see for example Head et al., 1973).

4.3.2 The t-Value Method

It is next of interest to consider an alternate expression for the terms $(K^2 - (\vec{k}_h^{(i)})^2)$ in Bethe's equation 2.9, page 20, which in turn leads to a new expression for the diagonal elements of the $\underline{A}$ matrix. This alternate approach is similar to one developed by Miyake (1959) for reflections in the zero order Laue zone. The expression to be presented here, however, can also be applied to reflections not in the zero order Laue zone. If the eigenvalue $\gamma^{(i)}$ is defined to be

$$\gamma^{(i)} = (k_o^{(i)})_z - K \tag{4.4}$$

then it can be seen from Fig. 14 that

$$\begin{aligned} K^2 - (\vec{k}_h^{(i)})^2 &= K^2 - \{(k_o^{(i)})_z + \rho_h\}^2 - \tau_h^2 \\ &= K^2 - \{K + (\gamma^{(i)} + \rho_h)\}^2 - \tau_h^2 \\ &= -2K(\gamma^{(i)} + \rho_h) - (\gamma^{(i)} + \rho_h)^2 - \tau_h^2 \\ &= -2K(\gamma^{(i)} + \rho_h)\{1 + \frac{(\gamma^{(i)} + \rho_h)}{2K}\} - \tau_h^2. \end{aligned} \tag{4.5}$$

If it is assumed that

$$\frac{\gamma^{(i)} + \rho_h}{2K} \simeq 0 \tag{4.6}$$

then

$$K^2 - (\vec{k}_h^{(i)})^2 \simeq -2K(\gamma^{(i)} + t_h) \tag{4.7}$$

where

$$t_h = -\frac{\tau_h^2}{2K} - \rho_h \, . \tag{4.8}$$

If equation 4.7 is substituted into Bethe's equation 2.9, page 20, then the eigenvalue equation

$$\underline{A}\underline{C}^{(i)} = \underline{\gamma}^{(i)}\underline{C}^{(i)} \tag{4.9}$$

can be obtained. In this equation, the off-diagonal elements are given by $A_{gh} = U_{g-h}/2K$, while the diagonal elements are the t-values of equation 4.8. The eigenvalues and eigenvectors of equation 4.9 can then be used to calculate the diffracted beam intensity.

4.3.3 The Exact Method

The third method which will be used to calculate the eigenvalues and eigenvectors of the $\underline{A}$ matrix is an exact approach which has not yet appeared in the literature. This method considers reflections in the zero Laue zone only, but it does not make the approximations inherent in the s-value and t-value approaches.

(If reflections other than those in the zero order zone are considered, then Bethe's equation cannot be cast in eigenvalue form.) In this approach, the term $K^2 - (\vec{k}_g^{(i)})^2$ is calculated from Fig. 14 in the following manner:

$$K^2 - (\vec{k}_g^{(i)})^2 = (K_z^2 + \tau_o^2) - ((k_o^{(i)})_z^2 + \tau_g^2)$$

$$= (K_z^2 - (k_o^{(i)})_z^2) + (\tau_o^2 - \tau_g^2).$$

$$= (K_z - (k_o^{(i)})_z)(K_z + (k_o^{(i)})_z) + \tau_o^2 - \tau_g^2. \quad (4.10)$$

If $\gamma^{(i)}$ is defined in the same way as for the s-value method, i.e.

$$\gamma^{(i)} = (k_o^{(i)})_z - K_z \quad (4.11)$$

then

$$\frac{K^2 - (\vec{k}_g^{(i)})^2}{2K} = -\gamma^{(i)}\left(\frac{K_z}{K} + \frac{\gamma^{(i)}}{2K}\right) + \frac{\tau_o^2 - \tau_g^2}{2K}$$

$$= -\Gamma^{(i)} + \frac{\tau_o^2 - \tau_g^2}{2K} \quad (4.12)$$

where

$$\Gamma^{(i)} = \gamma^{(i)}\left(\frac{K_z}{K} + \frac{\gamma^{(i)}}{2K}\right). \quad (4.13)$$

If the terms $(\tau_o^2 - \tau_g^2)/2K$ are used as the diagonal elements of the $\underline{A}$ matrix and the eigenvalues $\Gamma^{(i)}$ are calculated, then the exact eigenvalues $\gamma^{(i)}$ defined by equation 4.11 can be found from equation 4.13. The correct eigenvectors are those found by diagonalizing the $\underline{A}$ matrix. For reflections in the zero order Laue zone, the exact eigenvalues of equation 4.4 can be calculated in a similar way from equation 4.5.

4.3.4 A Comparison of the s-Value, t-Value and Exact Methods

Because the exact method is a new approach which does not make the approximations inherent in the s-value and t-value methods, it is possible for the first time to assess the accuracy of the two approximate methods. This was done by comparing the diffracted beam intensity calculated using each of the approximate methods with that found using the exact method. These calculations showed that for thin crystals the profiles were quite similar. As the thickness increased, however, significant differences in the diffracted beam intensity were found although the profile shape remained very much the same. An example of these differences is shown in Fig. 15. These calculations were carried out for the (110) dark field in molybdenum at 100 kV. It can be seen from this figure that the peaks in intensity obtained using the t-method are displaced slightly from those of the s-method and the exact method. This leads to significant differences in the diffracted beam

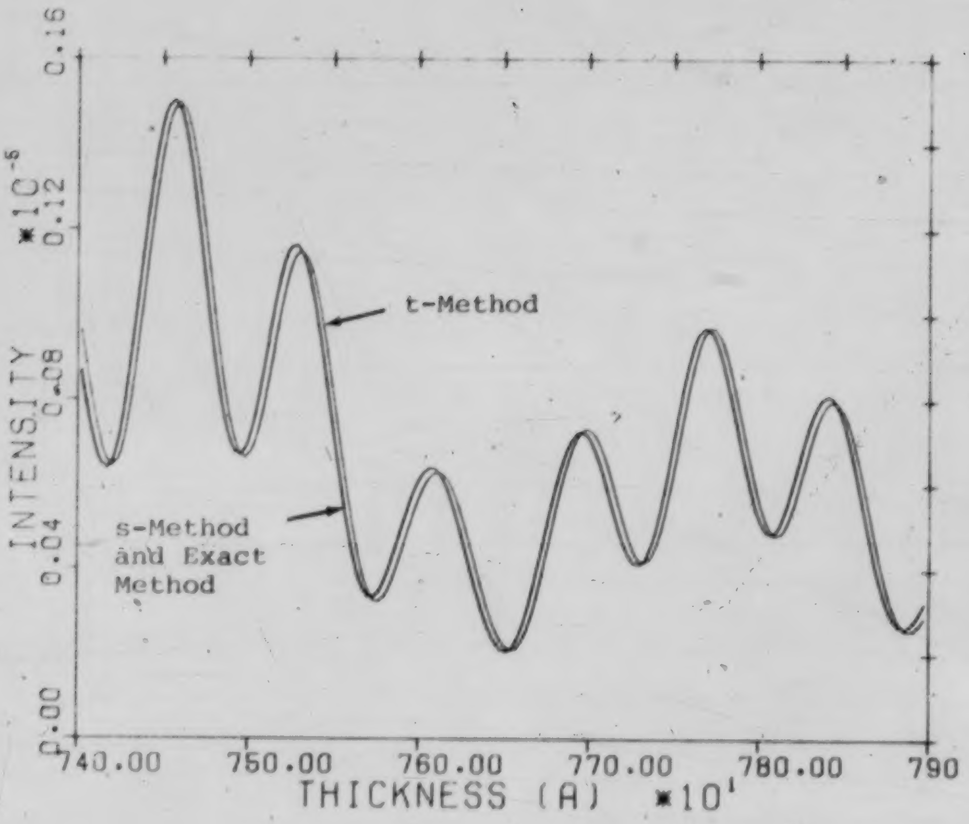

Fig. 15. A comparison of the diffracted beam intensities found in thick crystals using the t-method, s-method, and exact method. Thirteen reflections of the (110) systematic row in molybdenum were considered and $\delta = 3.5$.

intensity at a particular crystal thickness. For example, at a thickness of 7600 Å the intensities found by the t-method and exact method differ by 8 %. As can be seen from Fig. 15, good agreement was obtained between the s-method and exact method for thicker crystals.

The reason that the t-value method is a poorer approximation than the exact method can be seen by comparing the two methods analytically. This is most easily done by first showing that the t-method and the first order s-method approximation of equation 4.3a are equivalent. This can be shown by noting that the differences between the eigenvalues of a matrix will not be changed if a constant is added to each of the diagonal elements before diagonalization. Furthermore, the addition of this constant will not change the eigenvectors. If the constant $\tau_o^2/2K$ is added to all the t_g elements, then the t's of equation 4.8 become

$$t_h = \frac{1}{2K}(\tau_o^2 - \tau_h^2) \qquad (4.14)$$

for the zero order Laue zone. This expression for the diagonal elements is identical to the expression obtained when the s-values are calculated correct to the first order (see equation 4.3a). Accordingly, the eigenvalues and eigenvectors calculated by using the t-method are of the same accuracy as those calculated by using the first order s-value approximation of equation 4.3a.

The intensity profile differences which were found when the t-method was compared to the exact method can now be examined by comparing the first order s-value approximation to the exact method. Since the same diagonal elements are used in the $\underline{A}$ matrix in each case (compare equation 4.3a to equation 4.12), then the eigenvectors for each case will be identical. However, the eigenvalues obtained by diagonalizing the $\underline{A}$ matrix are used, without alteration, in calculating the intensity in the first order s-value case, while these same eigenvalues are corrected (see equation 4.13) before being used in the exact calculation. Accordingly, the eigenvalues of the first order s-method will differ slightly from the exact eigenvalues and this results in the slight displacement in the peaks in the intensity profiles in thick parts of the crystal (see Fig. 15). When a calculation is carried out using the more accurate s-values of equations 4.1 or 4.2, then the eigenvectors will no longer be exact. The eigenvalues, however, are more accurate and generally, improved agreement with the exact method is obtained.

For the diffracted beam intensity calculations presented in this thesis, either the s-value method (equations 4.1 or 4.2) or the exact method was used. The exact method is preferable when only reflections in the zero order Laue zone are considered because it is the most accurate and yet it does not take any more computing time than the s-value method. (The extra time required to correct the eigenvalues is compensated for by the simpler form of the diagonal elements of the $\underline{A}$ matrix). However, the t-method was used for plotting dispersion surface plots. The t-method is useful in this case because the eigenvalues and diagonal elements are defined with reference to a plane at distance K in the -z direction from the zero order Laue zone. This allows the dispersion surface and the K spheres about the reciprocal lattice points to be obtained by plotting the eigenvalues and the t_g elements respectively.

4.4 The Calculation of the Off-Diagonal Elements of the $\underline{A}$ Matrix

The gh off-diagonal element of the $\underline{A}$ matrix is equal to $U_{g-h}/2K$ where, for a crystal composed of only one atom type,

$$U_{g-h} = \frac{\beta}{\pi V_c} F_{g-h} \, f\left(\frac{\sin \theta_{g-h}}{\lambda}\right) \exp(-B|\vec{g}-\vec{h}|^2/4). \qquad (4.15)$$

(See for example, Howie, 1970.) In this expression, β is the relativistic mass correction factor for the incident electrons, V_c is the volume of the unit cell, F_{g-h} is the kinematical structure factor, and $f(\sin \theta_{g-h}/\lambda)$ is the atomic scattering factor for electrons. The scattering factors used in this thesis were those calculated by Doyle and Turner (1968) using relativistic Hartree-Fock atomic wave functions. Equation 4.15 also contains the Debye-Waller correction B. The B values used in this thesis were 0.51, 0.20, and 0.55, for gold, molybdenum, and aluminum respectively (Ibers and Vainshtein, 1962). For a particular crystal structure and accelerating voltage, the values of U_{g-h} tend to increase with atomic number and decrease with increasing $|\vec{g}-\vec{h}|$ as shown in Fig. 16.

4.5 The Calculation of the $\underline{A}'$ Matrix

In order to take absorption into account, it is necessary to calculate the terms $U'_{g-h}/2K$ of the $\underline{A}'$ matrix. The values of U'_{g-h} which were used were obtained from the ratios U'_g/U_g given by Humphreys and Hirsch (1968). The values of U'_g/U_g for gold, molybdenum, and aluminum are plotted in Fig. 17.

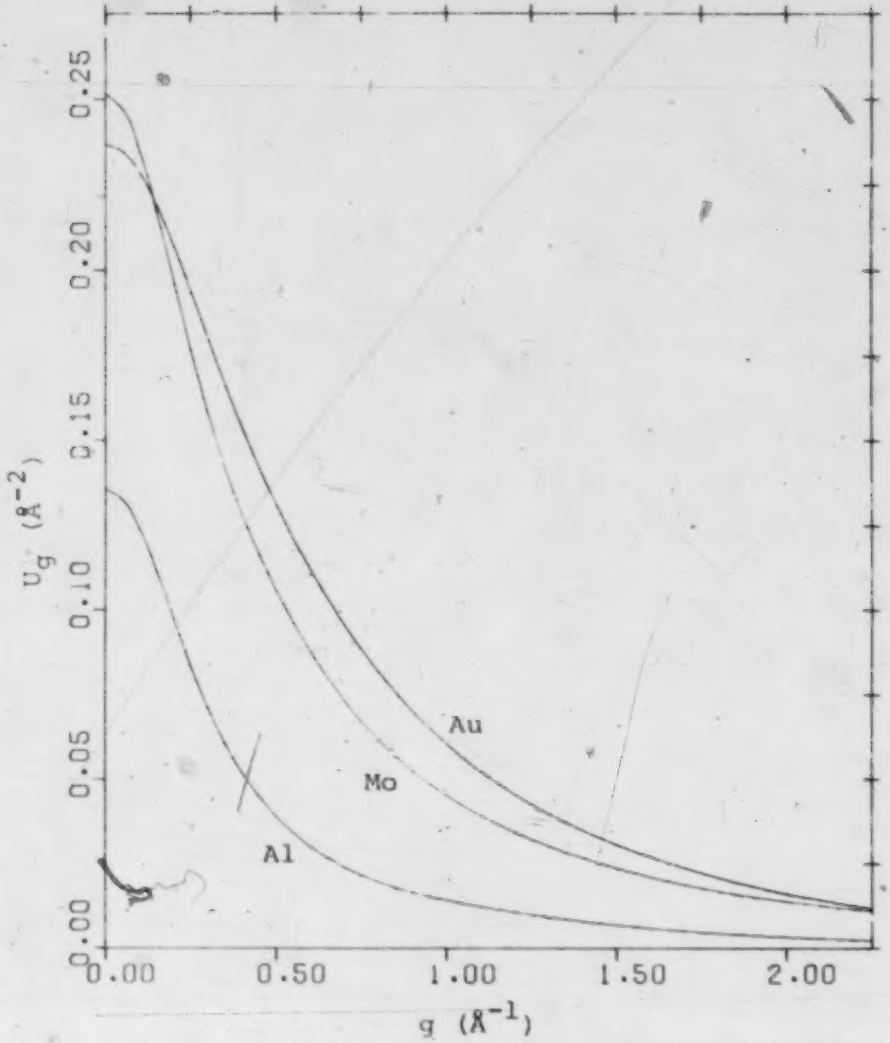

Fig. 16. Values of U_g as a function of g for 100 kV electrons in aluminum and gold (FCC crystal structure) and in molybdenum (BCC crystal structure). These materials have atomic numbers 13, 79, and 42 respectively.

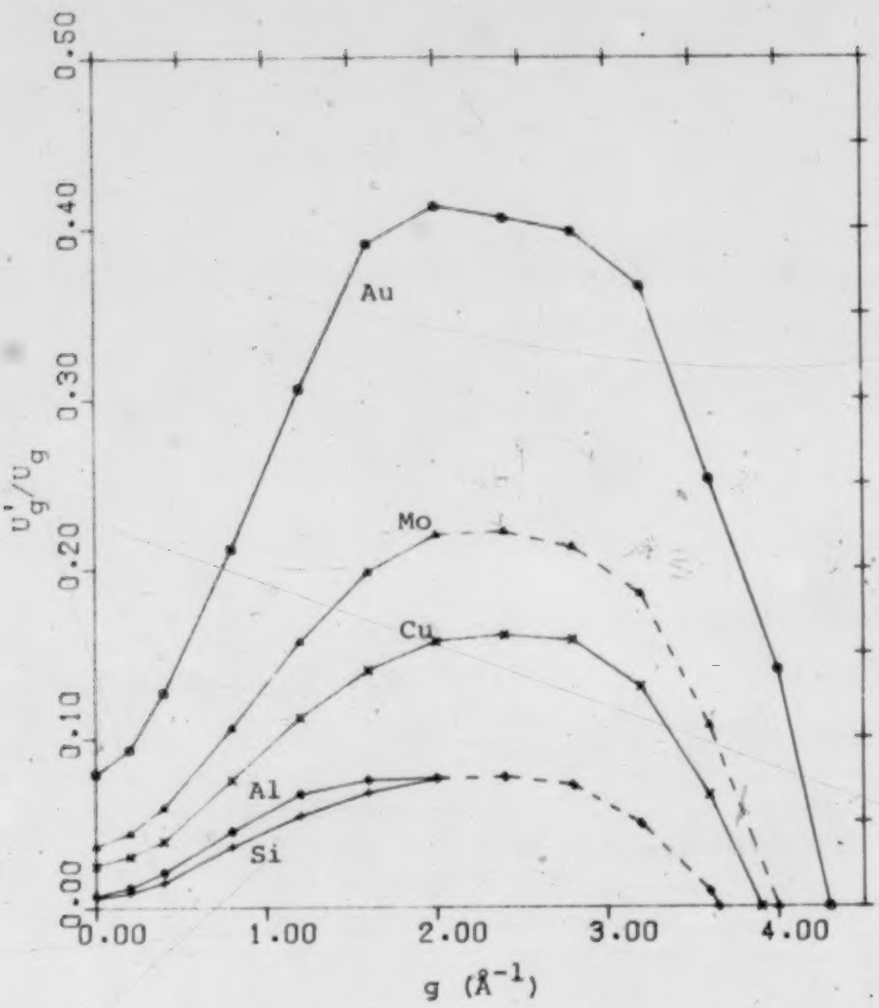

Fig. 17. Values of U_g'/U_g for 100 kV electrons obtained from the data presented by Humphreys and Hirsch (1968). The dashed lines are extrapolations of their results and were used to calculate U_g'/U_g for large values of g. The ratio U_g'/U_g was taken to be zero once these extrapolations intersected the g axis.

4.6 Matrix Diagonalization and the Calculation of Diffracted Beam Intensity

In comparing the kinematical, two-beam, and many-beam theories, the $\underline{A}$ matrix was diagonalized by using the subroutine EIGRS in the IMSL subroutine package (IMSL, 1974). This routine was used because it was found to be very accurate and required less computing time than other available routines. Equation 3.3 was then used to calculate the diffracted beam intensity. The intensity was generally obtained for thickness increments of 1 - 10 Å depending on how rapidly the intensity varied with thickness. In order to improve the accuracy to which the extinction distance could be calculated, IMSL (1974) smoothing routine ICS1VE was used to increase the number of points in the regions of the intensity peaks. The extinction distance was then obtained from the smoothed curve. The depth increment and the number of smoothed points close to each peak were determined in order to give an accuracy of better than 0.5% in calculating the extinction distance.

In examining approximations used to take the imaginary part of the lattice potential into account, it was necessary to diagonalize both real and complex matrices. In this case, the SSP (1970) routine EIGEN was used to diagonalize the real matrices. (The IMSL routine EIGRS was inconvenient because some of the eigenvectors of adjacent orientations were often multiplied by -1 and this led to complications in plotting the parameters $q^{(ij)}$. See Chapter 6.) The complex matrices were diagonalized by using the IMSL (1974) subroutine EIGCC.

All the computer programs were written in FORTRAN and executed on the IBM 360/67 computer of the Department of Computing Services at the University of Alberta. The calculated line graphs were plotted using an off-line model 925/1036 Calcomp Plotter.

CHAPTER 5

A COMPARISON OF THE KINEMATICAL, TWO-BEAM AND MANY-BEAM THEORIES

5.1 Introduction

It was indicated in Section 1.3.1 that the validity of the kinematical and two-beam theories for large values of δ will be examined in the first part of this thesis. This assessment will be carried out in this chapter by comparing these two theories to the nearly exact many-beam theory. The question which immediately arises is what method should be used to carry out this comparison. The method to be used in this thesis will be based on a comparison of intensity profiles obtained from each of the three theories. (These intensity profiles can be obtained experimentally by examining the images of wedge-shaped crystals.) This method was chosen because the shapes of these profiles are very sensitive to many-beam effects. (In this thesis, changes in the two-beam intensity profile which occur when additional reflections are considered will be referred to as many-beam effects.)

The next question which arises is what methods should be used to compare these profiles. The first method to be used will be based on a comparison of the average extinction distance in the many-beam profiles to the two-beam and kinematical extinction distances. The reason that the many-beam average extinction distance has been chosen is that, if only two primary Bloch waves are excited, this parameter is very nearly equal to the reciprocal of the spacing between the dispersion surface branches for these two Bloch waves. This is analogous to the concept of extinction distance in the two-beam theory which is equal to the reciprocal of the spacing between branches one and two of the dispersion surface. (A method similar to this has been employed by Goringe et al. (1966) in comparing the two-beam and many-beam extinction distances.)

The comparison of the many-beam average extinction distance to the kinematical and two-beam extinction distances, however, is of limited value in assessing the validity of the two analytical theories. The reason for this lies in the fact that secondary Bloch waves will not have a significant effect on the many-beam average extinction distance. These Bloch waves, however, can result in significant variations in the many-beam extinction distance. If these variations are large, then the kinematical and two-beam theories are poor approximations even though there may be good agreement between the many-beam average extinction distance and the results obtained from the two analytical theories. Therefore, in examining the validity of the two analytical theories, the variation with thickness in the many-beam extinction distance will also be examined.

Many-beam effects can be due to either systematic or non-systematic reflections. Accordingly, both these cases will be examined in this chapter.

5.2 A Comparison of the Kinematical, Two-Beam and Many-Beam Theories in the Systematic Case for Large Values of δ

In the first set of calculations, the extinction distances obtained using the kinematical, two-beam and many-beam theories were examined as a function of the deviation parameter δ for the (110) dark field intensity in molybdenum. The accelerating voltage used was 100 kV and, depending on the value of δ, from fourteen to sixteen reflections from the (110) systematic row were included in the many-beam calculations. Molybdenum was chosen because it is of medium atomic number and the accelerating voltage of 100 kV is commonly used experimentally. The first order dark field intensity was chosen because the contrast in this image is generally much better than in the bright field image and thus it is often used in experimental studies of extinction distance (see for example, Cann and Sheinin, 1974A). The validity of the two-beam and kinematical theories was assessed for values of $\delta > 3.5$. Values of $\delta < 3.5$ have previously been investigated by Sheinin (1967).

5.2.1 A Comparison of the Kinematical and Two-Beam Extinction Distances with the Many-Beam Average Extinction Distance

An examination of the many-beam intensity profiles for the (110) dark field in molybdenum showed that, for $\delta > 3.5$, the profiles were of two basic types. The first type is similar to that shown in Fig. 18(a). It can be seen from this figure that the intensity profile is sinusoidal in character over the range of thickness considered. The second type of profile which was obtained is similar to that shown in Fig. 18(b). This profile is sinusoidal in character up to a thickness of approximately 1000 Å, but, in contrast to the profile of Fig. 18(a), this second profile then becomes complex. In thicker parts of the crystal, the profile becomes sinusoidal in character again. It was found

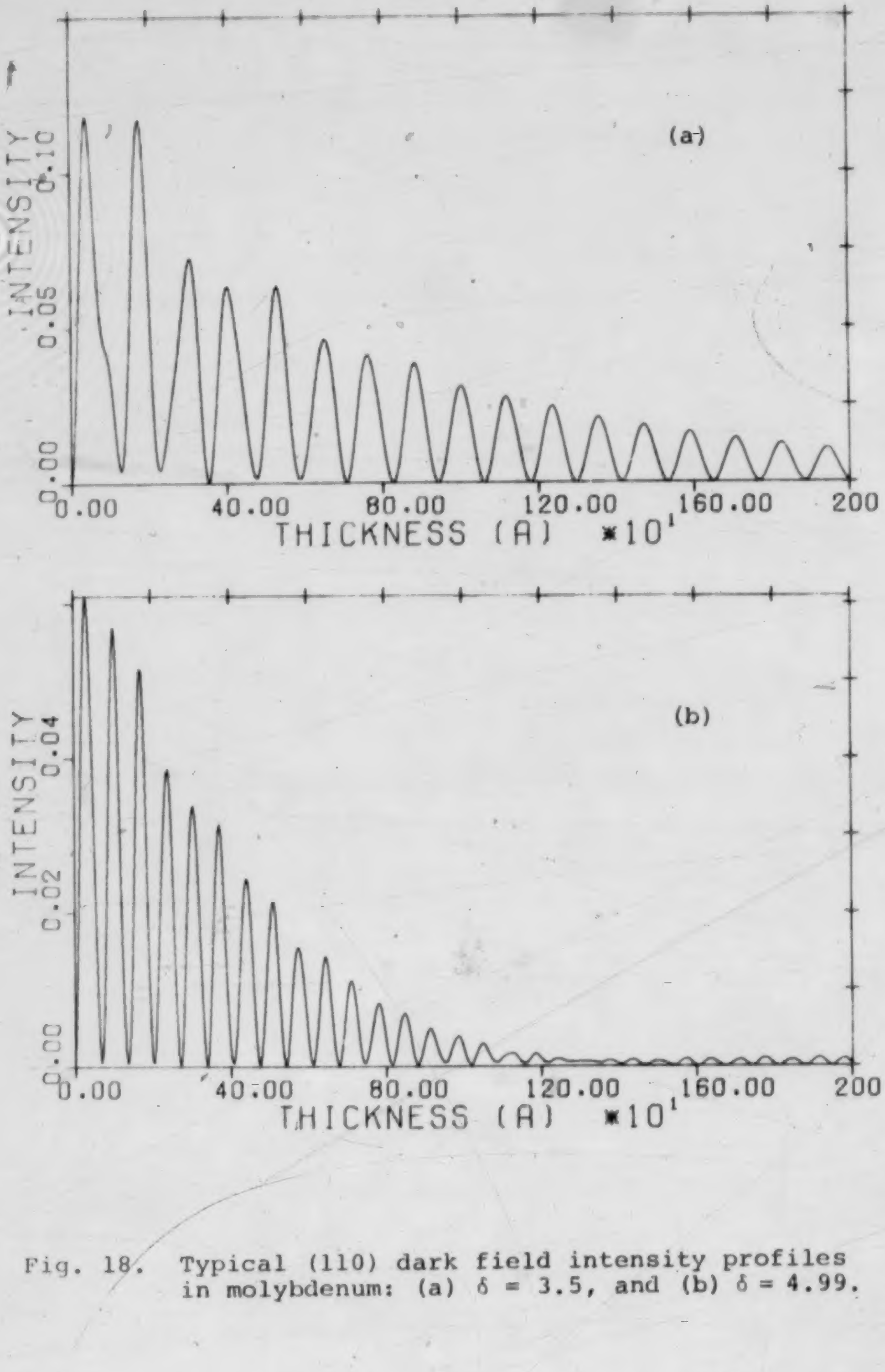

Fig. 18. Typical (110) dark field intensity profiles in molybdenum: (a) $\delta = 3.5$, and (b) $\delta = 4.99$.

that profiles of the type shown in Fig. 18(a) occurred for all values of δ except those close to 5.0 and 6.0.

As indicated in Section 5.1, the validity of the two-beam and kinematical theories will first be examined by comparing the extinction distances of the two analytical theories to the many-beam average extinction distance. The many-beam average extinction distance was first obtained for a thickness range of 0 to 1000 Å. This average extinction distance and the two-beam and kinematical extinction distances are shown in Fig. 19. It can be seen from this figure that the agreement between the three theories improves with increasing δ. Furthermore, the kinematical extinction distance is a considerably better approximation to the very nearly exact many-beam average extinction distance than is the two-beam extinction distance.

In order to examine how the many-beam average extinction distance changed with the thickness range considered, calculations were also performed for a thickness range of 0 to 1500 Å. The results are shown in Fig. 20. It can be seen that the many-beam average extinction distance shown in Fig. 20 is very similar to that shown in Fig. 19 except for values of δ close to 4.0, 5.0, and 6.0 where abrupt changes in the many-beam average extinction distance occur.

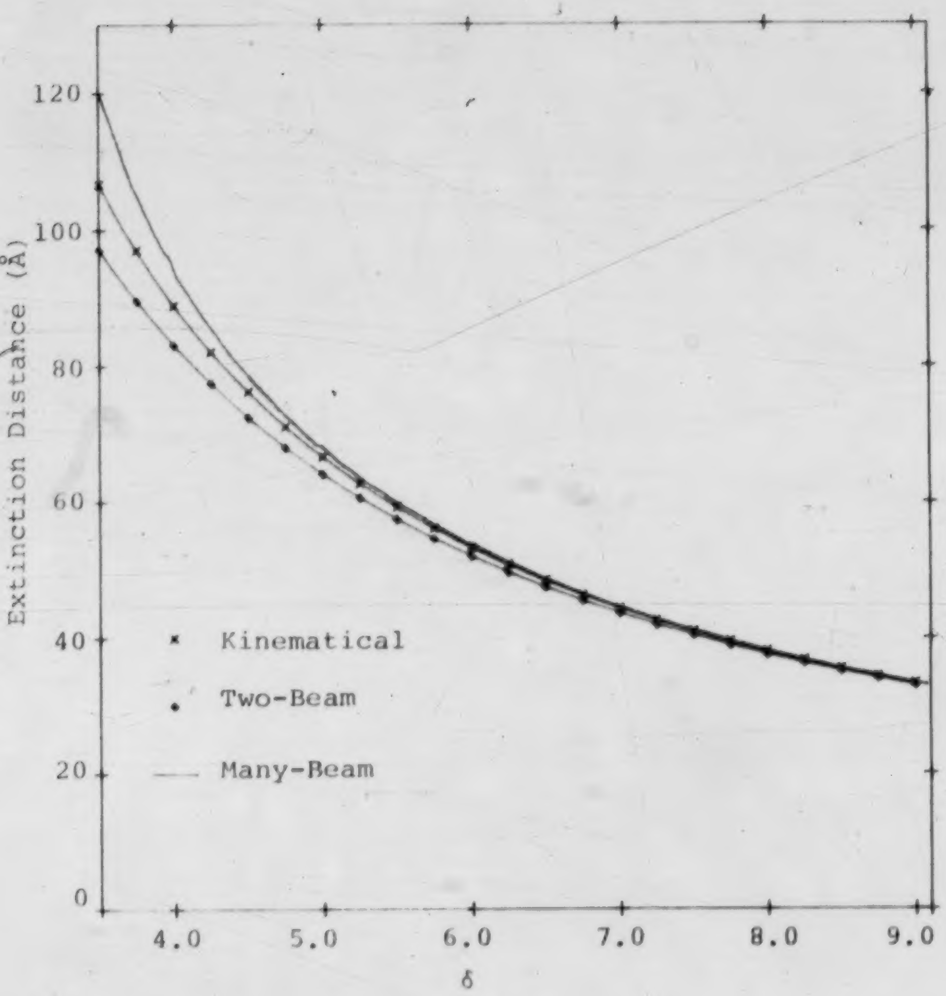

Fig. 19. The kinematical and two-beam extinction distances and the many-beam average extinction distance for the (110) dark field intensity in molybdenum. The many-beam average extinction distance was obtained for a thickness range of 0 to 1000 Å.

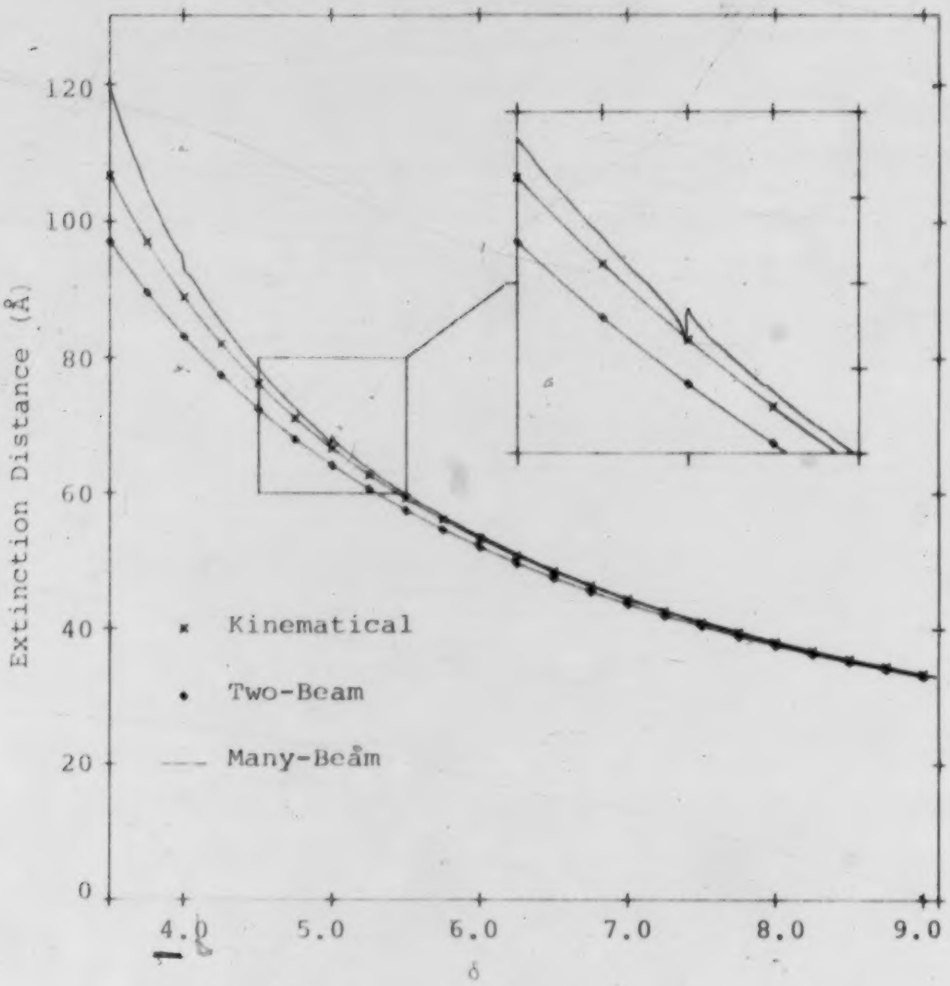

Fig. 20. The kinematical and two-beam extinction distances and the many-beam average extinction distance for the (110) dark field intensity in molybdenum. The many-beam average extinction distance was obtained for a thickness range of 0 to 1500 Å.

5.2.2 The Variation with Thickness of the Many-Beam Extinction Distance

As pointed out in Section 5.1, the results presented in the last section are of limited value for assessing the validity of the kinematical and two-beam theories because variations in extinction distance with thickness in the many-beam theory are averaged out. Since the analytical theories will be poor approximations if the variation in extinction distance is large, it is next of interest to examine this variation. The percentage variation in extinction distance was first obtained for the thickness range of 0 to 1000 Å. These results are shown in Fig. 21. It can be seen from this figure that there is a variation in the many-beam extinction distance of approximately 37% at $\delta = 3.5$. This variation then decreases rapidly with increasing δ to approximately 10% at $\delta = 4.8$. For values of $\delta > 4.8$ the variation decreases much more slowly to approximately 5% at $\delta = 9.0$.

In order to examine how the variation in extinction distance changes with the thickness range considered, calculations were performed for the thickness ranges 0 to 500 Å and 0 to 1500 Å. The percentage variation in extinction distance for the thickness range of 0 to 500 Å was very similar to that

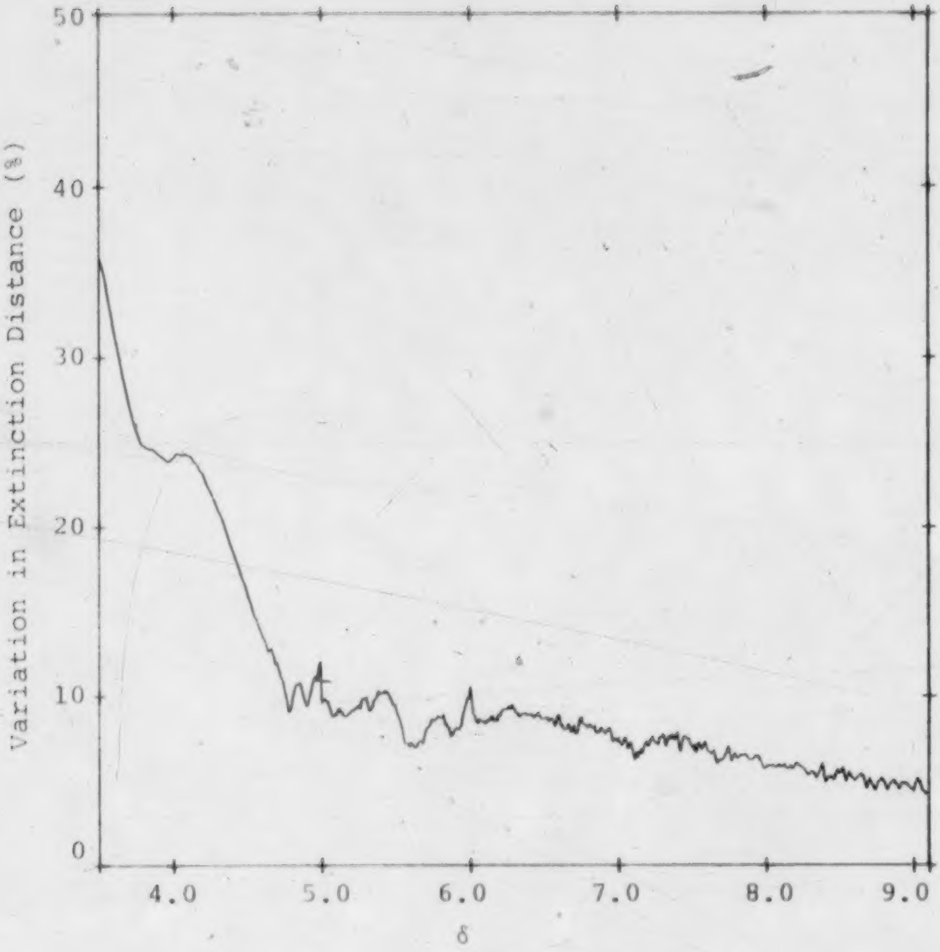

Fig. 21. The variation with thickness in the many-beam extinction distance for the (110) dark field intensity in molybdenum. The accelerating voltage used was 100 kV and a crystal thickness range of 0 to 1000 Å was considered.

shown in Fig. 21. The results obtained for the thickness range 0 to 1500 Å, on the other hand, are quite different and are shown in Fig. 22. It can be seen from this figure that large peaks occur for values of δ close to 5.0 and 6.0.

5.3 Analysis of the Results for the Systematic Case

The purpose of this section is to carry out an analysis of the results presented in Section 5.2. In this analysis, only the kinematical and many-beam theories will be compared. The reason for this can be seen from Fig. 19 which shows that, for large δ, there is good agreement between the kinematical and two-beam theories. This of course is a well-known result (see for example, Whelan, 1970) and occurs because the condition $|s_g 2K| >> |U_g|$ (see equation 3.18 of Section 3.4) is satisfied for large δ, i.e. large s_g. In comparing the kinematical and many-beam theories, the results for values of δ where a systematic reflection is close to its Bragg condition will be considered separately from results obtained when no systematic reflection is close to its Bragg condition. The reason for this is that the shapes of the intensity profiles obtained for these two cases are quite different (compare Figs. 18(a) and 18(b)).

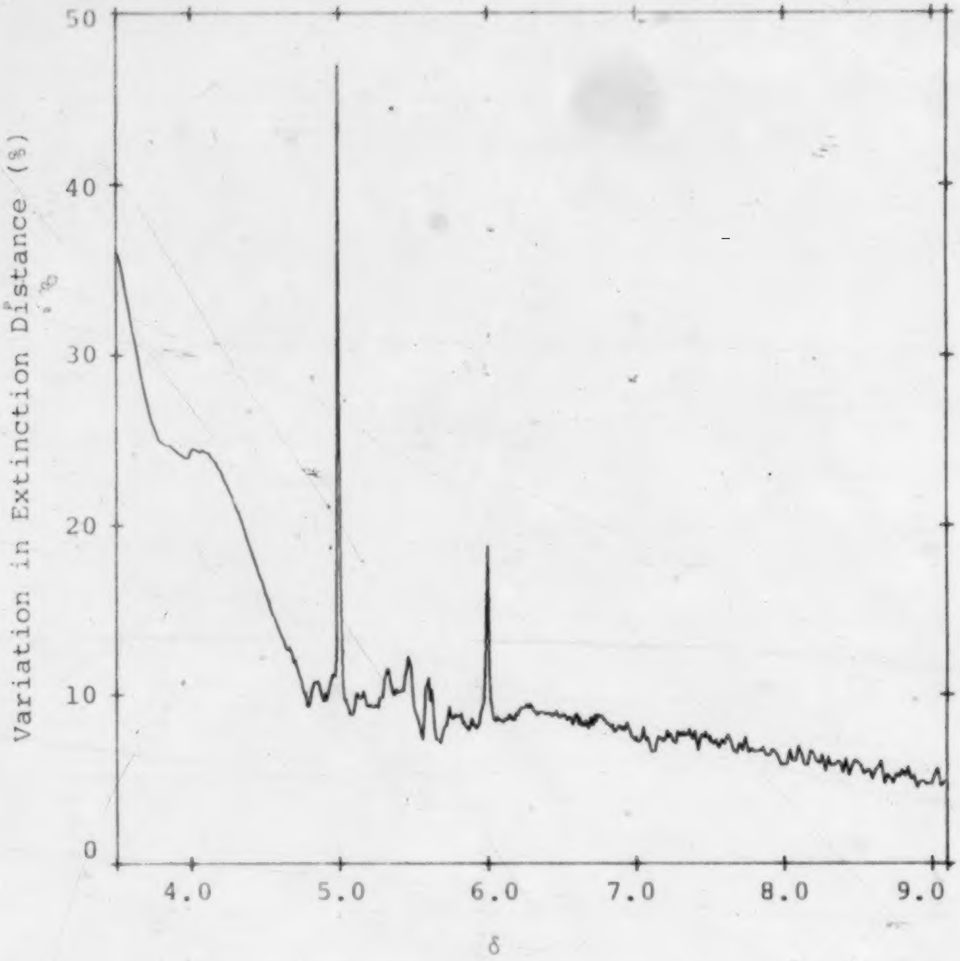

Fig. 22. The variation with thickness in the many-beam extinction distance for the (110) dark field intensity in molybdenum. A crystal thickness range of 0 to 1500 Å was considered.

5.3.1 An Analysis of the Results for Values of δ Where no Systematic Reflection is Close to its Bragg Condition

5.3.1(a) Numerical analysis of average extinction distance results

The results presented in Fig. 19 show that there is good agreement between the many-beam average extinction distance and the kinematical extinction distance when no systematic reflection is close to its Bragg condition. In order to explain this result, the number of primary and secondary Bloch waves in the many-beam calculation will be examined. (It should be noted that it is not the value of $C_o^{(i)}C_g^{(i)}$ but rather the value of $C_o^{(i)}C_g^{(i)}\exp(-2\pi q^{(i)}z)$ which determines the contribution made by Bloch wave i to the diffracted beam intensity at thickness z. It was found, however, that Bloch waves which were unimportant at thickness z were also unimportant at the top surface. Accordingly, a good indication of the number of primary and secondary Bloch waves could be obtained by examining the excitation amplitudes $C_o^{(i)}C_g^{(i)}$.) The magnitudes of the excitation amplitudes $C_o^{(i)}C_g^{(i)}$ for $\delta = 3.5$, 4.5, 5.5, 6.5, 7.5 and 8.5 are shown in Table 1. It should be noted that in this table the Bloch waves have been labelled using both the conventional method (see Section 2.1.1) and an alternate method referred to in

Table 1(a). The magnitudes of the Bloch wave excitation amplitudes $C_o^{(i)}C_g^{(i)}$ for the many-beam calculation discussed in the text. The primary Bloch waves are underlined. The Bloch waves have been labelled by using both the conventional scheme and the alternate K-sphere scheme described in Fig. 23.

$\delta = 3.5$			$\delta = 4.5$			$\delta = 5.5$		
Bloch Wave		$\lvert C_o^{(i)}C_g^{(i)}\rvert$	Bloch Wave		$\lvert C_o^{(i)}C_g^{(i)}\rvert$	Bloch Wave		$\lvert C_o^{(i)}C_g^{(i)}\rvert$
1	2g	.083	1	2g	.025	1	3g	.007
2	g	$\underline{.123}$	2	3g	.002	2	2g	.005
3	3g	.001	3	g	$\underline{.127}$	3	4g	.000
4	o	$\underline{.209}$	4	4g	.000	4	g	$\underline{.111}$
5	4g	.000	5	o	$\underline{.157}$	5	5g	.000
6	-g	.003	6	5g	.000	6	o	$\underline{.124}$
7	5g	.000	7	-g	.002	7	6g	.000

Table 1(b). The magnitudes of the Bloch wave excitation amplitudes $C_o^{(i)}C_g^{(i)}$ for the many-beam calculation discussed in the text. The primary Bloch waves are underlined. The Bloch waves have been labelled by using both the conventional method and the alternate K-sphere scheme described in Fig. 23.

$\delta = 6.5$			$\delta = 7.5$			$\delta = 8.5$		
Bloch Wave		$\lvert C_o^{(i)}C_g^{(i)}\rvert$	Bloch Wave		$\lvert C_o^{(i)}C_g^{(i)}\rvert$	Bloch Wave		$\lvert C_o^{(i)}C_g^{(i)}\rvert$
1	3g	.002	1	4g	.001	1	4g	.000
2	4g	.000	2	3g	.000	2	5g	.000
3	2g	.004	3	5g	.000	3	3g	.000
4	5g	.000	4	2g	.003	4	6g	.000
5	g	$\underline{.096}$	5	6g	.000	5	2g	.002
6	6g	.000	6	g	$\underline{.083}$	6	7g	.000
7	o	$\underline{.100}$	7	7g	.000	7	g	$\underline{.072}$
8	7g	.000	8	o	$\underline{.088}$	8	8g	.000
9	-g	.001	9	8g	.000	9	o	$\underline{.076}$
10	8g	.000	10	-g	.001	10	9g	.000

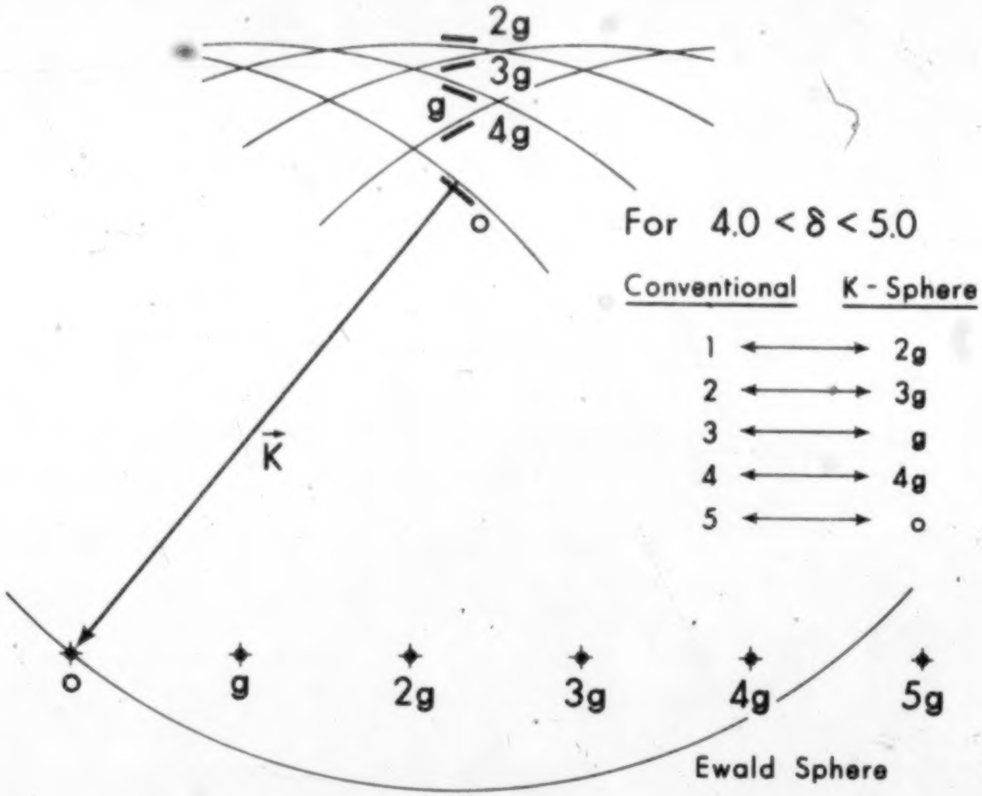

Fig. 23. The K-sphere scheme for labelling the branches of the dispersion surface. In this method, which is similar to a method used by Cockayne (1972), branch h of the dispersion surface is that branch which is closest to the sphere of radius K centered on the reciprocal lattice point h. For $4.0 < \delta < 5.0$ the relationship between the conventional method and the K-sphere method is shown. The relationship for a number of other values of δ can be obtained from Table 1. The K-sphere method does not apply when a systematic reflection is close to its Bragg condition.

this thesis as the K-sphere method (see Fig. 23). An analysis of Table 1 shows that two primary Bloch waves are excited in each case. In the conventional Bloch wave labelling scheme, these two primary Bloch waves are found to change when a high order systematic reflection passes through its Bragg condition. For example, the primary Bloch waves change from five and seven to six and eight as the value of δ passes through 7.0. The change occurs in such a manner, however, that the two primary Bloch waves are always labelled o and g in the K-sphere labelling scheme. The results obtained in Section 5.2.1 can now be explained by noting that the many-beam intensity profiles will be two-beam like in character (i.e. not complex) when there are only two primary Bloch waves. As indicated in Section 3.2.3, the average extinction distance for this two-beam like profile will very nearly be equal to the reciprocal of the separation between the two primary branches of the dispersion surface, i.e. the branches associated with the primary Bloch waves. It can be seen from Fig. 24 that these primary branches approach the spheres about o and g as δ increases. Since the reciprocal of the spacing between these spheres is the kinematical extinction distance, the agreement between the many-beam average

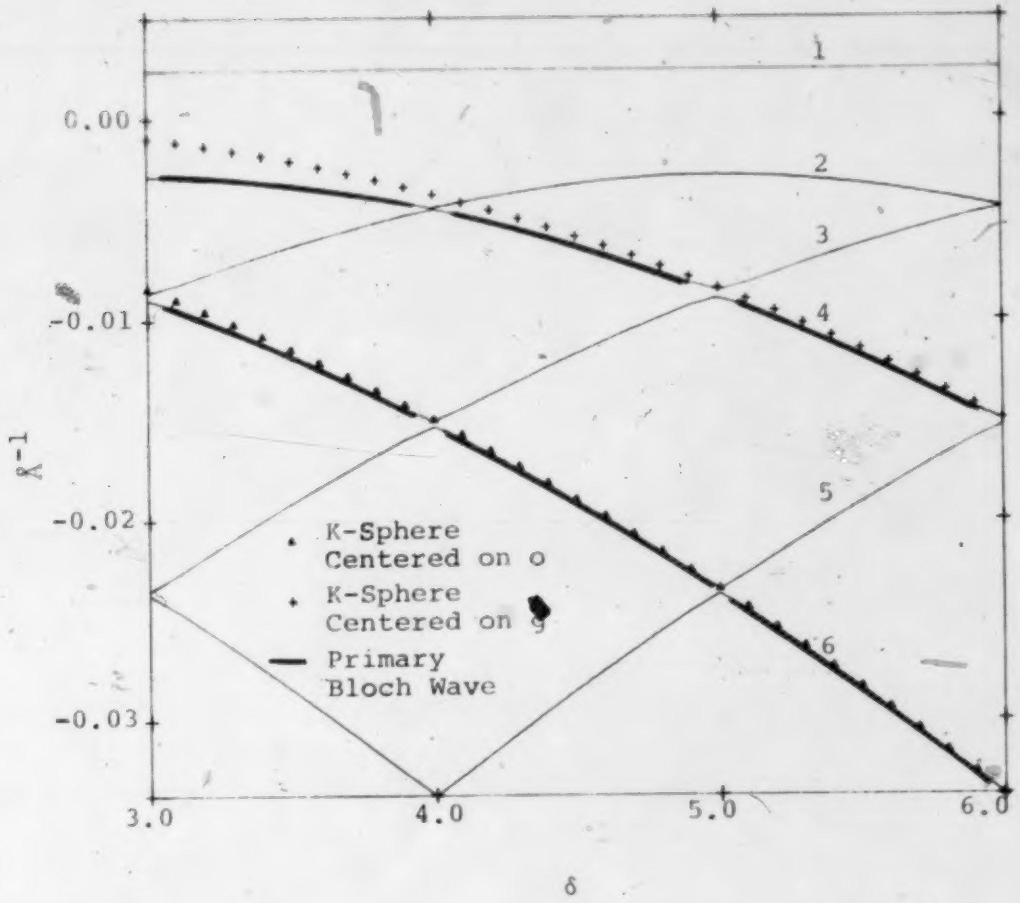

Fig. 24. A part of the many-beam dispersion surface for the systematic case. When a high order systematic reflection is not close to its Bragg condition, there are only two primary Bloch waves. These Bloch waves are associated with the dispersion surface branches closest to the spheres of radius K centered on o and g. When a high order systematic reflection passes through its Bragg condition, the primary Bloch waves in the conventional labelling scheme change as shown in the diagram.

extinction distance and the kinematical extinction distance improves with increasing δ.

5.3.1(b) Numerical analysis of the variation in extinction distance results

The variation in the many-beam extinction distance with thickness can also be explained by examining the magnitudes of the excitation amplitudes in Table 1. Although there are only two primary Bloch waves, several secondary Bloch waves are also excited. It can be seen from this table, for example, that the excitation amplitude of Bloch wave one is quite significant at $\delta = 3.5$ and that this excitation amplitude becomes progressively smaller with increasing δ. It was found that the percentage variation in extinction distance in Fig. 21 between values of δ of about 3.5 to 5.0 could be primarily attributed to this secondary Bloch wave. At higher values of δ, it was found that the variation in extinction distance could be attributed to secondary Bloch waves labelled 2g, -g and 3g in the K-sphere labelling scheme. Of these, Bloch wave 2g was usually the most important (see Table 1).

5.3.1(c) Analytical examination of the primary and secondary Bloch waves

The approach just presented successfully explains, from a numerical point of view, how many-beam effects arise in the case where no systematic reflection is close to its Bragg condition. However, further insight into how these many-beam effects arise can be obtained by deriving analytical expressions for the excitation coefficients of the primary and secondary Bloch waves. Since exact expressions for the eigenvalues and eigenvectors of a large $\underline{A}$ matrix cannot be obtained, an approximate approach based on the methods of matrix diagonalization outlined in Appendix A will be considered.

If the procedure given in Appendix A is used to diagonalize the many-beam $\underline{A}$ matrix, then the eigenvalues correct to first order are simply the elements on the diagonal of $\underline{A}$, i.e.

$$\gamma^{(o)} = 0, \quad \gamma^{(g)} = s_g \quad \ldots \quad \gamma^{(h)} = s_h \,. \qquad (5.1)$$

(In this approximate method for diagonalizing the $\underline{A}$ matrix, the eigenvalues and corresponding eigenvectors are labelled according to the K-sphere labelling scheme.) The eigenvalues of the $\underline{A}$ matrix correct to second order can be found from equation A.14 to be

$$\gamma^{(h)} = s_h - \sum_{g \neq h} \frac{(U_{g-h})^2}{(2K)^2(s_g - s_h)} \quad . \qquad (5.2)$$

As indicated in Appendix A, these second order eigenvalues will be a good approximation if the correction terms in the summation of equation 5.2 are small compared to s_h. Similarly, the orthogonal matrix of eigenvectors $\underline{C}$, correct to first order, can be calculated from equations A.9 and A.12. This matrix of eigenvectors, given in Table 2, will be a good approximation if the off-diagonal elements are small compared to the diagonal elements, i.e.

$$|2K(s_g - s_h)| >> |U_{g-h}| \ , \qquad (g \neq h) \ . \qquad (5.3)$$

Since the terms U_{g-h} are non-zero, the approximate expressions of equations 5.2 and Table 2 will break down if s_g approaches s_h $(g \neq h)$. For the systematic case, this can only occur if a systematic reflection is in its Bragg condition (see Fig. 25). The approximate eigenvalue and eigenvector expressions of equation 5.2 and Table 2 can therefore only be good approximations if no reflection is close to its Bragg condition.

It is next of interest to deduce which Bloch waves will be the primary Bloch waves. This can be done by comparing the magnitudes of the Bloch wave

Table 2. The first order approximation to the many-beam eigenvector matrix $\underline{C}$.

$$\underline{C} = \begin{bmatrix} C_o^{(o)} & C_o^{(g)} & C_o^{(2g)} & C_o^{(-g)} & C_o^{(3g)} & \cdots & C_o^{(h)} \\ C_g^{(o)} & C_g^{(g)} & C_g^{(2g)} & C_g^{(-g)} & C_g^{(3g)} & \cdots & C_g^{(h)} \\ \cdots & \cdots & \cdots & \cdots & \cdots & \cdots & \cdots \end{bmatrix}$$

$$\underline{C} = \begin{bmatrix} 1 & \frac{U_{-g}}{2Ks_g} & \frac{U_{-2g}}{2Ks_{2g}} & \frac{U_g}{2Ks_{-g}} & \frac{U_{-3g}}{2Ks_{3g}} & \cdots & \frac{U_{-h}}{2Ks_h} \\ \frac{-U_g}{2Ks_g} & 1 & \frac{-U_{-g}}{2K(s_g-s_{2g})} & \frac{-U_{2g}}{2K(s_g-s_{-g})} & \frac{-U_{-2g}}{2K(s_g-s_{3g})} & \cdots & \frac{-U_{g-h}}{2K(s_g-s_h)} \\ \cdots & \cdots & \cdots & \cdots & \cdots & \cdots & \cdots \end{bmatrix}$$

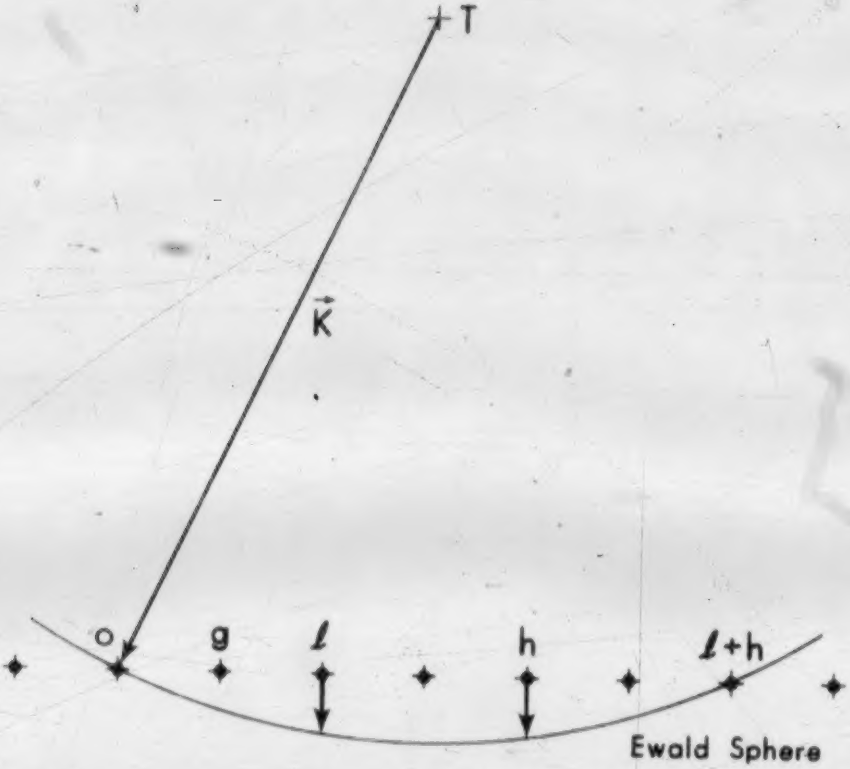

Fig. 25. The conditions under which the s-values of two different systematic reflections are equal. The s-value s_ℓ for any reflection ℓ will be equal to the s-value s_h for any other systematic reflection h only if the reflection ℓ+h is in its Bragg condition.

excitation amplitudes $C_o^{(h)}C_g^{(h)}$ obtained from the values of $C_o^{(h)}$ and $C_g^{(h)}$ given in Table 2. In assessing the relative magnitudes of the excitation amplitudes $C_o^{(h)}C_g^{(h)}$, it is important to note that the numerators of the terms $C_o^{(h)}$ and $C_g^{(h)}$ decrease rapidly in magnitude as $|\vec{h}|$ increases (see Fig. 16). This has been found to be the controlling factor in determining the relative magnitudes of the excitation amplitudes $C_o^{(h)}C_g^{(h)}$ (see Appendix B). The excitation amplitudes of high order Bloch waves (i.e. Bloch waves which in the K-sphere labelling scheme have a large $|\vec{h}|$) therefore tend to be smaller in magnitude than the excitation amplitudes of lower order Bloch waves. Since the magnitudes of the off-diagonal elements of the $\underline{C}$ matrix in Table 2 are much less than one (see Appendix B) while $C_o^{(o)} = C_g^{(g)} = 1$, the excitation amplitudes of Bloch waves o and g will be considerably larger in magnitude than the excitation amplitudes of the remaining Bloch waves. Bloch waves o and g are therefore primary Bloch waves. Since the magnitudes of the remaining excitation amplitudes decrease with increasing $|\vec{h}|$, the most important secondary Bloch waves are the low order Bloch waves such as 2g, -g and 3g. This is in agreement with the results presented in Table 1.

5.3.1(d) Analytical methods for comparing the kinematical extinction distance and the many-beam average extinction distance

It can be seen from Fig. 19 that the agreement between the kinematical extinction distance and the many-beam average extinction distance improves with increasing δ. This result can be explained by examining the first and second order eigenvalues of equations 5.1 and 5.2. Since there are only two primary Bloch waves o and g, the approximate value of the many-beam average extinction distance will be given by $1/|\gamma^{(o)}-\gamma^{(g)}|$. It can be seen from equation 5.2 that the magnitude of the second order correction to the eigenvalue $\gamma^{(o)}$ will depend on terms of the type

$$\sum_{h\neq o} - \frac{(U_{-h})^2}{(2K)^2 s_h} \quad . \qquad (5.4a)$$

Similarly, the second order corrections to the eigenvalue $\gamma^{(g)}$ are of the type

$$\sum_{h\neq g} \frac{(U_{g-h})^2}{(2K)^2 (s_g - s_h)} \quad . \qquad (5.4b)$$

On the other hand, if the eigenvalues correct to first order (equation 5.1) are used to obtain the extinction distance $1/|\gamma^{(o)} - \gamma^{(g)}|$, then the kinematical extinction distance $1/s_g$ is obtained. The difference between the many-beam average extinction distance and the kinematical extinction distance can therefore be seen by examining the magnitudes of the correction terms 5.4a and 5.4b. In examining the magnitude of these terms, it is important to note that the terms $(U_{-h})^2$ and $(U_{g-h})^2$ in the numerators decrease rapidly in magnitude with increasing $|\vec{h}|$. This has been found to be the controlling factor in determining the magnitude of the second order correction terms 5.4a and 5.4b. Because of this, the higher order terms are much less important and therefore can be neglected. The magnitude of the second order correction terms can therefore be examined by considering only terms of low order. However, the magnitude of these low order terms decreases with increasing δ because the denominators increase in magnitude (see Fig. 26). Accordingly, the many-beam average extinction distance and the kinematical extinction distance must approach one another with increasing δ, in agreement with the results presented in Fig. 19.

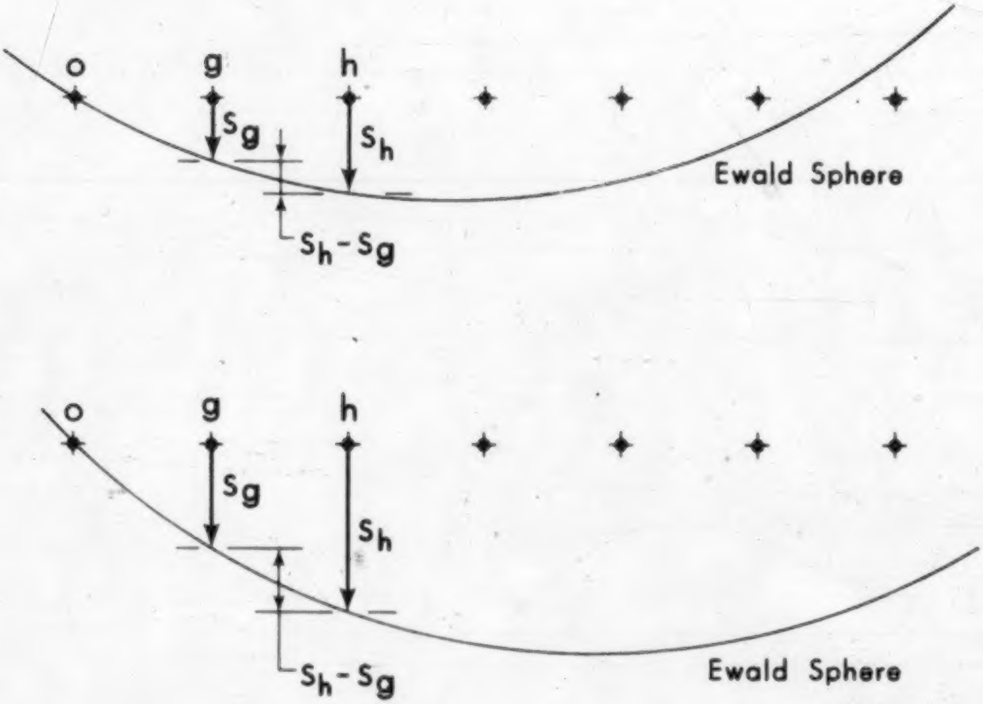

Fig. 26. A geometrical construction showing that, for large δ and a low order reflection h, the values s_h and $s_h - s_g$ increase with increasing δ.

5.3.2 Analysis of the Results for Orientations where a High Order Systematic Reflection is Close to its Bragg Condition

5.3.2(a) Numerical approach

The many-beam calculations of Section 5.2 showed that the variation in the extinction distance with thickness increased for values of δ close to the Bragg condition of a high order systematic reflection. In order to see how this effect arises, the excitation amplitudes $C_o^{(i)}C_g^{(i)}$ have been examined for orientations close to the Bragg condition of a high order systematic reflection. The results for $\delta = 4.97$, $\delta = 5.0$ and $\delta = 5.03$, given in Table 3, are typical of those obtained. It should be noted that the conventional Bloch wave labelling scheme is used. It can be seen from this table that as the value of δ passes through 5.0, the magnitudes of the excitation amplitudes of Bloch waves three and five decrease while those of four and six increase. For $\delta = 5.0$ it can be seen that all four Bloch wave excitation amplitudes are approximately of the same magnitude.

Because there are four primary Bloch waves for $\delta \approx 5.0$, the diffracted beam intensity can be written to a good approximation as

$$\phi_g = \sum_{i=3}^{6} D_i \exp(2\pi i\gamma^{(i)}z) \qquad (5.5)$$

Table 3. Typical Bloch wave excitation amplitudes for values of δ close to the Bragg condition of a high order systematic reflection. The primary Bloch waves are underlined.

$\delta = 4.97$		$\delta = 5.0$		$\delta = 5.03$	
Bloch Wave	$C_o^{(i)}C_g^{(i)}$	Bloch Wave	$C_o^{(i)}C_g^{(i)}$	Bloch Wave	$C_o^{(i)}C_g^{(i)}$
1	.041	1	.014	1	.013
2	.004	2	.004	2	.004
3	.101	3	.061	3	.021
4	.019	4	.058	4	.097
5	-.137	5	-.076	5	-.008
6	-.003	6	-.062	6	-.130
7	.002	7	.001	7	.000
8	-.000	8	.000	8	.002

where $D_i = C_o^{(i)} C_g^{(i)}$ and absorption has been neglected. The dispersion surface branches for these four primary Bloch waves are shown in Fig. 27. It can be seen from this figure that for δ close to 5.0, the eigenvalues of Bloch waves three and four differ by an amount equal to $\gamma^{(4)} - \gamma^{(3)} = c$. Since the terms D_3 and D_4 are of the same sign (see Table 3), these two Bloch waves will be in phase at the top surface of the crystal. Therefore, the contributions made by these Bloch waves to the diffracted beam amplitude will be out of phase at a thickness given by $z = |1/(2c)|$. Similar arguments can be used to show that Bloch waves five and six will be out of phase at a thickness $z = |1/(2d)|$ where $d = \gamma^{(6)} - \gamma^{(5)}$. However it can be seen from Fig. 27 that $d \approx c/2$. For the purposes of the qualitative argument to be presented here, it will therefore be assumed that Bloch waves five and six are in phase at a thickness $|1/(2c)|$.

Equation 5.5 can then be written

$$\phi_g = D'\exp(2\pi i\gamma^{(3)}z) + (D_5+D_6)\exp(2\pi i\gamma^{(5)}z) \qquad (5.6)$$

where

$$D' = D_3 + D_4\exp(2\pi icz) \ .$$

If it is assumed that $D_3 = D_4 = -D_5 = -D_6$ (this is very nearly the case as can be seen from Table 3),

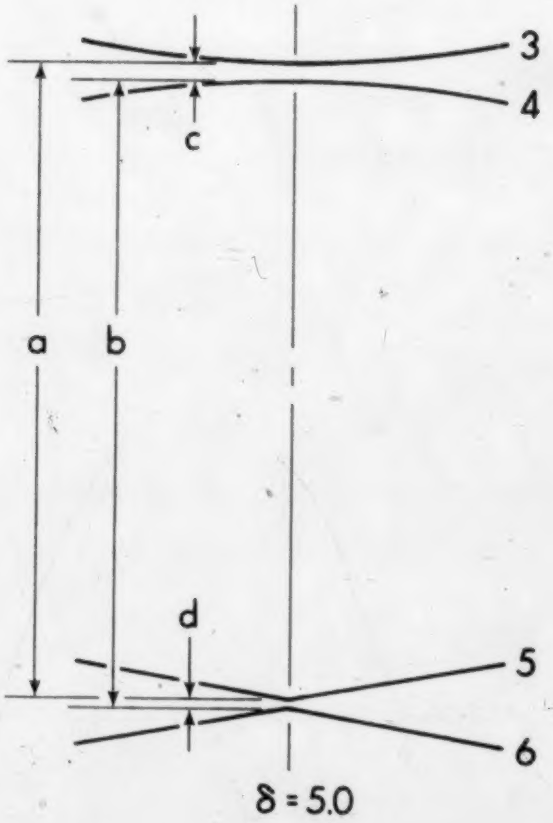

Fig. 27. A plot of a portion of the many-beam dispersion surface in the systematic case when the reflection 5g is close to its Bragg condition.

then the term D' will decrease in magnitude with increasing z and become very small for thicknesses close to $|1/(2c)|$. For thicknesses close to $|1/(2c)|$ the form of the intensity profile will be similar to that obtained when one primary Bloch wave (corresponding to the D_5+D_6 term) and other secondary Bloch waves (corresponding to the D' term and secondary Bloch waves such as 2g in the K-sphere labelling scheme) are excited. The beating between the primary Bloch wave and the secondary Bloch waves leads to a large variation in the extinction distance for thicknesses close to $|1/(2c)|$ as was in fact seen in Fig.18(b). A complex region was also observed in the diffracted beam intensity profiles close to $\delta = 6.0$ for reasons similar to those given above.

For values of δ close to 7.0, 8.0, and 9.0 complexity was not observed in the range of crystal thickness considered. The reason for this is that at these values of δ the separation c is considerably smaller than at $\delta = 5.0$ or $\delta = 6.0$. Therefore, the thickness at which complexity would occur is considerably larger. At these large thicknesses, the diffracted beam intensity is very small and this complexity is not significant.

5.3.2(b) Analytical approach

It is next of interest to examine the reason why more than two primary Bloch waves are excited for δ close to the Bragg condition of a high order systematic reflection. This can be seen by examining the magnitudes of the Bloch wave excitation amplitudes $C_o^{(h)} C_g^{(h)}$ obtained from the first order $\underline{C}$ matrix of Table 2. If a high order systematic reflection h approaches its Bragg condition, i.e. s_h approaches zero, then it can be seen from the $\underline{C}$ matrix in Table 2 that the term

$$C_o^{(h)} = \frac{U_{-h}}{2Ks_h} \tag{5.7}$$

becomes very large. In addition, the term

$$C_g^{(h-g)} = \frac{-U_h}{2K(s_g - s_{h-g})} \tag{5.8}$$

also becomes very large because s_g approaches s_{h-g} (see Fig. 25). Accordingly, Bloch waves h and h-g will become primary Bloch waves. Furthermore, the excitation amplitudes of all other secondary Bloch waves remain small. Clearly, therefore, for values of δ close to the Bragg condition of a high order systematic reflection, the four primary Bloch waves o, g, h-g, and h will be excited.

It should be noted that the above analysis shows that a high order systematic reflection h can have a significant effect on the intensity I_g in a perfect crystal when $s_h \approx o$ and when $s_h \approx s_g$. (Cockayne (1972) has previously used arguments similar to those just presented in order to show that, in the systematic case, these conditions should be avoided if weak-beam diffraction conditions are to be obtained.) In the systematic case, these two conditions reduce to the one condition that no systematic reflection should be close to its Bragg condition. However, it will be seen in the next section that these two conditions do not reduce to one in the non-systematic case, and therefore both conditions are important.

5.4 The Effect of Non-Systematic Reflections on Many-Beam Effects

In the many-beam calculations presented in Section 5.2, only systematic reflections were taken into account. In order to examine the role which non-systematic reflections play in many-beam effects, calculations including these reflections were also carried out. The results of these calculations will be presented and discussed in this section.

5.4.1 The Results of the Calculations which Included Non-Systematic Reflections

The calculations taking non-systematic reflections into account were carried out for the (110) dark field intensity in molybdenum. The crystal orientations which were considered are indicated in Fig. 28. The accelerating voltage used was 100 kV and the fifty most important reflections were included using Cann's criterion of equation 3.2 (Cann, 1973). An example of the variation in the extinction distance which was found for the thickness range 0 to 1500 Å is shown in Fig. 29. The crystal orientations considered in this figure were obtained by incrementing the point L from (3.25, 3.25, 4) to (3.25, 3.25, 7) (see Fig. 28). It can be seen from Fig. 29 that there is a variation in the extinction distance of at least 7% from all orientations and that there are many peaks present in the curve. As the thickness range used in calculating the percentage variation in extinction distance was increased, additional peaks were found. These peaks indicate that there are many orientations at which complexity is obtained. In the cases where no complexity was found, a many-beam average extinction distance was obtained. This average extinction distance was found to be within one or two percent of the kinematical extinction distance.

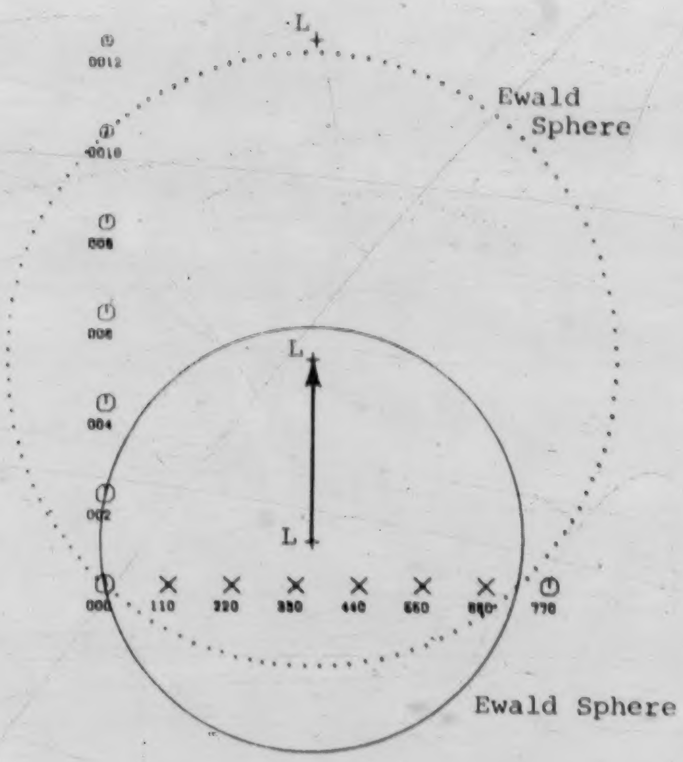

Fig. 28. A diffraction pattern indicating the crystal orientations considered in the calculations which took non-systematic reflections into account. The projection of the tie-point L was initially specified to have the coordinates (3.25,3.25,1). This coordinate was then incremented by (0,0,0.01) until a final coordinate of (3.25,3.25,12) was obtained.

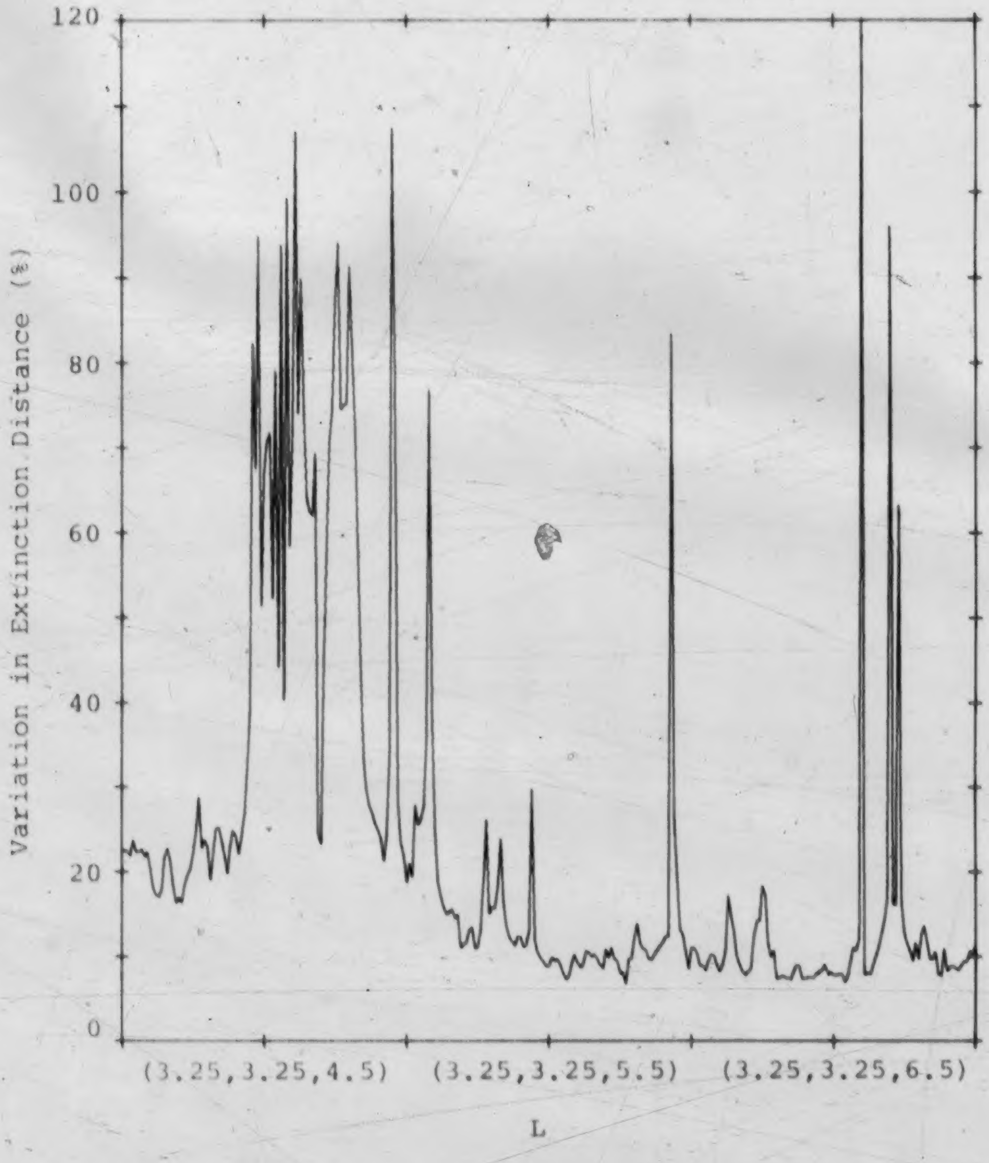

Fig. 29. The percentage variation in extinction distance for the (110) intensity in molybdenum when non-systematic reflections are taken into account. The crystal orientation is indicated by the coordinates of the projection of the tie-point (see Fig. 28). A crystal thickness range of 0 to 1500 Å was considered.

5.4.2 An Analysis of the Results for the Non-Systematic Case

An analysis of the results of Section 5.4.1 showed that complex profiles were obtained when more than two primary Bloch waves were excited. The additional primary Bloch waves were found to be excited for crystal orientations where a non-systematic reflection had a value of s_h close to zero or s_g. The reason why additional primary Bloch waves are excited at these orientations can be understood by examining the expression for the excitation amplitude

$$C_o^{(h)} C_g^{(h)} = - \frac{U_{-h} U_{g-h}}{(2K)^2 s_h (s_g - s_h)} \qquad (5.9)$$

for Bloch wave h obtained from the $\underline{C}$ matrix in Table 2. It can be seen from equation 5.9 that the excitation amplitude of Bloch wave h will become large as the value of s_h approaches zero or s_g. As a result, there will be three primary Bloch waves o, g, and h at these orientations and this results in a complex intensity profile.

In examining the reasons for the complexity in the intensity profiles, it was found that the effect of a non-systematic reflection h decreased as its order increased. The reason for this can be seen from equation 5.9. This equation shows that, for a particular value of s_h, the denominators will be constant and the numerators will be larger for the lower order Bloch wave. Accordingly, the excitation amplitude $C_o^{(h)}C_g^{(h)}$ will be larger in magnitude for lower order reflections.

The result that, when s_g is large, many-beam effects are important for $s_h \simeq 0$ or s_g is in agreement with the results reported by Cann and Sheinin (1974A, 1974B). These authors found that when the first order reflection g is close to its Bragg condition, the dark field intensity profile g becomes complex when a non-systematic reflection has an s-value close to one of the eigenvalues of a two-beam calculation including the reflections o and g. It can be seen from the expression for the two-beam eigenvalues given in equation 3.5 that, for large s_g, this condition reduces to the condition given in the previous paragraph.

The fact that a non-systematic reflection can be important for values of s_h close to zero or s_g is of significance in experimental observations of lattice defects under weak-beam diffraction conditions. Under these diffraction conditions it is desirable in most instances to avoid many-beam effects (Cockayne, 1972). It has been assumed in the literature that the effect of a non-systematic reflection can be avoided if these reflections are far from their Bragg conditions. The results presented in this thesis show that the effects of a non-systematic reflection can also be large if $s_h = s_g$. Therefore, this condition should also be avoided if weak-beam diffraction conditions are to be obtained. Since the value of s_g is large under weak-beam conditions, this means that non-systematic reflections can have a marked effect even though they are far from their Bragg conditions.

The results discussed above also show that in theoretical calculations of weak-beam contrast it is necessary to take all reflections into account which have s_h values close to zero or s_g. Since this fact is not reflected in Cann's strong-beam criterion of equation 3.2, an improved criterion needs to be developed.

5.5 The Effect of Atomic Number, Accelerating Voltage, and the Order of the Systematic Row on Many-Beam Effects

In the last three sections, the dependence of many-beam effects on the deviation parameter δ was examined. These many-beam effects were found to depend on the magnitudes of the excitation amplitudes of the primary Bloch waves

$$C_o^{(g)} C_g^{(g)} = -C_o^{(o)} C_g^{(o)} = -\frac{U_{-g}}{\tau_o^2 - \tau_g^2} \qquad (5.10)$$

relative to the excitation amplitudes of the secondary Bloch waves

$$C_o^{(h)} C_g^{(h)} = \frac{U_{-h} U_{g-h}}{(\tau_o^2 - \tau_h^2)(\tau_g^2 - \tau_h^2)} \quad . \tag{5.11}$$

(In order to simplify the analysis to be carried out in this section, the t-values of equation 4.8 will be used for the diagonal elements of the $\underline{A}$ matrix. When the eigenvector matrix $\underline{C}$ is calculated correct to first order, the primary and secondary excitation amplitudes are given by equations 5.10 and 5.11. In these equations, τ_h is the distance from the projection of the tie-point onto the systematic row to the reflection h. See Fig. 14.) The importance of many-beam effects was also found to depend on the magnitude of the second order corrections for the many-beam eigenvalues $\gamma^{(o)}$ and $\gamma^{(g)}$. The magnitude of these correction terms determines the difference between the many-beam average extinction distance, correct to second order, and the kinematical extinction distance which is obtained from the first order approximations for $\gamma^{(o)}$ and $\gamma^{(g)}$. Using the t-method, the second order correction terms 5.4 are of the form

$$\frac{-(U_{-h})^2}{2K(\tau_o^2-\tau_h^2)} \quad \text{and} \quad \frac{-(U_{g-h})^2}{2K(\tau_g^2-\tau_h^2)} \quad . \tag{5.12}$$

It will be shown in this section that the magnitudes of the excitation amplitudes of equations 5.10 and 5.11 and the magnitudes of the eigenvalue correction terms 5.12 depend on atomic number, the accelerating voltage and the order of the systematic row.

5.5.1 The Effect of Atomic Number on Many-Beam Effects

In this section, the effect of atomic number on the Bloch wave excitation amplitudes of equations 5.10 and 5.11 and on the eigenvalue correction terms 5.12 will be considered. As materials of higher atomic number are considered, the scattering factors used to calculate the Fourier coefficients U_h in equation 4.4 will increase (see Hirsch et al., 1965). If two materials of the same crystal structure and nearly equal lattice parameters are compared, values of U_h of the higher atomic number material will tend to be larger than the corresponding values for the lower atomic number material (see Fig. 16). Since the lattice parameters are similar for the two cases, the corresponding t-values will be nearly equal. For a particular accelerating voltage, this means that the magnitude of the excitation amplitudes of the secondary Bloch waves (equation 5.10) and those of the primary Bloch waves (equation 5.11) will both increase with atomic number.

However, if the terms U_{-h} and U_{g-h} of equation 5.11 and the single term U_{-g} in equation 5.10 all increase by approximately the same factor, then the secondary Bloch waves will become relatively more important. This should lead to an increased variation in the extinction distance in the higher atomic number material. Furthermore, the correction terms 5.12 for the many-beam eigenvalues will also be larger for the higher atomic number material. This should lead therefore to a greater difference between the many-beam average extinction distance and the kinematical extinction distance for higher atomic number materials.

In order to see if these effects do in fact occur, calculations were carried out for the high and low atomic number materials gold and aluminum. These materials are both face centered cubic in structure and have lattice parameters which are very nearly equal. The accelerating voltage used in this calculation was 100 kV and sixteen reflections of the (111) systematic row were considered. The percentage variation in the extinction distance for the (111) dark field intensity was obtained for crystals twenty extinction distances thick. The results are shown in Table 4 for $\delta = 6.5$, $\delta = 7.5$ and $\delta = 8.5$. It can be seen from this table that there is a

Table 4. A comparison of many-beam effects in materials of high and low atomic number.

Material	% variation in extinction distance			% difference between the many-beam average extinction distance and the kinematical extinction distance at $\delta = 6.5$
	$\delta = 6.5$	$\delta = 7.5$	$\delta = 8.5$	
Gold	15.4	13.0	9.6	1.0
Aluminum	3.4	3.0	2.1	0.1

considerable increase in the variation of the extinction distance with thickness for the higher atomic number material. The percentage difference between the many-beam average extinction distance and the kinematical extinction distance was also found to be larger for higher atomic number materials as shown in Table 4. Clearly, these results indicate that many-beam effects increase markedly in materials of high atomic number and therefore the kinematical theory becomes a poorer approximation.

5.5.2 The Effect of Changes in the Accelerating Voltage on Many-Beam Effects

It is next of interest to examine how the excitation amplitudes of the primary and secondary Bloch waves (equations 5.11 and 5.10) and the second order corrections to the eigenvalues (terms 5.12) change as the accelerating voltage is changed. As the accelerating voltage is increased, the magnitude of U_h increases because the relativistic correction term β used in calculating this term increases (see equation 4.15). The numerators of the excitation amplitudes of equations 5.10 and 5.11 therefore increase as the accelerating voltage is increased, while the denominators of these terms remain constant.

(It should be noted that if s-values are used for the diagonal of the $\underline{A}$ matrix, it is not clear how the denominators $2Ks_h(s_g-s_h)$ of the excitation amplitudes change with accelerating voltage since both the s-values and K change. The t-values rather than the s-values were used in equations 5.10, 5.11 and 5.12 in order to overcome this problem.) Since all the terms U_{-h} increase by the same factor β, the excitation amplitudes of the secondary Bloch waves will increase with respect to those of the primary Bloch waves o and g by a factor β. Accordingly, the variation in extinction distance should increase with an increase in the accelerating voltage.

The effect of increases in the accelerating voltage on the many-beam average extinction distance can be seen by examining the first and second order approximations for the eigenvalues of the two primary Bloch waves. When the t-method is used to calculate the first order approximation to the many-beam eigenvalues, the difference between the eigenvalues of the two primary Bloch waves o and g is found to be $|\tau_o^2-\tau_g^2|/(2K)$. (This is simply the difference between the elements t_o and t_g on the diagonal of the $\underline{A}$ matrix and is equal to the reciprocal of the kinematical extinction distance.) As the accelerating voltage increases, the quantity $|\tau_o^2-\tau_g^2|/(2K)$ changes by a factor of 1/K. The second order corrections to the eigenvalues of the primary Bloch waves o and g also change by a factor 1/K. However, in addition, the numerators of these terms increase because the terms U_{-h} increase. Therefore, the correction terms become more significant for higher accelerating voltages. Accordingly, the percentage difference between the many-beam average extinction distance and the kinematical extinction distance should increase as the accelerating voltage increases.

In order to see if these effects do in fact occur, calculations were carried out for the (110) dark field intensity in molybdenum. The results for accelerating voltages of 100 kV and 1000 kV are shown in Table 5. Sixteen reflections of the (110) systematic row were included and the calculations were carried out for $\delta = 6.5$, 7.5 and 8.5. The variation in extinction distance and the many-beam average extinction distance were obtained for crystals twenty extinction distances thick. It can be seen from Table 5 that there is a considerable increase in the variation of the extinction distance as the accelerating voltage is increased. It can also be seen from Table 5 that the percentage difference between the many-beam average extinction distance and the kinematical extinction distance increases

Table 5. The effect of changes in the accelerating voltage on many-beam effects in molybdenum.

kV	% variation in the extinction distance			% difference between the many-beam average extinction distance and the kinematical extinction distance at $\delta = 6.5$
	$\delta = 6.5$	$\delta = 7.5$	$\delta = 8.5$	
100	8.9	6.9	5.1	0.4
1000	20.1	15.9	8.5	1.8

with accelerating voltage. Clearly then, these results show that many-beam effects also increase markedly with accelerating voltage and as a result the kinematical theory becomes a poorer approximation.

In order to examine the role of the relativistic correction term β, calculations were also carried out in which no relativistic mass correction was applied to the terms U_{g-h} (i.e., $\beta = 1.0$). These results are shown in Table 6. It can be seen from this table that there is good agreement between the results obtained using the different accelerating voltages. This result is of interest since the increase in many-beam effects with voltage has been studied by many authors (see for example Goringe et al., 1966; Howie, 1966, 1970; Fukuhara, 1966; and Botros and Sheinin, 1974). These results have been attributed to the relativistic increase in the U's as well as an increase in the radius of the Ewald sphere. However, the results presented above show that the increase in many-beam effects which occurs with accelerating voltage is purely a relativistic effect. The fact that the radius of the Ewald sphere does not have an influence on many-beam effects is a general result first pointed out by Uyeda (1968) and can be seen by examining the $\underline{A}$ matrix when the t-values are used for the diagonal elements.

Table 6. The effect of changes in the accelerating voltage on many-beam effects in molybdenum when the terms U_h are not relativistically corrected.

kV	% variation in the extinction distance			% difference between the many-beam average extinction distance and the kinematical extinction distance at $\delta = 6.5$
	$\delta = 6.5$	$\delta = 7.5$	$\delta = 8.5$	
100	7.7	5.7	4.1	0.3
1000	7.5	5.8	4.2	0.3

5.5.3 The Effect of the Order of the Systematic Row on Many-Beam Effects

It is lastly of interest to examine how many-beam effects depend on the order of the systematic row. If a lower order systematic row is considered (for example, a (110) row instead of a (200) row), then the numerators in the expressions for the excitation amplitudes of equations 5.10 and 5.11 and in the second order eigenvalue correction terms 5.12 will increase (see Fig. 16). Furthermore, the denominators in these terms will tend to decrease in magnitude since the values of τ_h decrease. Accordingly, the excitation amplitudes of the secondary Bloch waves should increase with respect to the excitation amplitudes of the primary Bloch waves o and g. Therefore, there should be a larger variation in the extinction distance for the lower order systematic row. In addition, there should be a larger difference between the kinematical and many-beam average extinction distances. The reason for this lies in the fact that the second order eigenvalue correction terms 5.12 will be larger for the lower order row because the numerators increase and the denominators decrease. On the other hand, the difference $|\tau_o^2 - \tau_g^2|/(2K)$ between the primary Bloch wave eigenvalues $\gamma^{(o)}$ and $\gamma^{(g)}$ correct to first order will decrease for the lower order row. Accordingly, the percentage difference between the many-beam average extinction distance and the kinematical extinction distance should be larger for the lower order systematic row.

In order to see if these effects do in fact occur, calculations were carried out for the (110) and (200) systematic rows in molybdenum. The accelerating voltage used was 100 kV and sixteen reflections were included. The percentage variation in the extinction distance for the (110) and (200) dark fields is shown in Table 7. The crystal thickness considered was twenty extinction distances and the calculations were carried out for $\delta = 6.5$, $\delta = 7.5$ and $\delta = 8.5$. It can be seen from this table that there is a considerable decrease in the variation of the extinction distance with thickness for the higher order systematic row. The percentage difference between the many-beam average extinction distance and the kinematical extinction distance was also found to decrease. These results show that many-beam effects increase markedly when a lower order systematic row is considered and therefore the kinematical theory is a poorer approximation.

Table 7. A comparison of many-beam effects for high and low order systematic rows.

Systematic Row	% variation in extinction distance at			% difference between the many-beam average extinction distance and the kinematical extinction distance at $\delta = 6.5$
	$\delta = 6.5$	$\delta = 7.5$	$\delta = 8.5$	
(110)	8.9	6.9	5.1	0.4
(200)	3.1	2.4	1.6	0.04

5.6 Summary and Conclusions

In the past, the validity of the kinematical theory for large values of δ has been assessed by comparing it to the two-beam theory. In this thesis, the validity has been assessed by comparing the kinematical theory to the more exact many-beam theory. Two methods were used to carry out this comparison. The first method is similar to the method traditionally used to assess the validity of the kinematical theory and involves a comparison of the kinematical extinction distance to the many-beam average extinction distance. The results of this comparison showed that, if no systematic reflection was close to its Bragg condition, the kinematical and many-beam theories were in good agreement. This first method, however, has serious limitations because the many-beam average extinction distance is not sensitive to the effects associated with the presence of secondary Bloch waves. Accordingly, a second method was also used to compare the two theories. In this method the variation in the many-beam extinction distance with thickness was examined. This method showed that there were significant variations in the many-beam extinction distance even when no systematic reflections were close to the Bragg condition. This result shows that the kinematical theory is a poorer approximation than it had previously been considered to be.

When these two methods were used to compare the two theories close to the Bragg condition of a high order systematic reflection, many-beam effects were found to become very important, i.e. the intensity profiles became complex. The kinematical theory is therefore a very poor approximation for these diffraction conditions. The kinematical and many-beam theories were also compared when non-systematic reflections were included in the many-beam calculation. It was found that complexity could occur in the many-beam profiles if the s-value of a non-systematic reflection was close in value to zero or s_g. The kinematical theory is therefore a very poor approximation at these diffraction conditions. This is an important result because it shows that a non-systematic reflection can have an important effect when it is close to its Bragg condition. However, a non-systematic reflection can also have an important effect when it is not in the Bragg condition provided that $s_h \approx s_g$. This second condition has not previously been mentioned in the literature and is important in experimental observations of lattice defects under weak-beam diffraction conditions.

The effects of atomic number, accelerating voltage, and the order of the systematic row were also examined. It was found that the kinematical theory became a poorer approximation as atomic number or accelerating voltage increased or if a lower order systematic row was considered.

CHAPTER 6

EXACT AND APPROXIMATE METHODS FOR TAKING ABSORPTION INTO ACCOUNT IN THE DYNAMICAL THEORY OF ELECTRON DIFFRACTION

6.1 Introduction

The effects of absorption are taken into account in the dynamical theory of electron diffraction by the addition of an imaginary part to the lattice potential (for a recent review see Dederichs (1972) or Kambe and Molière (1970)). The approach widely adopted in the literature to the solution of the Schrodinger wave equation including this potential is to assume that the imaginary part is much smaller than the real part, thus permitting first order perturbation theory for the non-degenerate state to be used. There are, however, several limitations to this approach. Firstly, this form of perturbation theory is only applicable to diffraction conditions for which Bloch wave degeneracies do not occur. (In this thesis the term Bloch wave degeneracy will be taken to mean an equality in the kinetic energies of the Bloch waves.) During the last several years, however, there has been considerable interest in phenomena in which the occurrence of a Bloch wave degeneracy is involved. For example, the critical voltage effect (Lally et al.,1972), which results in the minimization of the diffracted beam intensity of a second order systematic reflection, is associated with the degeneracy of Bloch waves two and three. Also, when non-systematic reflections are taken into account in the dynamical theory, Bloch wave degeneracies are found to occur under certain diffraction conditions (Gjønnes and Høier, 1971; Cann and Sheinin, 1972, 1974A, 1974B).

A second limitation of the standard theory is that it is not applicable to diffraction conditions which result in quasi-degenerate or close level states. Close level states (i.e. nearly degenerate Bloch waves or close dispersion surfaces) occur for a wide variety of diffraction conditions. For example, they occur in the case where systematic reflections are taken into account and when a reflection is close to or in its Bragg condition. Some of these levels become particularly close for certain critical accelerating voltages. Close levels also occur at certain orientations in calculations which include non-systematic reflections.

A third limitation of the standard method for calculating absorption coefficients is that it is a first order approximation based on the assumption that the imaginary part of the lattice potential is much smaller than the real part. Sheinin and Andrew (1974) in a recent paper have shown that this assumption, although valid for the lighter elements, may not be valid for heavier elements because the imaginary part of the potential increases with increasing atomic number.

The limitations of the standard method clearly indicate that the development of alternative methods of taking absorption into account is desirable. Approximate methods, which enable calculations to be carried out under conditions of exact degeneracy, have been developed by Sheinin and Cann (1973) and Serneels and Gevers (1973B). Serneels and Gevers have also developed expressions based on second and higher order perturbation theory for the non-degenerate state which can be employed when the imaginary part of the lattice potential is no longer a small perturbation. As yet, however, no approximate methods have been developed for handling the case of quasi-degenerate or close level states.

An alternative to the approximate methods discussed above is to perform calculations which make no assumptions about the size of the perturbation or about how close the kinetic energies of the Bloch waves are to one another. One method, referred to in this thesis as the exact method, has been used by Thomas (1972) and Lally et al. (1972) in calculations of critical voltage phenomena. This method, based on the Bloch wave concept, simply diagonalizes the complex matrix ($\underline{A} + i\underline{A}'$) which occurs in the eigenvalue formulation of the equations of the dynamical theory (see equation 6.3). Other methods not formulated on the Bloch wave concept are also available, as for example, the multi-slice method of Cowley and Moodie (see Goodman and Moodie, 1974) and the Howie and Whelan (1961) differential equation approach. All these theories are useful from a computational point of view, but they do not give any insight into the interactions between Bloch waves which result from the introduction of the complex lattice potential. In this chapter an alternative approach which permits these interactions to be studied will be presented. The theory is based on generalized perturbation theory and diagonalizes, without approximation, the complex matrix ($\underline{A} + i\underline{A}'$) of the exact theory. Because this approach is a perturbation approach, the solution to the equations of the dynamical theory including absorption depend explicitly on the mixing of the unperturbed Bloch waves. This new formulation of the theory has the following advantages over the methods previously available:

(a) It offers insight into the changes in the mechanisms of image contrast which result from the introduction of the complex lattice potential. These changes involve the mixing of Bloch waves.

(b) The relationship between the lower order approximations, based on perturbation techniques, and the exact theory can be seen simply and directly.

(c) An approximate method, based on perturbation theory and capable of handling quasi-degenerate states can be developed for calculating diffracted beam intensities. This method, referred to in this thesis as the sub-matrix method, gives considerable saving in computing time while, at the same time, giving very close agreement with those theories which do not make perturbation approximations.

In Sections 6.2 and 6.3 of this chapter, the theory will be developed in its exact form. This will be followed in Section 6.4 by a discussion of some properties of the parameters $q^{(ij)}$ which represent the mixing between pairs of Bloch waves. The reduction of the exact theory to approximate methods for taking absorption into account will then be considered in the remaining sections.

6.2 The Solution of the Equations of the Dynamical Theory Including Absorption Using Generalized Perturbation Theory

As shown in Chapter 2, the high energy electrons in the crystal can be described in the dynamical theory of electron diffraction by Bloch waves of the form

$$|b^{(i)}> = \exp(2\pi i\vec{k}^{(i)}\cdot\vec{r})|u^{(i)}>$$

$$= \exp(2\pi i\vec{k}^{(i)}\cdot\vec{r}) \sum_g C_g^{(i)} \exp(2\pi i\vec{g}\cdot\vec{r}) \ . \qquad (6.1)$$

The Fourier coefficients $\underset{\sim}{C}_g^{(i)}$ and the Bloch wave vectors $\vec{k}^{(i)}$ can be found by solving the eigenvalue equation

$$\underline{\underline{A}}\underline{C}^{(i)} = \gamma^{(i)}\underline{C}^{(i)} \ . \qquad (6.2)$$

When the effects of absorption are taken into account by introducing an imaginary part to the lattice potential, the eigenvalue equation 6.2 becomes

$$(\underline{A} + i\underline{A}')\underline{C}'^{(n)} = \gamma'^{(n)}\underline{C}'^{(n)} \qquad (6.3)$$

where $i\underline{A}'$ is a matrix in which the elements iA'_{gh} are proportional to the Fourier coefficients of the imaginary part of the lattice potential $iU'(\vec{r})$ through the relation $iA'_{gh} = iU'_{g-h}/2K$. The matrix $(\underline{A} + i\underline{A}')$ is no longer Hermitian and thus has complex eigenvalues and eigenvectors. The real eigenvalues and eigenvectors $\gamma^{(i)}$ and $\underline{C}^{(i)}$ in equation 6.2 have therefore been rewritten in equation 6.3 as the complex quantities $\gamma'^{(n)}$ and $\underline{C}'^{(n)}$ respectively.

The approach to be taken in this thesis to the solution of equation 6.3 makes no assumptions regarding the size of the perturbation $i\underline{\Delta}'$ or the spacing of the levels and is based on generalized perturbation theory. In this approach, the eigenvectors of a perturbed equation are written in terms of a linear combination of the eigenvectors of an unperturbed equation (see for example Raimes, 1961). Accordingly, it is assumed in solving equation 6.3, referred to in this thesis as the perturbed equation, that the N eigenvectors and the corresponding eigenvalues of the unperturbed equation 6.2 are known. Since the eigenvalues of this unperturbed equation are discrete and the eigenvectors $\underline{C}^{(i)}$ form a complete orthonormal set, the eigenvector elements $C_g'^{(n)}$ of the perturbed equation can be written exactly as the linear combination

$$C_g'^{(n)} = \sum_i a_i^{(n)} C_g^{(i)} \qquad (6.4a)$$

or in matrix form

$$\underline{C}'^{(n)} = \underline{\underline{C}}\,\underline{a}^{(n)} \; . \qquad (6.4b)$$

In this equation $\underline{\underline{C}}$ is a matrix in which the columns are the eigenvectors of equation 6.2 and $\underline{a}^{(n)}$ is a column vector containing the ith coefficient in the linear combination as the ith element. The eigenvector $\underline{C}'^{(n)}$ in equation 6.4b can then be substituted into equation

6.3 to give

$$(\underline{A} + i\underline{A}')\underline{\underline{C}}\underline{\underline{a}}^{(n)} = \gamma'^{(n)}\underline{\underline{C}}\underline{\underline{a}}^{(n)} \; . \qquad (6.5)$$

This expression can then be multiplied by $\underline{C}^{-1}$, the inverse of $\underline{C}$, to give

$$[\underline{C}^{-1}\underline{\underline{A}}\underline{\underline{C}} + i\underline{C}^{-1}\underline{A}'\underline{C}]\underline{a}^{(n)} = \gamma'^{(n)}\underline{a}^{(n)} \; . \qquad (6.6)$$

Equation 6.6 can be expressed in a more convenient form by defining the parameters

$$q^{(ij)} = (1/2K)\langle u^{(i)}|U'|u^{(j)}\rangle = (1/2K)\sum_{g}\sum_{h} C_h^{(i)}C_g^{(j)}U'_{g-h}$$

and $\qquad q^{(ii)} = q^{(i)} \; , \qquad (6.7)$

where $q^{(i)}$ is the absorption coefficient of the Bloch wave as normally defined in the literature (see equation 2.29). The use of equations 6.7 and 6.2 then allows equation 6.6 to be rewritten in matrix form as follows

$$\begin{bmatrix} \gamma^{(1)}+iq^{(1)} & iq^{(12)} & iq^{(13)} & \cdots \\ iq^{(21)} & \gamma^{(2)}+iq^{(2)} & iq^{(23)} & \cdots \\ iq^{(31)} & iq^{(32)} & \gamma^{(3)}+iq^{(3)} & \cdots \\ \cdots & \cdots & \cdots & \cdots \end{bmatrix} \begin{bmatrix} a_1^{(n)} \\ a_2^{(n)} \\ a_3^{(n)} \\ \cdots \end{bmatrix} = \gamma'^{(n)} \begin{bmatrix} a_1^{(n)} \\ a_2^{(n)} \\ a_3^{(n)} \\ \cdots \end{bmatrix}$$

(6.8)

This equation can then be abbreviated to the eigenvalue equation

$$\underline{\underline{B}}\underline{a}^{(n)} = \gamma'^{(n)}\underline{a}^{(n)} . \qquad (6.9)$$

It can be seen from equations 6.7 and 6.8 that the perturbed eigenvalue equation 6.9 can be solved only by first solving the unperturbed equation 6.2.

Since no assumptions have been made about how close the levels are to one another or about the size of the perturbation, the eigenvalues $\gamma'^{(n)}$ of the perturbed equation 6.3 can be found without approximation by diagonalizing the complex matrix $\underline{\underline{B}}$ in equation 6.9. The corresponding eigenvectors, $\underline{a}^{(n)}$, of this matrix can then be substituted into equation 6.4b to construct without approximation the eigenvectors $\underline{C}'^{(n)}$ of equation 6.3. If $\underline{C}$ is orthogonal and $\underline{a}^{(n)}$ is normalized, then $\underline{C}'^{(n)}$ will also be normalized.

The form of the wave functions including absorption can be found from equation 6.1 by substituting the complex eigenvector elements $C_g'^{(n)}$ for the unperturbed elements $C_g^{(i)}$ and the complex wave vectors $\vec{k}'^{(n)}$ for $\vec{k}^{(i)}$, where $k_z'^{(n)} = (\gamma'^{(n)} + K_z)$. The perturbed wave functions, $|b'^{(n)}>$, can then be written in the form

$$|b'^{(n)}> = \exp(2\pi i\vec{k}'^{(n)}\cdot\vec{r}) \sum_g C_g'^{(n)} \exp(2\pi i\vec{g}\cdot\vec{r}) . \qquad (6.10)$$

Clearly these wave functions are also Bloch waves since equation 6.10 has the form of a plane wave modulated by a function $|u'^{(n)}> = \sum_g C_g'^{(n)}\exp(2\pi i\vec{g}\cdot\vec{r})$ which has the periodicity of the lattice. It is of interest to express the Bloch functions $|u'^{(n)}\rangle$ in terms of the parameters characteristic of the unperturbed Bloch waves. This can be done by substituting equation 6.4a into equation 6.10 to obtain

$$\begin{aligned} |b'^{(n)}\rangle &= \exp(2\pi i\vec{k}'^{(n)}\cdot\vec{r})\,|u'^{(n)}\rangle \\ &= \exp(2\pi i\vec{k}'^{(n)}\cdot\vec{r})\sum_i a_i^{(n)}|u^{(i)}\rangle \;. \end{aligned} \qquad (6.11)$$

This equation indicates that the perturbed Bloch functions $|u'^{(n)}\rangle$ are in fact linear combinations of the unperturbed Bloch functions $|u^{(i)}\rangle$. This can be interpreted as indicating that the perturbation (the imaginary part of the lattice potential) results in a mixing of the Bloch waves characteristic of the system without absorption. It can further be seen from equation 6.7 that the off-diagonal elements, $q^{(ij)}$, of the $\underline{B}$ matrix represent the mixing which occurs between a particular pair of unperturbed Bloch waves, i and j, since these elements depend explicitly on the Bloch functions $|u^{(i)}\rangle$ and $|u^{(j)}\rangle$. The appearance of these $q^{(ij)}$ elements allows the importance of the mixing of Bloch waves to be assessed. In Section 6.4, some relevant properties of these elements will be discussed. The importance of this mixing on the diffracted beam intensity will then be considered in Chapter 7.

6.3 Calculation of Diffracted Beam Intensities

The calculation of diffracted beam intensities in the dynamical theory involves a determination of the extent to which the various Bloch waves in the crystal are excited. In the standard method, this is done relatively simply since the orthogonality of the $\underset{\sim}{C}$ matrix leads to the result that the excitation coefficient of a particular Bloch wave, $|b^{(i)}>$, is equal to $C_o^{(i)}$. This result, however, is not valid in the general case since the matrix of eigenvectors is no longer orthogonal. The purpose of this section is to outline the procedure involved in calculating diffracted beam intensities in this case.

The method for calculating diffracted beam intensities from the Bloch wave functions, $|b'^{(n)}>$, of the perturbed system is analogous to the method used in the standard Bloch wave formulation of the dynamical theory (see Section 2.1.2). The starting point for the calculation is the total wave function for the electrons in the crystal

$$\Psi = \sum_n X^{(n)} |b'^{(n)}> = \sum_n X^{(n)} \sum_g C_g'^{(n)} \exp(2\pi i(\vec{k}'^{(n)} + \vec{g})\cdot\vec{r}) \qquad (6.12)$$

where $X^{(n)}$ is the excitation coefficient for the wave function $|b'^{(n)}>$ of equation 6.10. If equation 6.12 is then sorted into incident and diffracted beams and the resulting terms are multiplied by the phase term $\exp(-2\pi i\vec{K}\cdot\vec{r})$, the expression for the diffracted beam intensity is found to be

$$|\phi_g|^2 = \left|\sum_n X^{(n)} C_g'^{(n)} \exp(2\pi i\gamma'^{(n)} z)\right|^2. \qquad (6.13)$$

The eigenvalues $\gamma'^{(n)}$ in this equation can be found by diagonalizing the matrix $\underline{B}$, and the eigenvector elements $C_g'^{(n)}$ can be found by substituting the eigenvectors of the $\underline{A}$ and $\underline{B}$ matrices into equation 6.4a. The excitation coefficients can be determined from the boundary conditions at the top surface of the crystal, i.e.

$$\phi_o = 1\ , \qquad \phi_g = 0 \qquad (g \neq 0) \qquad (6.14)$$

where ϕ_o is the amplitude of the directly transmitted beam and ϕ_g are the amplitudes of the diffracted beams. Equation 6.13 together with 6.14 gives

$$\underline{C}'\underline{X} = \underline{u} \qquad (6.15)$$

where $\underline{C}'$ is a matrix having the elements $C_g'^{(n)}$ in the g^{th} row and n^{th} column, $\underline{X}$ is a column vector containing the excitation coefficients $X^{(n)}$ in the n^{th} row, and $\underline{u}$ is a column vector containing the diffracted beam amplitudes 1, 0, 0, ... of equation 6.14. The excitation coefficients $X^{(n)}$, required in equation 6.13, can then be found by obtaining numerical solutions to the nonhomogeneous system of linear equations 6.15. In contrast to the standard theory, these coefficients are, in general, complex.

Although the excitation coefficients can be found from equation 6.15, an alternate form of this equation can be obtained by substituting in equation 6.15 the matrix form of equation 6.4, $\underline{C}' = \underline{C}\underline{a}$, where $\underline{a}$ is a matrix which has as its columns the column vectors $\underline{a}^{(n)}$. Using the orthogonality of the $\underline{C}$ matrix and multiplying by $\underline{C}^{-1}$ from the left then gives

$$\underline{a}\underline{X} = \underline{G} \tag{6.16}$$

where $\underline{G}$ is a column vector containing the elements $C_o^{(i)}$ in the i^{th} row. The excitation coefficients required in equation 6.13 can then be found by solving the nonhomogeneous system of linear equations 6.16. This alternate method for calculating the excitation coefficients leads to convenient simplifications in the approximate diffracted beam intensity expressions to be derived in Section 6.6 of this chapter.

6.4 Some Properties of the $q^{(ij)}$ Elements of the $\underline{B}$ Matrix

Before examining the approximations which can be made in diagonalizing the $\underline{B}$ matrix (see equation 6.9 of Section 6.3), it is first of interest to discuss some of the properties of the off-diagonal elements of this matrix. The first important property is that for centrosymmetric crystals $q^{(ij)} = q^{(ji)}$, i.e. the $\underline{B}$ matrix is symmetric. This can be seen from the definition of $q^{(ij)}$ in equation 6.7, Section 6.2, together with the fact that for centrosymmetric crystals $\underline{A}' = (\underline{A}')^T$, the transpose of $\underline{A}'$, and $\underline{C}^{-1} = \underline{C}^T$. These relationships give

$$\underline{q} = \underline{C}^{-1}\underline{A}'\underline{C} = \underline{C}^T(\underline{A}')^T\underline{C} = (\underline{C}^T\underline{A}'\underline{C})^T = (\underline{C}^{-1}\underline{A}'\underline{C})^T = \underline{q}^T \qquad (6.17)$$

where $\underline{q}$ is a matrix formed by the imaginary elements of $\underline{B}$.

Another important property of the $\underline{q}$ matrix is that, under certain diffraction conditions, some of the off-diagonal elements are identically zero. For example, if a centrosymmetric crystal is oriented so that the systematic reflection mg is in its exact Bragg condition and only a systematic row of reflections is considered, then the eigenvectors of the unperturbed equation 6.2 are either symmetric, with

$$C^{(i)}_{\frac{m+n}{2}} = C^{(i)}_{\frac{m-n}{2}} \qquad (6.18a)$$

or anti-symmetric with

$$C^{(i)}_{\frac{m+n}{2}} = -\,C^{(i)}_{\frac{m-n}{2}} \qquad (6.18b)$$

where n = 0,2,4,... for m even and n = 1,3,5,... for m odd (Metherell and Fisher, 1969). If eigenvector elements $C_h^{(i)}$ and $C_g^{(j)}$ are substituted into equation 6.7, it can be shown by using equations 6.18a,b that, for a centrosymmetric crystal, the value of $q^{(ij)}$ is identically equal to zero, provided that one of the Bloch waves is symmetric and the other is anti-symmetric. A particular example of this second property has previously been noted by Serneels and Gevers (1974), who showed that the matrix elements describing the mixing between Bloch waves two and three are identically zero in a critical voltage calculation carried out precisely at 2g in the Bragg condition.

A third property of the $q^{(ij)}$ elements can be obtained by comparing these elements for values of the deviation parameter δ which are equal in magnitude but opposite in sign (see Fig. 30). For the systematic row of reflections shown in this figure, the $\underline{A}$ matrix for $\delta = y/g$ can be written

$$\underline{A}(y) = \begin{pmatrix} t_o(y) & \frac{U_{-g}}{2K} & \frac{U_g}{2K} & \cdots \\ \frac{U_g}{2K} & t_g(y) & \frac{U_{2g}}{2K} & \cdots \\ \frac{U_{-g}}{2K} & \frac{U_{-2g}}{2K} & t_{-g}(y) & \cdots \\ \cdots & \cdots & \cdots & \cdots \end{pmatrix} \qquad (6.19)$$

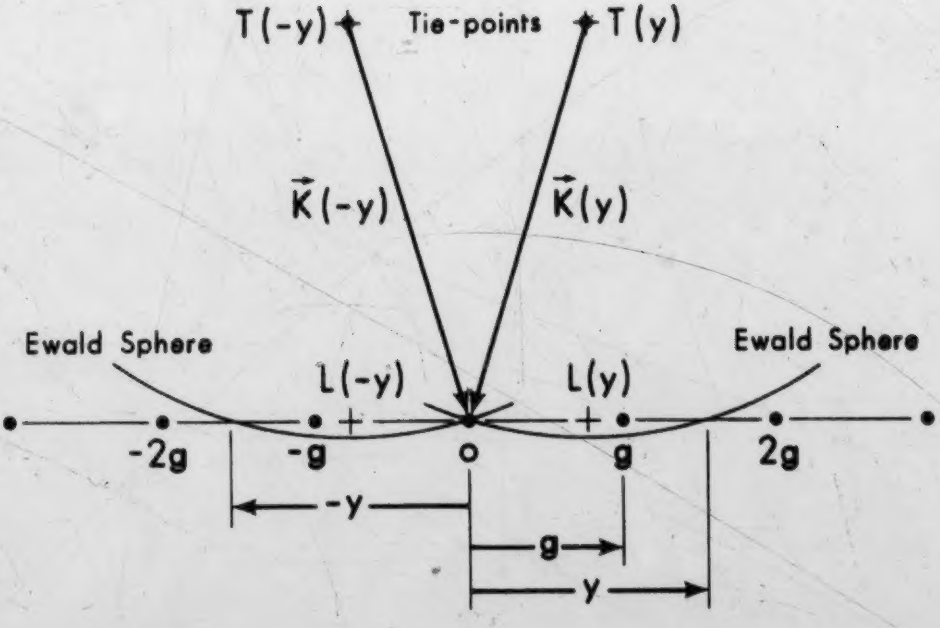

Fig. 30. The Ewald sphere construction for deviation parameters $\delta = y/g$ and $\delta = -y/g$ which are equal in magnitude but opposite in sign. The points L(y) and L(-y) are the perpendicular projections of the tie-points T(y) and T(-y) onto the systematic row.

The elements on the diagonal of this matrix are the t-value elements of equation 4.8, i.e.

$$t_h(y) = -\frac{(\tau_h(y))^2}{2K} \qquad (6.20)$$

where $\tau_h(y)$ is the distance from the point L(y) to the reciprocal lattice point h (see Fig. 30). (For simplicity, the t-method approximation for calculating the diagonal elements of the $\underline{A}$ matrix will be used in this section. This will not affect the arguments presented, however, since these arguments will be based on the eigenvectors of the $\underline{A}$ matrix, and the eigenvectors found using the t-method are exact. See Section 4.3.4.) Similarly, the $\underline{A}$ matrix for $\delta = -y/g$ can be written

$$\underline{A}(-y) = \begin{bmatrix} t_o(-y) & \frac{U_g}{2K} & \frac{U_{-g}}{2K} & \cdots \\ \frac{U_{-g}}{2K} & t_{-g}(-y) & \frac{t_{-2g}}{2K} & \cdots \\ \frac{U_g}{2K} & \frac{U_{2g}}{2K} & t_g(-y) & \cdots \\ \cdots & \cdots & \cdots & \cdots \end{bmatrix} \qquad (6.21)$$

Since $\tau(y)$ is the distance from the point L(y) to the reciprocal lattice point h, it can be seen from equation 6.20 and Fig. 30 that

$$t_h(y) = t_{-h}(-y) \quad . \qquad (6.22)$$

Furthermore, for centrosymmetric crystals, $U_g = U_{-g}$. Accordingly the $\underline{A}$ matrices of equations 6.19 and 6.21 are identical. The real, normalized eigenvectors of these matrices will therefore be equal, except for an arbitrary multiplicative factor of ±1, i.e.

$$\begin{pmatrix} C_o^{(i)}(y) \\ C_g^{(i)}(y) \\ C_{-g}^{(i)}(y) \\ \cdots \end{pmatrix} = \pm \begin{pmatrix} C_o^{(i)}(-y) \\ C_{-g}^{(i)}(-y) \\ C_g^{(i)}(-y) \\ \cdots \end{pmatrix} . \qquad (6.23)$$

Therefore, from equation 6.23 and the definition of $q^{(ij)}$ in equation 6.7

$$q^{(ij)}(y) = \frac{1}{2K} \sum_g \sum_h C_h^{(i)}(y) C_g^{(j)}(y) U'_{g-h}$$

$$= \pm \frac{1}{2K} \sum_g \sum_h C_{-h}^{(i)}(-y) C_{-g}^{(j)}(-y) U'_{-(g-h)}$$

$$= \pm\, q^{(ij)}(-y) \ . \qquad (6.24)$$

The $q^{(ij)}$ elements are therefore equal in magnitude for values of the deviation parameter δ which are equal in magnitude but opposite in sign. With the proper choice of the arbitrary sign in equation 6.23, the $q^{(ij)}$ elements for these values of δ can be identically equal.

A fourth property of the elements $q^{(ij)}$ is that, when only systematic reflections are considered,

$|q^{(ij)}|$ is a periodic function of the deviation parameter $\delta.\vec{\ell}$ This property can be derived by comparing the $\underset{\sim}{A}$ matrix at $\delta = y/g$ to

the $\underset{\sim}{A}$ matrix at $\delta = (y + 2\ell)/g$

where $\vec{\ell}$ is a reciprocal lattice vector (see Fig. 31). The $\underset{\sim}{A}$ matrix at $\delta = (y + 2\ell)/g$ can be written

$$\underset{\sim}{A}(y+2\ell) = \begin{pmatrix} t_g(y+2\ell) & \frac{U_{-g}}{2K} & \frac{U_g}{2K} & \cdots \\ \frac{U_g}{2K} & t_{2g}(y+2\ell) & \frac{U_{2g}}{2K} & \cdots \\ \frac{U_{-g}}{2K} & \frac{U_{-2g}}{2K} & t_o(y+2\ell) & \cdots \\ \cdots & \cdots & \cdots & \cdots \end{pmatrix} \qquad (6.25)$$

Since $t_h(y)$ is the distance from the point $L(y)$ to the reciprocal lattice point h, it can be seen from equation 6.20 and Fig. 31 that

$$t_{h+\ell}(y+2\ell) = t_h(y) \ . \qquad (6.26)$$

Therefore, the $\underset{\sim}{A}$ matrices in equations 6.19 and 6.25 are identical, i.e. $\underset{\sim}{A}(y) = \underset{\sim}{A}(y+2\ell)$. Accordingly, the real, normalized eigenvectors of these matrices will be equal except for an arbitrary multiplicative factor of ± 1, i.e.

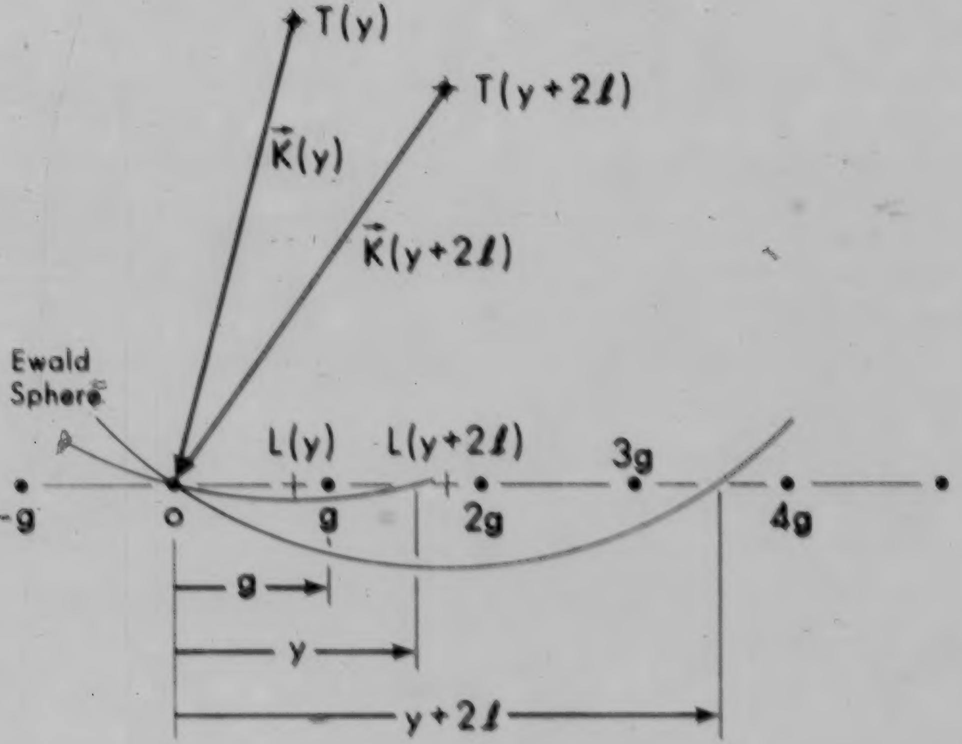

Fig. 31. The Ewald sphere construction for deviation parameters $\delta = y/g$ and $\delta = (y + 2\ell)/g$ where $\vec{\ell}$ is a reciprocal lattice vector. The points L(y) and L(y + 2ℓ) are the perpendicular projections of the tie-points T(y) and T(y + 2ℓ) onto the systematic row.

$$\begin{bmatrix} C_o^{(i)}(y) \\ C_g^{(i)}(y) \\ C_{-g}^{(i)}(y) \\ \cdots\cdot \end{bmatrix} = \pm \begin{bmatrix} C_g^{(i)}(y+2\ell) \\ C_{2g}^{(i)}(y+2\ell) \\ C_o^{(i)}(y+2\ell) \\ \cdots\cdot \end{bmatrix} \qquad (6.27)$$

From equation 6.27 and the definition of $q^{(ij)}$ in equation 6.7 it can then be seen that

$$\begin{aligned} q^{(ij)}(y) &= \frac{1}{2K} \sum_g \sum_h C_h^{(i)}(y) C_g^{(j)}(y) U'_{g-h} \\ &= \pm \frac{1}{2K} \sum_g \sum_h C_{h+\ell}^{(i)}(y+2\ell) C_{g+\ell}^{(j)}(y+2\ell) U'_{g+\ell-h-\ell} \\ &= \pm q^{(ij)}(y+2\ell) \quad . \end{aligned} \qquad (6.28)$$

The magnitude of the elements $q^{(ij)}$ is thus a periodic function of δ with a period equal to $2\ell/g$. If $\vec{\ell} = \vec{g}$ where $|\vec{g}|$ is the distance from o to g in Fig. 31, then the period is 2.0 in units of δ. Metherell and Fisher (1969) have previously shown this result for the diagonal elements $q^{(ii)} = q^{(i)}$ of the $\underline{B}$ matrix. Their argument is based on Bloch's theorem and can be extended to prove the result of equation 6.28.

In order to illustrate the way in which the magnitudes of the terms $q^{(ij)}$ vary with δ, thirteen beam calculations for the (220) systematic row in gold have been carried out. The results are shown in Fig. 32. It can be seen from this figure that the values of $|q^{(ij)}|$ are symmetrical about $\delta = 0.0$ and that they are a periodic function of δ with a period equal to 2.0. Furthermore, for $\delta = n$ where n is an integer, some of the values of $q^{(ij)}$ are zero because Bloch waves of opposite symmetry are involved.

6.5 The Relationship Between the Exact Approach and the Low Order Perturbation Theory Approaches

In Section 6.2, the exact solution to the equations of the dynamical theory of electron diffraction including absorption was formulated in terms of a matrix $\underline{\underline{B}}$ whose off-diagonal elements, $iq^{(ij)}$, were seen to represent the mixing which occurs between pairs of Bloch waves. In this section the assumptions concerning the importance of Bloch wave mixing which must be made in order to reduce the exact theory to the low order perturbation theories previously presented in the literature will be considered. The mathematical procedure which will be used is discussed in detail in Appendix A.

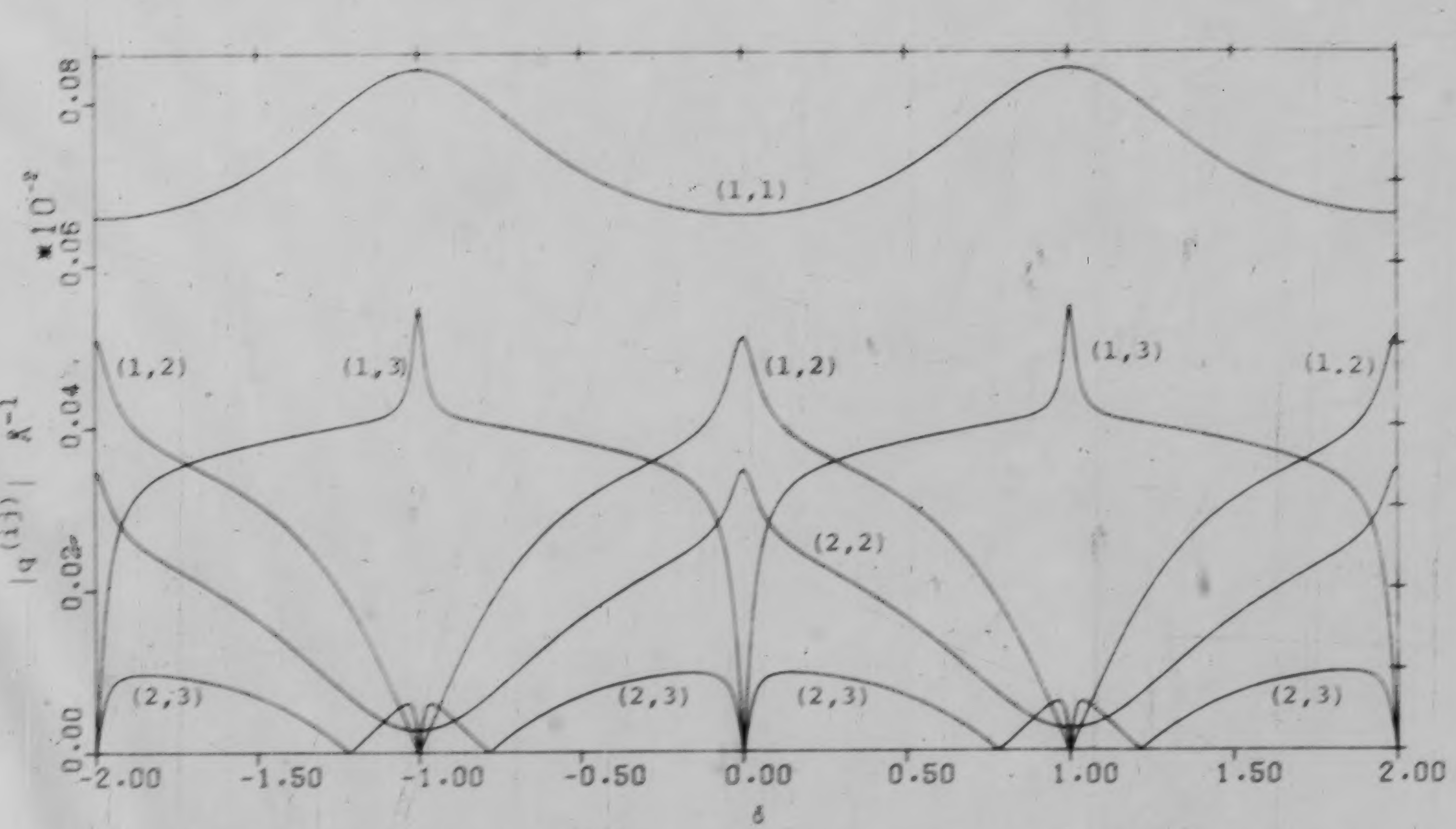

Fig. 32. Typical values of $|q^{(ij)}|$ in gold as a function of the deviation parameter δ. Thirteen reflections of the (220) systematic row were considered and the accelerating voltage was 100 kV.

6.5.1 The First Order Approximation to the Solution of the Perturbed Equation

The low order perturbation theory approaches discussed in Section 6.1 can be developed from the exact theory by calculating approximate expressions for the eigenvalues and eigenvectors of the $\underline{B}$ matrix. In order to calculate the eigenvalues of the $\underline{B}$ matrix correct to first order, it is assumed that different Bloch waves do not mix and, therefore, that all the off-diagonal elements of the $\underline{B}$ matrix are zero. Under this first order approximation the $\underline{B}$ matrix then takes the diagonal form

$$\underline{B} \approx \begin{bmatrix} \gamma^{(1)}+iq^{(1)} & 0 & 0 & \cdots\cdot \\ 0 & \gamma^{(2)}+iq^{(2)} & 0 & \cdots\cdot \\ 0 & 0 & \gamma^{(3)}+iq^{(3)} & \cdots\cdot \\ \cdots & \cdots & \cdots & \cdots \end{bmatrix} \qquad (6.29)$$

The perturbed eigenvalues $\gamma'^{(n)}$ of this approximate $\underline{B}$ matrix are then equal to the standard theory eigenvalues $\gamma^{(n)} + iq^{(n)}$ found using first order perturbation theory for the non-degenerate state. The corresponding eigenvectors $\underline{a}^{(n)}$ of the approximate $\underline{B}$ matrix can be written as columns of the unit matrix $\underline{I}$ (see equation A.5 of Appendix A). Reference to equation 6.4b then shows that the perturbed eigenvector matrix $\underline{C}'$ can be approximated by the unperturbed eigenvector matrix $\underline{C}$

and that the Bloch wave functions $|b'^{(n)}>$ then become those used in the standard first order perturbation approach, namely

$$|b'^{(n)}> = |b^{(n)}> . \qquad (6.30)$$

It therefore can be seen that if the assumption is made that the imaginary part of the lattice potential does not result in mixing between any of the Bloch waves, the exact solution reduces to the incomplete first order perturbation theory solution for the non-degenerate state, referred to as the standard theory.

6.5.2 The Second Order Approximation to the Solution of the Perturbed Equation

In the second order approximate solution to the matrix $\underline{B}$, the effect of Bloch wave mixing is taken into account in an approximate manner by assuming that the mixing between two particular Bloch waves i and j will only affect the eigenvalues and eigenvectors of Bloch waves i and j. Within this second order approximation, then, the only off-diagonal elements of the matrix $\underline{B}$ which are taken into account in the calculation of the corrected eigenvalue and eigenvector of a particular Bloch wave i are $iq^{(ij)}$ and $iq^{(ji)}$ where $j = 1,N$ $(j \neq i)$ and N is the number of beams taken into account.

In order to calculate the perturbed eigenvalue $\gamma'^{(n)}$ of the matrix $\underline{B}$ correct to second order, it is first convenient to cast the perturbed eigenvalue equation 6.9 in the form

$$(\underline{B} - \{\gamma'\})\underline{a}^{(n)} = 0 \tag{6.31}$$

where $\{\gamma'\}$ is a diagonal matrix containing the diagonal elements $\gamma'^{(n)}$. If it is assumed in equation 6.31 that the first order eigenvalues on the diagonal of the matrix $\underline{B}$ are non-degenerate, and that the second order corrections to the eigenvalues are small, then, to a good approximation the diagonal terms $\gamma^{(m)} + iq^{(m)} - \gamma'^{(n)}$ can be set equal to $\gamma^{(m)} + iq^{(m)} - \gamma^{(n)} - iq^{(n)}$ for $m \neq n$. Furthermore, if it is assumed, as mentioned above, that only the off-diagonal terms in the $\underline{B}$ matrix which involve Bloch wave n directly will have an important effect on $\gamma'^{(n)}$ then all other off-diagonal elements can be neglected and can be considered to be zero. Under these second order approximations, equation 6.31 becomes

$$\begin{pmatrix} \gamma^{(1)}+iq^{(1)}-\gamma'^{(1)} & iq^{(12)} & iq^{(13)} & \cdots \\ iq^{(21)} & \gamma^{(2)}+iq^{(2)}-\gamma^{(1)}-iq^{(1)} & 0 & \cdots \\ iq^{(31)} & 0 & \gamma^{(3)}+iq^{(3)}-\gamma^{(1)}-iq^{(1)} & \\ \cdots & \cdots & \cdots & \cdots \end{pmatrix} \begin{pmatrix} a_1^{(n)} \\ a_2^{(n)} \\ a_3^{(n)} \\ \cdots \end{pmatrix} = 0 \tag{6.32}$$

As shown in Appendix A, the eigenvector $\underline{a}^{(n)}$ can be obtained by solving all but the n^{th} equation represented by the matrix equation 6.32 to give

$$P_j^{(n)} = - \frac{iq^{(jn)}}{\gamma^{(j)} + iq^{(j)} - \gamma^{(n)} - iq^{(n)}} \qquad (j \neq n) \qquad (6.33a)$$

where $P_j^{(n)} = \frac{a_j^{(n)}}{a_n^{(n)}}$ ~~and~~ $\cancel{P_n^{(n)}} = 1$. (6.33b)

Since it has been assumed that the first order eigenvalues are non-degenerate, the denominator in equation 6.33a will be large and it can therefore be assumed that $P_j^{(n)} << 1$ $(j \neq n)$. Therefore the column vector $\underline{P}^{(n)}$, whose elements are $P_j^{(n)}$, can be considered to be normalized and the eigenvector $\underline{a}^{(n)}$ can be taken to be equal to $\underline{P}^{(n)}$. The eigenvector elements of $\underline{C}'^{(n)}$ can then be found from equation 6.4b to be

$$\underline{C}'^{(n)} = \underline{\underline{C}}\underline{P}^{(n)}$$

$$\text{or} \qquad \underline{C}' = \underline{\underline{C}}\underline{\underline{P}} \qquad (6.34)$$

where $\underline{P}$ is a matrix whose n^{th} column contains the eigenvector $\underline{P}^{(n)}$. It can be seen from equations 6.33 and 6.34 that the corrections to the first order eigenvectors obtained from second order perturbation theory are complex. If, however, it is assumed that

$$|\gamma^{(j)} - \gamma^{(n)}| >> |q^{(j)} - q^{(n)}| . \qquad (6.35)$$

then these corrections reduce to the purely imaginary first order corrections derived by Wilkens et al. (1973) and Serneels and Gevers (1973B). The fact that, in the present analysis, this first order result is forthcoming from second order perturbation theory is consistent with the fact that, in perturbation theory, the calculation of the perturbed energies to a given order requires the knowledge of the wave functions to the next lower order.

It is next of interest to obtain the second order corrections to the first order eigenvalues. This can be done, as shown in Appendix A, by substituting the expressions for $a_j^{(n)}$ obtained from equations 6.33 into the n^{th} equation of 6.32 to give

$$\gamma'^{(n)} = \gamma^{(n)} + iq^{(n)} - \sum_{j \neq n}^{N} \frac{(iq^{(nj)})^2}{\gamma^{(j)} + iq^{(j)} - \gamma^{(n)} - iq^{(n)}} . \quad (6.36)$$

It should be noted that this second order approximate solution gives both a real and an imaginary correction to the first order eigenvalues $\gamma^{(n)} + iq^{(n)}$. This differs from the purely real correction derived by Serneels and Gevers (1973B) using second order perturbation theory for the non-degenerate state. However, if the assumption in equation 6.35 is again made, 6.36 gives the purely real correction derived by these authors.

It is also of interest to consider the calculation of the excitation coefficients required to calculate diffracted beam intensity in the second order theory. In the standard theory this task is simplified since these coefficients can be shown to be the terms in the first column of $\underline{C}^{-1}$, the inverse of the $\underline{C}$ matrix. Since $\underline{C}$ is orthogonal, the excitation coefficients are simply equal to $C_o^{(i)}$, $i = 1,N$. In the general case when the eigenvector matrix $\underline{C}'$ is complex, the excitation coefficients are still equal to the first column of $(\underline{C}')^{-1}$. However, $\underline{C}'$ is not orthogonal and $(\underline{C}')^{-1} \neq (\underline{C}')^{T}$. The calculation of the excitation coefficients in this case therefore requires that the first column of $(\underline{C}')^{-1}$ be obtained by other means. It is possible in the second order approximation, however, to calculate approximate expressions for the excitation coefficients by deriving an approximation to $(\underline{C}')^{-1}$. If it is assumed that $|P_j^{(n)}| << 1$ for $j \neq n$, then $\underline{P}^{-1}$ can be approximated by $\underline{P}^{T}$, the transpose of $\underline{P}$, if terms involving the products of the small off-diagonal elements of $\underline{P}$ are neglected in comparison to the elements of $\underline{P}$. (This can be seen most easily by multiplying $\underline{P}$ by $\underline{P}^{T}$, using the fact that $P_j^{(i)} = -P_i^{(j)}$ and examining the approximations required to make this product equal to the unity matrix.) The inverse of $\underline{C}'$ then becomes

$$(\underline{C}')^{-1} = (\underline{C}\underline{P})^{-1} = \underline{P}^{-1}\underline{C}^{-1} \approx \underline{P}^{T}\underline{C}^{T} = (\underline{C}')^{T}. \qquad (6.37)$$

The excitation coefficient, $X^{(n)}$, can therefore be approximated by $C_o'^{(n)}$ for the second order case in a manner similar to the standard theory. Wilkens et al. (1973) have previously given expressions for $(\underline{C}')^{-1}$, but in their second order theory $(\underline{C}')^{-1}$ was not shown to be approximately equal to $(\underline{C}')^{T}$.

6.6 The Sub-Matrix Approach

In the second order approximation of the previous section, mixing between different Bloch waves was taken into account in an approximate way by assuming that the second order corrections to the eigenvalues were small. It can be seen from equation 6.36 however, that these corrections will become large as $q^{(ij)}$ increases or as the term $\gamma^{(j)} + iq^{(j)} - \gamma^{(n)} - iq^{(n)}$ becomes small. Since the $q^{(ij)}$ terms tend to increase as the atomic number increases (see Section 7.2) and certain of the terms $\gamma^{(j)} + iq^{(j)} - \gamma^{(n)} - iq^{(n)}$ can become small, for example, near critical voltage diffraction conditions, it is of interest to develop an approximate method for diagonalizing the $\underline{B}$ matrix which can be used when the low order perturbation solutions for the non-degenerate state do not apply. Such an approximation, termed the sub-matrix approach, will be developed in this section.

In the sub-matrix approach it is assumed that the mixing between some Bloch waves is important and should be taken into account, while the mixing between others is not important and can be neglected. This approach is similar to that used in quasi-degenerate perturbation theory where some of the unperturbed levels are assumed to be sufficiently close that mixing between these close levels must be considered. As the simplest example of this method, let it be assumed that the mixing between only two of the Bloch waves is important. (The procedure can easily be generalized to take into account the mixing between more than two Bloch waves.) If, for example, it is the mixing between Bloch waves two and three that is considered to be important then the $\underline{B}$ matrix takes the approximate form

$$\underline{B} \approx \begin{bmatrix} \gamma^{(1)}+iq^{(1)} & 0 & 0 & 0 & \cdots \\ 0 & \gamma^{(2)}+iq^{(2)} & iq^{(23)} & 0 & \cdots \\ 0 & iq^{(32)} & \gamma^{(3)}+iq^{(3)} & 0 & \cdots \\ 0 & 0 & 0 & \gamma^{(4)}+iq^{(4)} & \cdots \\ \cdots & \cdots & \cdots & \cdots & \cdots \end{bmatrix} \tag{6.38}$$

The perturbed eigenvalues $\gamma'^{(n)}$ $(n \neq 2,3)$ of this matrix are then found to be those of the standard theory, while the perturbed eigenvalues $\gamma'^{(2)}$ and $\gamma'^{(3)}$ can be found by diagonalizing the sub-matrix

$$= \begin{pmatrix} \gamma^{(2)}+iq^{(2)} & iq^{(23)} \\ iq^{(32)} & \gamma^{(3)}+iq^{(3)} \end{pmatrix} . \qquad (6.39)$$

The eigenvectors $\underline{a}^{(n)}$ of this sub-matrix can then be incorporated into the matrix $\underline{a}$ which has as columns the eigenvectors of the $\underline{B}$ matrix in equation 6.38. This produces an $\underline{a}$ matrix of the form

$$\underline{a} \approx \begin{pmatrix} 1 & 0 & 0 & 0 \ldots \\ 0 & a_2^{(2)} & a_2^{(3)} & 0 \ldots \\ 0 & a_3^{(2)} & a_3^{(3)} & 0 \ldots \\ 0 & 0 & 0 & 1 \ldots \\ \ldots & \ldots & \ldots & \ldots \end{pmatrix} . \qquad (6.40)$$

The perturbed Bloch wave functions in the sub-matrix approach can now be obtained from equation 6.10. For those Bloch waves which are not considered to mix, the Bloch wave functions can be seen to be those of the standard theory, while for those which are considered to mix, in this case 2 and 3,

$$|b'^{(n)}\rangle = \exp(2\pi i\vec{k}'^{(n)}\cdot\vec{r})\{a_2^{(n)}|u^{(2)}\rangle + a_3^{(n)}|u^{(3)}\rangle\}. \; (n=2,3) \qquad (6.41)$$

Thus Bloch waves 2 and 3 in the perturbed state are formed from a linear combination of unperturbed Bloch functions.

In order to calculate the diffracted beam intensity using the sub-matrix approach, it is first necessary to calculate the Bloch wave excitation coefficients. The general method for calculating these coefficients has been given in Section 6.3 where it was shown that $X^{(n)}$, the excitation coefficient of Block wave n, can be found from the expression

$$\underline{\underline{a}}\,\underline{X} = \underline{G} \quad . \tag{6.42}$$

In this equation, $\underline{\underline{a}}$ is a matrix whose nth column is the eigenvector $\underline{a}^{(n)}$ of the $\underline{B}$ matrix, $\underline{X}$ is a column vector containing $X^{(n)}$ in the nth row, and $\underline{G}$ is a column vector containing $C_o^{(n)}$ in the nth row. The $\underline{a}$ matrix of equation 6.40 can therefore be substituted into 6.42 to give

$$\begin{bmatrix} 1 & 0 & 0 & 0 \ldots \\ 0 & a_2^{(2)} & a_2^{(3)} & 0 \ldots \\ 0 & a_3^{(2)} & a_3^{(3)} & 0 \ldots \\ 0 & 0 & 0 & 1 \ldots \\ \ldots & \ldots & \ldots & \ldots \end{bmatrix} \begin{bmatrix} X^{(1)} \\ X^{(2)} \\ X^{(3)} \\ X^{(4)} \\ \ldots \end{bmatrix} = \begin{bmatrix} C_o^{(1)} \\ C_o^{(2)} \\ C_o^{(3)} \\ C_o^{(4)} \\ \ldots \end{bmatrix} \quad . \tag{6.43}$$

It can be seen by inspection that $X^{(n)} = C_o^{(n)}$ for $n \neq 2,3$, and that $X^{(2)}$ and $X^{(3)}$ can be found from the reduced set of simultaneous equations

$$\begin{bmatrix} a_2^{(2)} & a_2^{(3)} \\ a_3^{(2)} & a_3^{(3)} \end{bmatrix} \begin{bmatrix} X^{(2)} \\ X^{(3)} \end{bmatrix} = \begin{bmatrix} C_o^{(2)} \\ C_o^{(3)} \end{bmatrix} . \qquad (6.44)$$

The expression for diffracted beam intensity, for the present example, can therefore be written as

$$I_g = |\phi_g|^2 = \Big| \sum_{n=2,3} X^{(n)} C_g'^{(n)} \exp(2\pi i \gamma'^{(n)} z) + \sum_{n \neq 2,3} C_o^{(n)} C_g^{(n)} \exp(2\pi i \gamma'^{(n)} z) \Big|^2 \qquad (6.45)$$

where $\gamma'^{(n)}$ $(n \neq 2,3)$ are the eigenvalues, $\gamma^{(n)} + iq^{(n)}$, of the standard theory and $\gamma'^{(n)}$ $(n = 2,3)$ are the eigenvalues of the sub-matrix in expression 6.39.

6.7 A Criterion for Determining which Bloch Wave Mixing Terms are Important in the Sub-Matrix Approach

In order to be able to most conveniently apply the sub-matrix approach, it is clearly desirable to have some criterion for determining which Bloch wave mixing terms should be taken into account. The method to be presented in this thesis is based on the fact that the contribution of a particular Bloch wave to the intensity of the g^{th} diffracted beam is determined by the excitation amplitude $X_o^{(i)} C_g^{(i)}$. In the standard theory where Bloch wave mixing is neglected, this amplitude is simply $C_o^{(i)} C_g^{(i)}$. Bloch wave mixing will, in general, result in a change in this excitation amplitude which can be determined, to first order, by equations 6.33 and 6.34. It can be seen from these equations that the mixing of Bloch wave i with other Bloch waves j leads to a first order correction to the g^{th} component of eigenvector i given by

$$C_g'^{(i)} = C_g^{(i)} + \sum_{j \neq i} P_j^{(i)} C_g^{(j)} \quad . \tag{6.46}$$

Since it was also shown in Section 6.5.2 that, correct to first order, the excitation coefficient $X^{(i)}$ of Bloch wave i is $C_o'^{(i)}$, the first order excitation amplitude becomes

$$\begin{aligned} X^{(i)} C_g'^{(i)} &= C_o'^{(i)} C_g'^{(i)} \\ &= [C_o^{(i)} + \sum_{j \neq i} P_j^{(i)} C_o^{(j)}][C_g^{(i)} + \sum_{j \neq i} P_j^{(i)} C_g^{(j)}] \\ &= C_o^{(i)} C_g^{(i)} + \sum_{j \neq i} P_j^{(i)} C_o^{(i)} C_g^{(j)} + \sum_{j \neq i} P_j^{(i)} C_o^{(j)} C_g^{(i)} \end{aligned} \tag{6.47}$$

where terms of second order in $P_j^{(i)}$ have been neglected. (It has been found numerically that, when the corrections to all the excitation amplitudes $C_o^{(i)} C_g^{(i)}$ $(i = 1,N)$ are considered, all the significant corrections arise from terms of first order in $P_j^{(i)}$.) If it is further assumed that $|\gamma^{(j)} - \gamma^{(n)}| >> |q^{(j)} - q^{(n)}|$ in equation

6.33a then, to a first approximation, the mixing between Bloch waves i and j leads to an imaginary correction to the excitation amplitude of Bloch wave i of

$$\Delta_g^{(i)j} = - \frac{iq^{(ij)}}{\gamma^{(j)} - \gamma^{(i)}} (C_o^{(i)} C_g^{(j)} + C_o^{(j)} C_g^{(i)}) . \qquad (6.48)$$

The mixing between the same two Bloch waves will also lead to a correction, $\Delta^{(j)i}$, to the excitation amplitude of Bloch wave j of $-\Delta^{(i)j}$. An indication of the importance of mixing between Bloch waves i and j can now be found by comparing the magnitude of $\Delta_g^{(i)j}$ to the magnitudes of the excitation amplitudes of the most important Bloch waves present. In order to facilitate this comparison, it has been found convenient to express $|\Delta_g^{(i)j}|$ as a percentage of the magnitude of the largest $C_o^{(n)} C_g^{(n)}$ term. The use of these excitation amplitude correction factors in determining the Bloch wave mixing terms to be taken into account in a particular submatrix calculation will be illustrated in Section 7.5.

6.8 Summary

In this chapter, generalized perturbation theory has been used to derive an exact solution to the matrix form of the equations of the dynamical theory of electron diffraction including absorption. It has been shown that the introduction of the imaginary potential leads to a mixing of the unperturbed Bloch waves characteristic of the system without absorption. The first and second order approximate solutions to the generalized theory were then considered and the relationship between these approaches and the perturbation approaches previously presented in the literature was discussed. A new perturbation approach, termed the sub-matrix approach, which is capable of handling non-degenerate, quasi-degenerate, and degenerate states, was then developed.

In the next chapter, the importance of Bloch wave mixing in calculations of diffracted beam intensity will be examined. The different methods for taking this mixing into account will then be compared.

CHAPTER 7

THE IMPORTANCE OF BLOCH WAVE MIXING IN CALCULATIONS OF DIFFRACTED BEAM INTENSITY

7.1 Introduction

In the previous chapter, the dynamical theory of electron diffraction including absorption was formulated in terms of a matrix $\underline{B}$ whose off-diagonal elements were seen to represent the mixing between pairs of Bloch waves. In this chapter the importance of these elements in calculations of diffracted beam intensity will be considered.

7.2 The Effect of Atomic Number on the Importance of Bloch Wave Mixing

In order to illustrate the importance of Bloch wave mixing, two sets of calculations have been carried out. In the first of these, the importance of this mixing in materials of differing atomic number has been examined. This approach has been adopted because the off-diagonal elements of the $\underline{B}$ matrix are a function of U_g', which in turn increase with atomic number (Humphreys and Hirsch, 1968). Table 8 shows the first four rows and columns of $\underline{B}$ matrices for the low atomic number material aluminum and the high atomic

Table 8. The first four rows and columns of typical $\underline{B}$ matrices for a thirteen beam calculation in gold and aluminum. The values to the right indicate the amounts by which the real and imaginary parts of the eigenvalues of these $\underline{B}$ matrices differ from the elements on the diagonal of $\underline{B}$ before diagonalization.

$\underline{B}$ matrix Gold $(\times 10^{-3})$ Å^{-1}				Change in diagonal element upon diagonalization $(\times 10^{-6})$ Å^{-1}	
				real	imaginary
7.9+0.67i	0.38i	0.34i	0.30i	-32.	0.53
0.38i	-0.3+0.24i	0.096i	0.28i	10.	0.27
0.34i	0.096i	-3.7+0.25i	0.029i	8.7	-0.71
0.30i	0.28i	0.029i	-25.+0.32i	2.9	-0.034

$\underline{B}$ matrix Aluminum $(\times 10^{-3})$ Å^{-1}				Change in diagonal element upon diagonalization $(\times 10^{-6})$ Å^{-1}	
				real	imaginary
7.3+0.023i	0.018i	0.017i	0.011i	-0.85	0.001
0.018i	-0.015+0.018i	0.009i	0.017i	-1.2	0.007
0.017i	0.009i	-3.6+0.017i	0.003i	-0.42	-0.015
0.011i	0.017i	0.003i	-25.+0.019i	-0.42	-0.011

number material gold. In calculating these matrices, thirteen reflections of the (220) systematic row were included, the deviation parameter was $\delta = 1.8$, and the accelerating voltage was 100 kV. (The $\underline{B}$ matrix elements of Table 8 include the mixing between Bloch waves one to four and are very similar to the $\underline{B}$ matrices which would be obtained from a calculation which only included the four most important reflections $\bar{2}\bar{2}0$ to 440.) It can be seen from Table 8 that the off-diagonal $\underline{B}$ elements are more than a factor of ten larger for gold than for aluminum. The Bloch wave mixing introduced by the imaginary part of the lattice potential is thus more significant for high atomic number materials than for low atomic number materials.

It is next of interest to consider the effects of the Bloch wave mixing described above on the eigenvalues of the matrix $\underline{B}$. This has been done by simply calculating the differences between the exact and standard theory eigenvalues. In carrying out these calculations, it is important to note that the amount by which the standard theory eigenvalues $(\gamma^{(i)} + iq^{(i)})$, which are equal to the diagonal elements of the matrix $\underline{B}$, are modified by the inclusion of the off-diagonal elements depends on the process of matrix diagonalization. In this process, the importance of the off-diagonal elements depends both on the values of these elements as well as on the values and differences between the diagonal elements. In order to assess the importance of the off-diagonal elements in materials of different atomic number, it is therefore important to compare $\underline{B}$ matrices in which the corresponding diagonal elements are as nearly equal as possible. Reference to Table 8 shows that the $\underline{B}$ matrices for gold and aluminum meet this requirement. The results shown in the right column of Table 8 indicate that the difference between the exact eigenvalues $\gamma'^{(n)}_i$ and the eigenvalues $(\gamma^{(i)} + iq^{(i)})$ of the standard theory are considerably greater in gold than in aluminum. This indicates that Bloch wave mixing leads to larger changes in the eigenvalues for materials of high atomic number than for materials of low atomic number.

In order to see the effect which Bloch wave mixing has on the diffracted beam intensity, the matrices of Table 8 and the methods outlined in Section 6.3 have been used to calculate the bright field, first order, and second order intensities in gold and aluminum for particular values of crystal thickness. Each intensity was then compared to the corresponding intensity found using the standard theory. The comparison involved expressing the differences between the intensities found by the two methods as a percentage of the intensity found from the standard first order theory. The average amounts by which the two theories differed for thicknesses between 0 Å and 3000 Å is shown in Table 9. It can be seen that, for each of the diffracted beam intensities considered, the differences are larger for the high atomic number material. For the diffraction conditions considered, the differences for the first order dark field are larger than those for the bright field while the second order dark field differences are the largest of all.

As an illustration of the differences just discussed, the second order dark field intensity profiles in gold obtained using the standard and exact theories are shown in Fig. 33. These profiles are typical of all those obtained in comparing the standard and exact theories in that there is very little difference in the overall shape of the profile or in the peak to peak spacing. There is, however, significant difference in the diffracted beam intensities found using the standard and exact theories. For the second order dark field profile in gold shown in Fig.33, this difference amounts to an average of 15%.

In summary, the results of this section indidate that Bloch wave mixing can have an important effect on diffracted beam intensity and that this effect is greater in high atomic number materials.

Table 9. The average percentage difference in the intensities for gold and aluminum found using the standard and exact theories. The diffraction conditions used are indicated in the text.

	Average percentage difference in intensity	
	Gold	Aluminum
Bright Field (o)	1.	.04
First Order (g)	5.	.6
Second Order (2g)	15.	2.

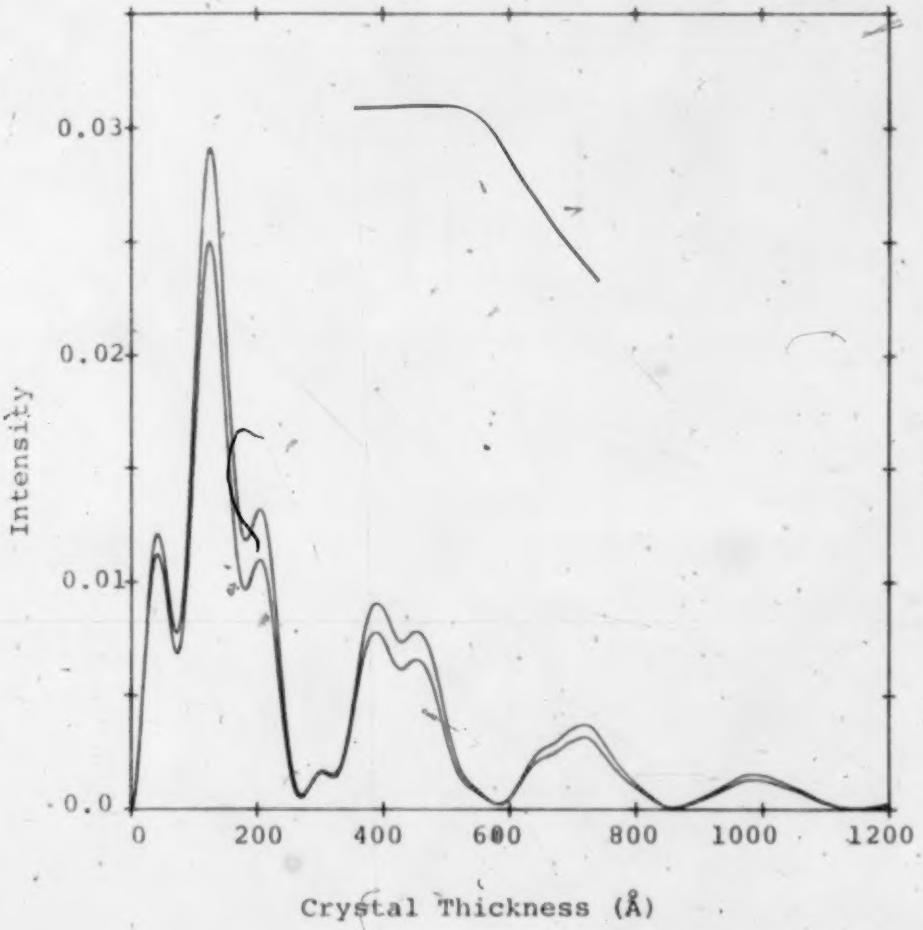

Fig. 33. The exact theory (upper curve) and standard theory (lower curve) second order dark field intensity profiles for gold at $\delta = 1.8$. The diffraction conditions used were the same as those for Tables 8 and 9.

7.3 The Effect of Quasi-Degenerate Diffraction Conditions on the Importance of Bloch Wave Mixing

7.3.1 Anomalous Absorption Effects in Diffracted Beam Intensity Profiles

As indicated in Section 7.2, the effect of the off-diagonal elements of the $\underline{B}$ matrix depends on the differences between the diagonal elements. It is therefore of interest to investigate the effects of the off-diagonal elements near the critical voltage where, for the second order reflection near its Bragg condition, two of the Bloch states have nearly equal kinetic energies. (For a more complete description of the critical voltage effect, see Chapter 8.) Under these quasi-degenerate conditions, two of the diagonal elements of the $\underline{B}$ matrix are nearly equal. In this second set of calculations, the importance of Bloch wave mixing near the critical voltage in the medium atomic number material molybdenum was investigated. The standard and exact theory profiles for the second order dark field at the critical voltage of 74 kV are shown in Fig. 34. In this calculation, thirteen reflections of the (110) systematic row were considered and the deviation parameter was $\delta = 2.004$. These diffraction conditions are close to those at

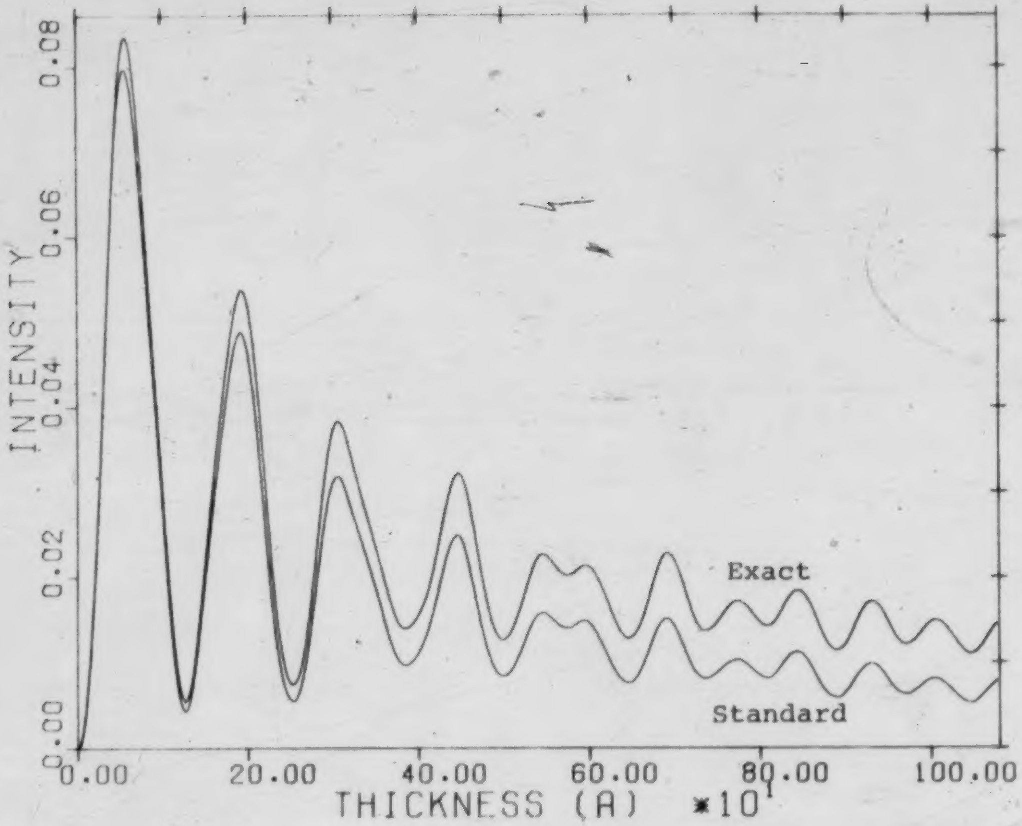

Fig. 34. The second order dark field intensity for the (110) systematic row in molybdenum at the critical voltage of 74 kV and for $\delta = 2.004$.

which Bloch waves two and three are degenerate and at which these Bloch waves make important contributions to the (220) dark field intensity (Lally et al., 1972). It can be seen from Fig. 34 that there is no appreciable change in the overall shape of the intensity profiles found using the two theories and that the peak to peak spacing is not noticeably altered. There are, however, large differences in the diffracted beam intensities found using the two theories, and these differences increase with thickness. The differences vary from a few percent in thin parts of the crystal to 100% at 1200 Å. Although some differences were also found for the bright field and first order intensity profiles, the largest differences between the two theories were for the second order dark field.

It is of interest to note in Fig. 34 that Bloch wave mixing acts in such a way that the effects of anomalous absorption are enhanced (see Section 2.2.3). (It should be noted, however, that this effect was found to arise because of changes in the eigenvectors and not from changes in the absorption coefficients $q^{(i)}$.) Accordingly, the contrast $((I_{max}-I_{min})/(I_{max}+I_{min}))$ in thick parts of the crystal is less for the exact theory than for the standard theory. This point is of interest since Lally et al. (1972) have shown that the reduction in the second order dark field intensity which occurs near the critical voltage lowers the background intensity and leads to improved visibility of defects. The results of Fig. 34 show that if this reduction in the background intensity (i.e. the improved contrast) is to be properly assessed in intensity calculations, then Bloch wave mixing should be taken into consideration.

7.3.2 The Effect of Bloch Wave Mixing on Rocking Curves

In order to determine the range of δ over which the differences between the standard and exact theories are large, rocking curve calculations have been carried out in molybdenum at the critical voltage. (A rocking curve is simply a plot of the diffracted beam intensity, at some specified crystal thickness, as a function of the deviation parameter δ. See Hashimoto et al., 1962 for example.) In these calculations, thirteen reflections of the (110) systematic row were again considered, the accelerating voltage was 74 kV (the critical voltage) and the deviation parameter was varied from $\delta = 2.0$ to $\delta = 2.1$. The second order dark field rocking curves for the crystal thickness of 3000 Å are shown in Figs. 35(a) and 35(b). It can be seen from Fig. 35(b) that there is good agreement between the standard and exact theories precisely at $\delta = 2.0$. This

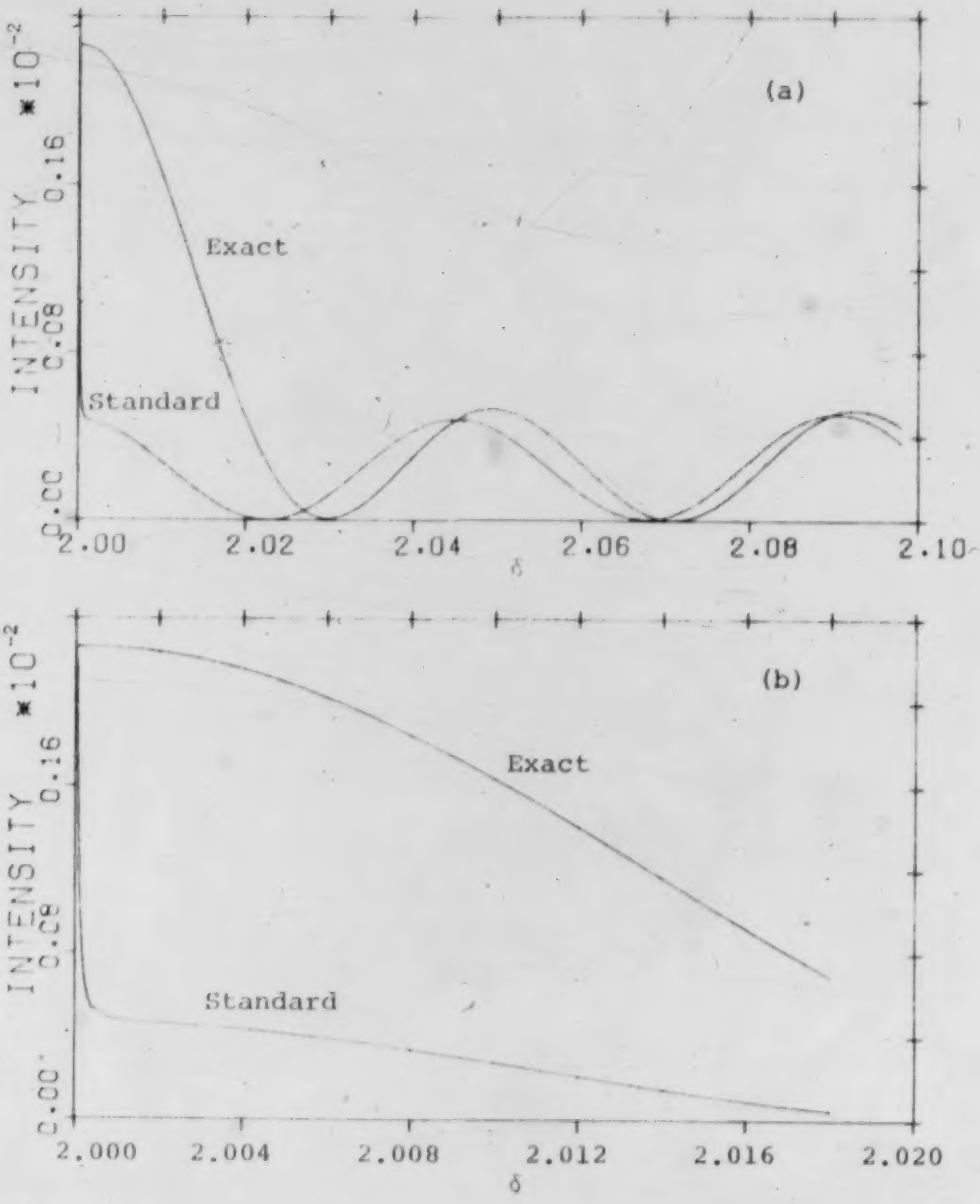

Fig. 35. Second order dark field rocking curves for molybdenum close to $\delta = 2.0$ obtained using the standard and exact theories. Thirteen systematic reflections of the (110) row were included in the calculation, the accelerating voltage was 74 kV (the critical voltage) and the crystal thickness was 3000 Å.

good agreement results from the fact that Bloch waves two and three are of opposite symmetry precisely at $\delta = 2.0$ and therefore do not mix (see Section 6.4). For $\delta > 2.0$ to approximately $\delta = 2.02$ there is a large difference between the intensities found using the two theories. For $\delta > 2.02$ the differences are still apparent but become smaller. Clearly, the results of Fig. 35 indicate that Bloch wave mixing is important at the critical voltage over a range of values of δ close to $\delta = 2.0$ and should be taken into account in rocking curve calculations. This finding is important since standard theory rocking curves have been used by Lally et al. (1972) to illustrate the reduction in the second order dark field intensity which occurs at the critical voltage.

Rocking curves were also obtained at the critical voltage but for values of δ close to the symmetry position ($\delta = 0.0$). Under these diffraction conditions, Bloch waves two and three are again quasi-degenerate. The standard and exact theory rocking curves obtained for the bright field at a thickness of 3000 Å are plotted in Fig. 36. It can be seen from this figure that, for small non-zero values of δ, the intensity calculated using the exact theory is considerably less than the intensity obtained using the

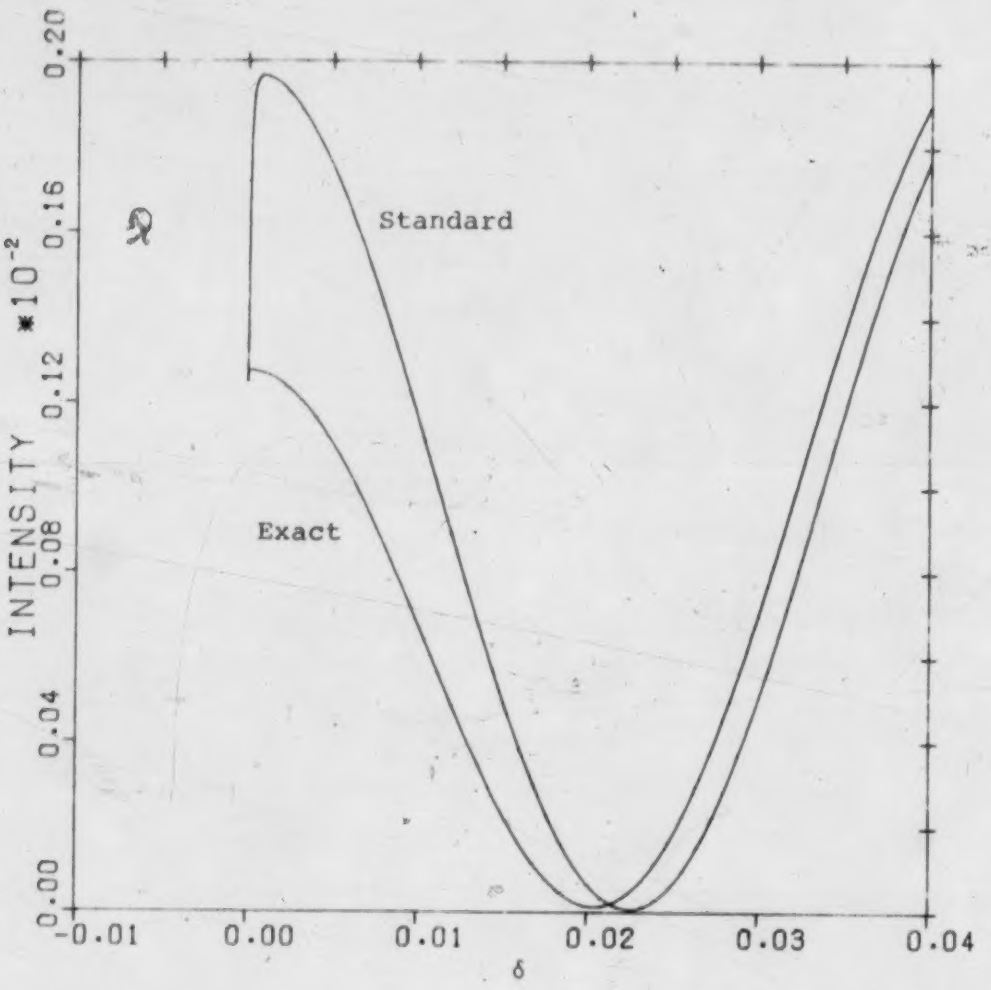

Fig. 36. Bright field rocking curves for molybdenum close to the symmetry position ($\delta = 0.0$) obtained using the standard and exact theories. Thirteen reflections of the (110) systematic row were considered, the accelerating voltage was 74 kV (the critical voltage) and the crystal thickness was 3000 Å.

standard theory. (This is the reverse of the situation close to $\delta = 2.0$ in Fig. 35 where the standard theory intensity was less than that of the exact theory.) However, good agreement was obtained precisely at $\delta = 0.0$ because, for this orientation, Bloch waves two and three are of opposite symmetry and therefore do not mix. Significant differences were also found between the standard and exact theories in rocking curves obtained from the first and second order dark field intensities.

In order to examine whether it is necessary to be very close to the critical voltage in order to obtain large differences between the standard and exact theories, calculations were also carried out at voltages somewhat removed from the critical voltage. The (220) rocking curve for molybdenum at a thickness of 1000 Å is plotted in Fig. 37 for δ close to 2.0 and for an accelerating voltage of 100 kV. It can be seen from this figure that significant differences between the standard and exact theories still occur. As would be expected, these differences were found to decrease as calculations were carried out for voltages further from the critical voltage. However, good agreement between the two theories far from the critical voltage could only be obtained in low atomic number materials.

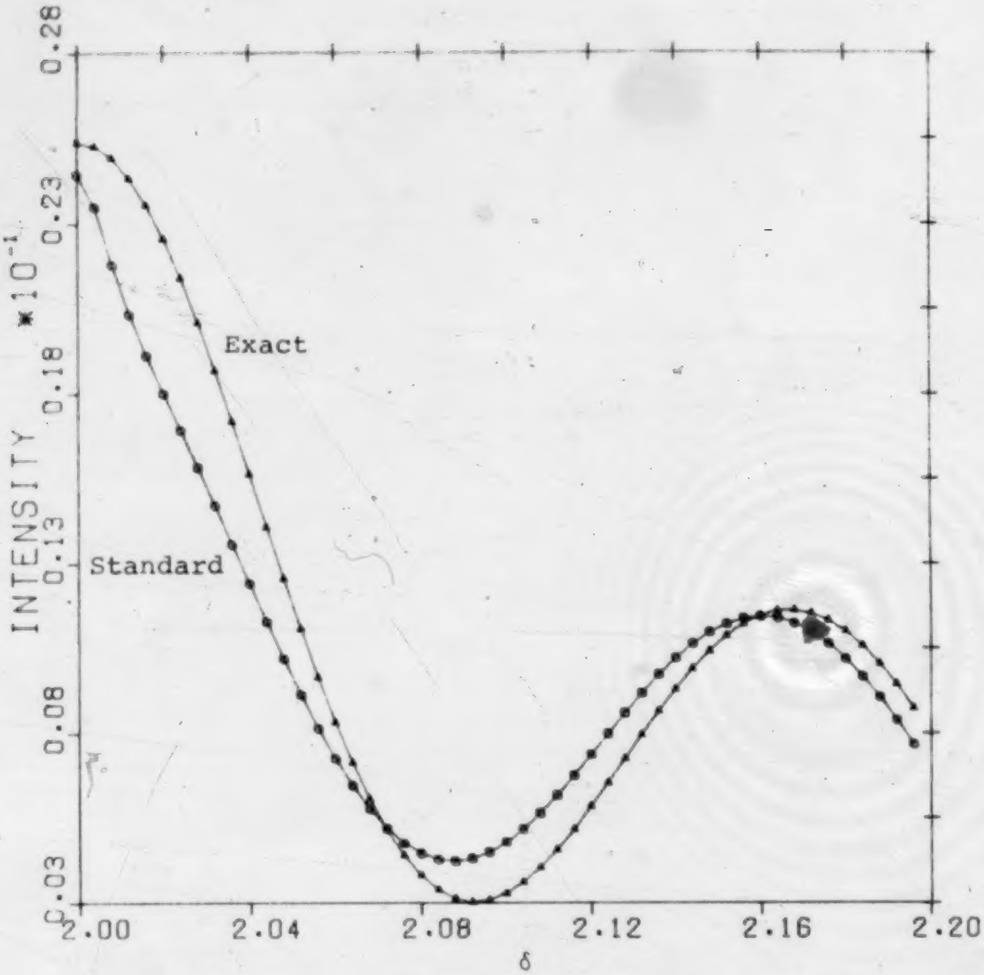

Fig. 37. Second order dark field rocking curves for molybdenum close to $\delta = 2.0$ obtained using the standard and exact theories. Thirteen systematic reflections of the 110 row were considered, the accelerating voltage was 100 kV, and the crystal thickness was 1000 Å.

In conclusion, it can be seen from the results presented in this section that Bloch wave mixing can have a very significant effect on the diffracted beam intensity when calculations are carried out under quasi-degenerate diffraction conditions.

7.4 Discussion

The calculations described in Section 7.3 have shown that the importance of Bloch wave mixing is determined to a very considerable extent by how close certain of the diagonal elements of the $\underline{B}$ matrix are to one another. Since the values of the diagonal elements for a given material are in turn determined by the crystal orientation and the accelerating voltage, the importance of including the off-diagonal elements of the $\underline{B}$ matrix in a given calculation also depends on these factors. In attempting to assess the importance of Bloch wave mixing, it is therefore important for the electron microscopist to note that there is a wide variety of diffraction conditions, in addition to those at the critical voltage mentioned above, which give rise to relatively close values of the diagonal elements of the matrix $\underline{B}$. A familiar example is the case where a high order systematic reflection is in the Bragg condition. Under these circumstances, some of the Bloch waves which contribute significantly to the intensity of certain of the diffracted beams are associated with branches of the dispersion surface which very nearly touch (i.e., the Bloch waves have nearly equal eigenvalues $\gamma^{(i)}$). Since the absorption coefficients $q^{(i)}$ are normally much less than the eigenvalues $\gamma^{(i)}$, this would imply that the values of the diagonal elements of the $\underline{B}$ matrix $(\gamma^{(i)} + iq^{(i)})$, associated with these Bloch waves, would be nearly equal.

Another example, not so familiar but perhaps more important, is the case where non-systematic reflections are taken into account. It has been shown by several authors (Gjønnes and Høier, 1971; Cann and Sheinin, 1972, 1974A, 1974B; Sheinin and Cann, 1973) that at orientations close to a non-systematic reflection in the Bragg condition, Bloch wave degeneracies or touching branches of the dispersion surface occur. Again, this means that, for the Bloch waves concerned, equal or nearly equal values of the real parts of the diagonal elements of the $\underline{B}$ matrix will be obtained. Sheinin and Cann (1973) have shown that at such degeneracies, effects of Bloch wave mixing are considerable. The calculations in Section 7.3.2 for the quasi-degenerate case near the critical voltage would indicate that the Bloch wave mixing which would occur near the degeneracy of the non-systematic case would also give rise to significant effects. It is clear from these considerations, therefore, that there are many possible diffraction conditions for which the effects of Bloch wave mixing should be taken into account.

7.5 A Comparison of Approximate and Exact Methods for Taking Absorption into Account

In this section the standard, second order, sub-matrix and exact methods of taking absorption into account will be compared. The comparison has been carried out by calculating diffracted beam intensities in gold for diffraction conditions where no Bloch wave degeneracies were involved, and also in molybdenum close to a Bloch wave degeneracy.

In the gold calculations, thirteen reflections of the (220) systematic row were considered, the accelerating voltage was 100 kV and the deviation parameter was $\delta = 1.8$. (These are the same diffraction conditions as were used for the gold calculations in Section 7.2.) In order to determine the size of the sub-matrix to be used, the excitation amplitude correction factors derived in Section 6.7 were calculated. The results obtained for bright-field, first order dark field and second order dark field are shown in Table 10. It is clear from this table that, for these diffraction

Table 10. Parameters indicating the effect of Bloch wave mixing on the standard theory excitation amplitudes $C_o^{(i)} C_h^{(i)}$ in gold. The effect of mixing between pairs of Bloch waves not shown was small and was therefore neglected.

	Bloch wave i,j	$\Delta_h^{(i)j}$ (%)
Bright Field (h = o)	1,2	2.3
	2,3	0.60
	2,4	0.17
First Order Dark Field (h = g)	1,2	16.
	1,3	1.6
	2,3	1.3
Second Order Dark Field (h = 2g)	2,3	25.
	1,2	7.8
	1,3	6.1

conditions, the effect of Bloch wave mixing on diffracted beam intensity should increase with increasing order of the reflection considered. This is in good agreement with the differences found between the standard and exact theories for this orientation (see the gold results in Table 9). Table 10 also shows that in second order dark field calculations, for example, only mixing between Bloch waves 1, 2 and 3 need be taken into account. Accordingly, in calculations of second order dark field intensity, the sub-matrix used was analogous to the one shown in expression 6.39, Section 6.6, except that values of $q^{(ij)}$, $i = 1,3$ and $j = 1,3$, were included. The results obtained from the calculations of diffracted beam intensity showed that the second order theory was in better agreement with the exact theory than was the standard theory. The best agreement, however, was found by using the sub-matrix approach. For example, at a thickness of 450 Å, it was found that the exact theory differed from the standard, second order, and sub-matrix theories by 15%, 8.5% and 0.24% respectively. Although there is very good agreement between the sub-matrix and exact theories, this agreement could be improved by expanding the size of the sub-matrix. In the limit as the sub-matrix size becomes equal to that of the $\underline{B}$ matrix, the sub-matrix theory becomes equivalent to the exact theory.

In comparing the different theories it is also important to compare the computing times which each theory requires. From a numerical point of view, there is no point in using an approximate theory if the exact theory is just as fast. The total computing time which each of the theories required in order to calculate the eigenvalues and eigenvectors of the $\underline{A} + i\underline{A}'$ matrix and the excitation coefficients was therefore obtained. For the gold calculations just considered, it was found that the sub-matrix approach was the fastest and that the times taken by the second order and the exact theories were larger by factors of two and three respectively. Clearly, the sub-matrix approach can lead to a significant saving of computing time while still giving results in excellent agreement with the exact theory.

In order to compare the different theories close to a Bloch wave degeneracy, the standard, second order, sub-matrix and exact theories were used to calculate second order dark field rocking curves in molybdenum at the critical voltage. In these calculations, the only large excitation amplitude correction factor was found to result from mixing between Bloch waves two and three. Accordingly, a sub-matrix was used which took only mixing between these Bloch waves into account. The rocking curves which were obtained are shown in Fig. 38. In this calculation, thirteen reflections of the (110) systematic row were considered, the second order dark field intensity was calculated at a thickness of 3000 Å, and the accelerating voltage was 74 kV (the critical voltage). It can be seen from Fig. 38 that the sub-matrix approach is a very good approximation for all values of δ while the second order theory breaks down close to $\delta = 2.0$, i.e. close to a Bloch wave degeneracy. As already discussed in Section 7.3, the standard theory is a poor approximation over this range of orientations except for $\delta = 2.0$. An examination of the computing times required by the different theories showed that the sub-matrix approach was much faster than either the second order or exact theories. These results obtained close to a Bloch wave degeneracy again illustrate that the sub-matrix approach can give a considerable saving in computing time and still give very close agreement with the exact theory.

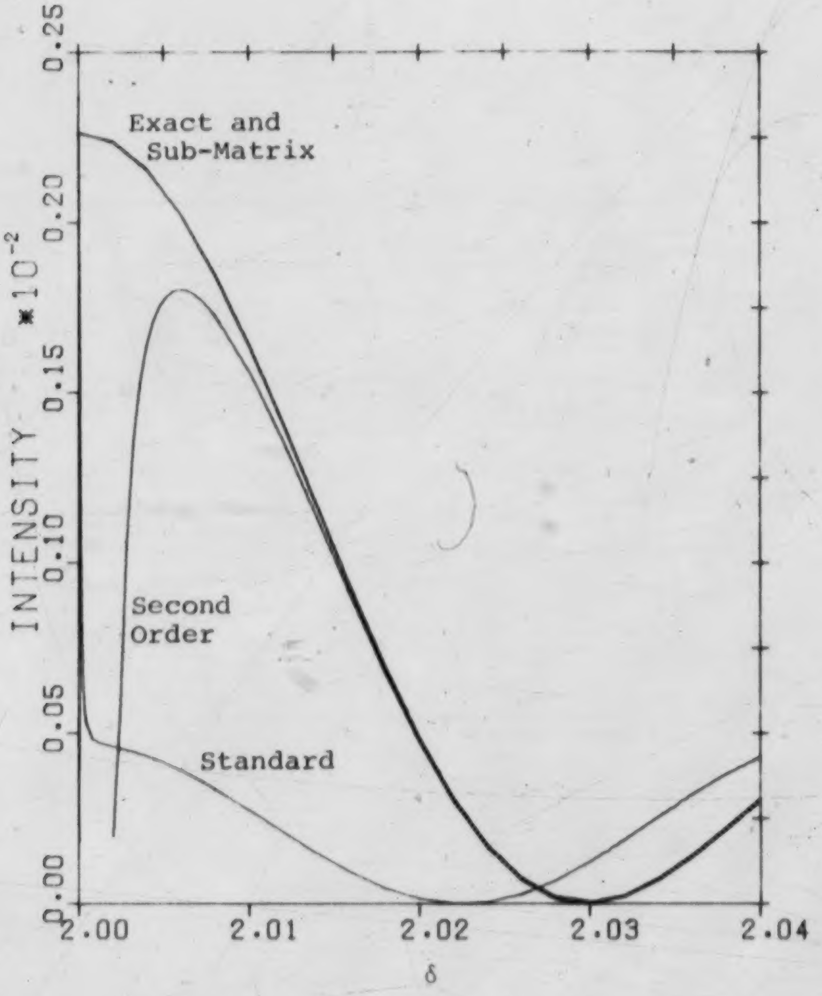

Fig. 38. Second order dark field rocking curves for molybdenum close to $\delta = 2.0$ obtained using the standard, second order, sub-matrix, and exact theories. Thirteen systematic reflections of the (110) row were included, the accelerating voltage was 74 kV (the critical voltage) and the crystal thickness was 3000 Å.

CHAPTER 8

THE IMPORTANCE OF BLOCH WAVE MIXING IN THE CRITICAL VOLTAGE EFFECT

8.1 Introduction

In the last chapter, it was found that the effects of Bloch wave mixing are important when high atomic number materials are considered or when the crystal is oriented so that quasi-degenerate diffraction conditions are obtained. It is next of interest to examine a particular phenomenon in which this Bloch wave mixing is important and must be taken into account in order to obtain a physical understanding of the contrast mechanisms involved. The critical voltage effect, which has received considerable attention in the literature in the past several years, is such a phenomenon and will therefore be considered in this chapter.

8.2 A Review of the Critical Voltage Effect

Before examining the role of Bloch wave mixing in the critical voltage effect, it is first of interest to briefly review the physical nature of this effect. The critical voltage effect was discovered experimentally by Nagata and Fukuhara (1967) and Uyeda (1968).

These authors found that for $\delta = 2.0$ and a certain incident electron energy, the intensity of a second order reflection became very weak. This reduction in intensity was also observed by Watanabe and Uyeda (1968) in the vanishing of second order Kikuchi lines. Following Metherell and Fisher (1969) and Lally et al. (1972) this effect has come to be known as the critical voltage effect.

The critical voltage effect has generated a great deal of interest in the literature because it has been found that the voltage at which the minimization in second order intensity occurs (i.e. the critical voltage) is very sensitive to values of atomic scattering factors, structure factors, and the lattice parameter. The effect has therefore been used in the accurate determination of atomic scattering factors, Debye temperatures, the degree of ordering of partially ordered alloys, and lattice parameter changes (see for example, Watanabe et al., 1968; Lally et al., 1972; Butler, 1972, 1973; Thomas et al., 1974). The effect has also been found to be useful in increasing the visibility of defect contrast (Lally et al., 1972).

There are two approaches which have been used in the literature to explain the minimization in the second order dark field intensity at the critical voltage. The first approach is due to Uyeda (1968) and is based on Bethe's second order approximation (Bethe, 1928). In this approach, it is assumed that two strong beams, o and 2g, are included in the $\underline{A}$ matrix and that the effect of other weak beams such as g can be taken into account by calculating a modified value ${}^{m}U_{2g}$ for the Fourier coefficient U_{2g}. (See Uyeda (1968) for the expression for this modified Fourier coefficient.) For a particular value of the accelerating voltage, ${}^{m}U_{2g}$ is found to go to zero and the $\underline{A}$ matrix becomes diagonal. Since the eigenvector matrix $\underline{C}$ is then a unit matrix, the excitation amplitudes $C_o^{(i)}C_{2g}^{(i)}$ of the two Bloch waves are zero and no diffracted beam is obtained.

However, this first approach indicates that the intensity I_{2g} becomes zero at the critical voltage whereas in fact the intensity decreases to some non-zero value (Lally et al., 1972). In order to more accurately describe the critical voltage effect, a second explanation based on Bloch wave symmetry arguments was presented by Metherell and Fisher (1969) and Lally et al. (1972). This second approach considers the contribution which each Bloch wave makes to the diffracted beam intensity

$$I_{2g} = \left|\sum_i C_o^{(i)}C_{2g}^{(i)}\exp(2\pi i(\gamma^{(i)}+iq^{(i)})z)\right|^2 . \qquad (8.1)$$

For δ exactly equal to 2.0 it is found that, at the top surface of the crystal, Bloch waves one, two and three are primary Bloch waves and of these, Bloch wave one is the least important. Furthermore, it is found that the absorption coefficient of Bloch wave one is much larger than those of Bloch waves two and three. The diffracted beam intensity expression 8.1 can therefore be written

$$I_{2g} = \left| \sum_{i=2,3} C_o^{(i)} C_{2g}^{(i)} \exp(2\pi i(\gamma^{(i)} + iq^{(i)})z) + \Delta \right|^2 \qquad (8.2)$$

where Δ represents the contribution of all Bloch waves except two and three. The magnitude of Δ is very small unless the crystal is very thin, in which case Bloch wave one can make a significant contribution.

The reduction in the intensity which occurs at the critical voltage can now be understood by examining the excitation amplitudes and the eigenvalues of Bloch waves two and three in equation 8.2. The values for these parameters at the exact Bragg condition of the (222) reflection in copper close to the critical voltage are shown in Fig. 39. It can be seen from this figure that as the accelerating voltage is increased from 250 to 390 kV, the excitation amplitudes of Bloch waves two and three remain nearly equal in magnitude and of opposite sign while the eigenvalues of these Bloch waves approach each other in value. At 390 kV the eigenvalues are degenerate and the excitation amplitudes of Bloch

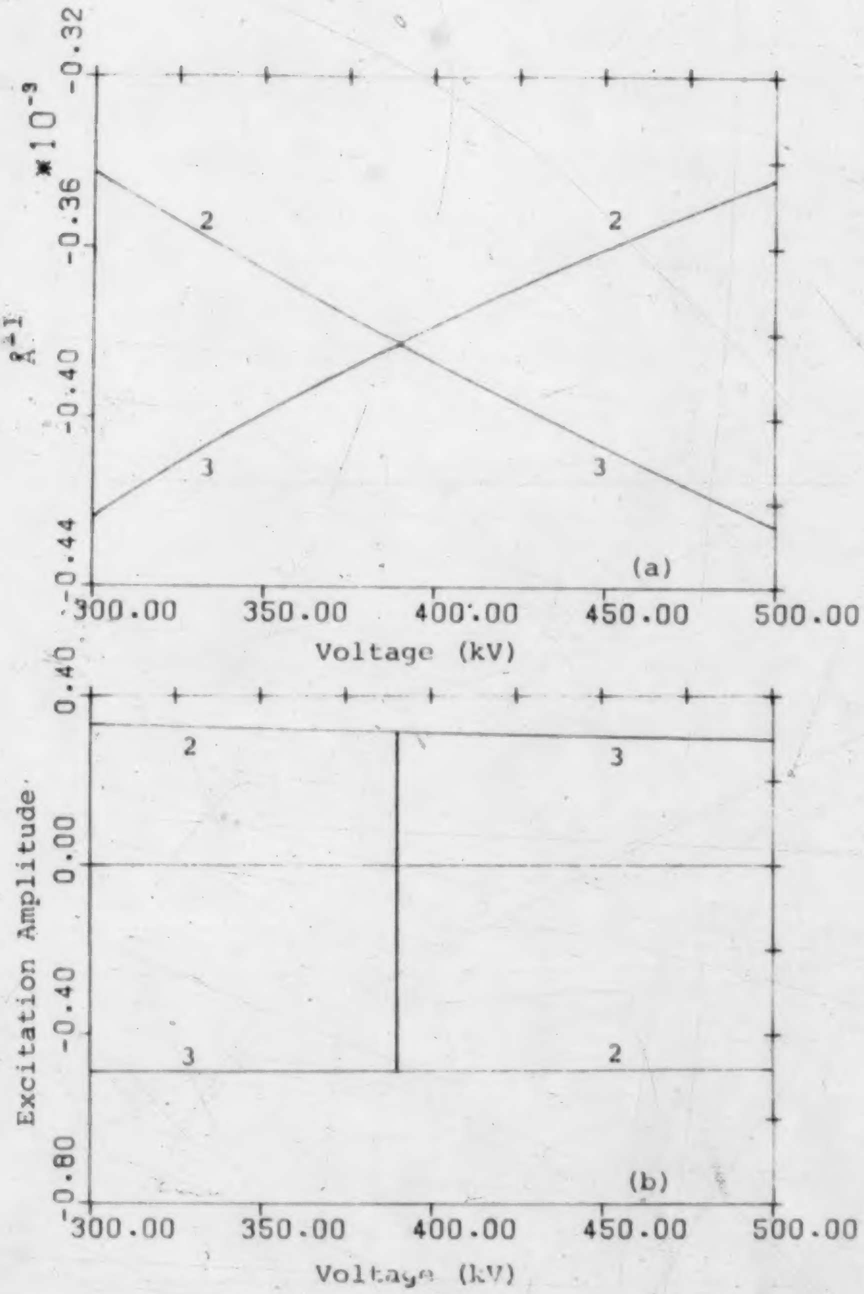

Fig. 39. This figure shows (a) the eigenvalues and (b) the excitation amplitudes for Bloch waves two and three close to the critical voltage in copper. Thirteen reflections of the (111) systematic row were taken into account and δ was taken to be 2.0.

waves two and three are interchanged. This interchange results from a change in the symmetry of Bloch waves two and three (for example, Bloch wave two is symmetric below 390 kV and becomes anti-symmetric above 390 kV). Lally et al. (1972) have defined the voltage at which this change in symmetry occurs to be the critical voltage. With an increase in accelerating voltage beyond the critical voltage, the excitation amplitudes of Bloch waves two and three remain nearly equal in magnitude and of opposite sign while the difference between the eigenvalues increases.

The reason for the reduction in the diffracted beam intensity I_{2g} at the critical voltage can now be understood by noting that at the critical voltage $\gamma^{(2)} = \gamma^{(3)}$ while the excitation amplitudes of these Bloch waves are nearly equal in magnitude and are of opposite sign. It can be seen from equation 8.2, therefore, that the contributions made by these two Bloch waves will interfere destructively and a minimum in the intensity results. An example of this reduction in the diffracted beam intensity is shown in Fig. 40. In obtaining the results presented in this figure, thirteen reflections of the (111) systematic row were included, δ was taken to be exactly 2.0 and the intensity was calculated for a crystal thickness of 5000 Å. It can be seen from Fig. 40 that the intensity is very

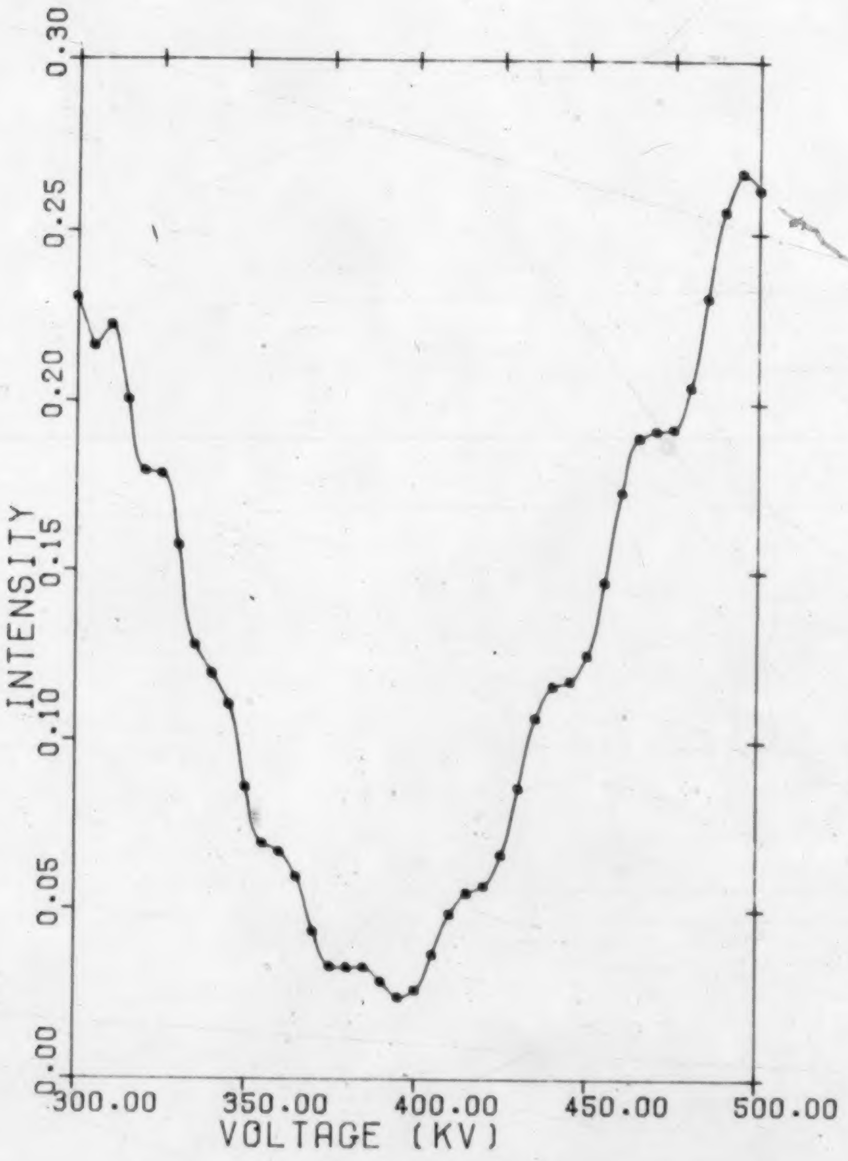

Fig. 40. The critical voltage intensity minimum for the (222) intensity in copper.

much reduced close to the critical voltage of 390 kV but is not equal to zero. This result is in better agreement with experiment than Bethe's second order approximation. (As indicated earlier in this section, the approach based on Bethe's approximation shows that the intensity becomes zero at the critical voltage.) Therefore, Bethe's approximation has been restricted to determining approximate values for the critical voltage (Uyeda, 1968; Watanabe et al., 1968), while the second approach based on the many-beam theory has been used in the detailed investigations into the critical voltage effect (Metherell and Fisher, 1969; Lally et al., 1972; Thomas, 1972; Butler, 1972, 1973; Thomas et al., 1974; Serneels and Gevers, 1974; Gevers et al., 1974, 1975; Andrew and Sheinin, 1974A, 1974B).

8.3 Critical Voltage Effects for Small Departures from the Exact Second Order Bragg Condition

As indicated in the previous section, the critical voltage is defined in the literature as being the voltage at which the symmetries of Bloch waves two and three are interchanged. This change in symmetry occurs at the exact Bragg condition of a second order reflection when Bloch waves two and three are degenerate. It has previously been shown by Serneels and Gevers (1974) that, for δ exactly equal to 2.0, the mixing between these degenerate Bloch waves is not important because $q^{(23)} = 0$ (see also Section 6.4). However, the diffraction conditions which give rise to the exact degeneracy cannot in general be obtained experimentally because of such factors as beam divergence, specimen bending and the lack of precision which is inherent in determining the crystal orientation. Furthermore, it has been found by the author of this thesis that conditions equivalent to the exact degeneracy cannot be attained in numerical calculations of diffracted beam intensity at the critical voltage. This arises because the number of significant figures in computer calculations is limited to some finite value. It was therefore felt to be of interest to investigate the importance of Bloch wave mixing on the critical voltage effect at small departures from the exact Bragg condition of the second order reflection. The results of this investigation will be presented in this section.

8.3.1 An Examination of the Critical Voltage Intensity Minimum at Small Departures from $\delta = 2.0$

The first question which arises is to what extent does the critical voltage intensity minimum occur for $\delta \neq 2.0$. As will be seen in this section, the answer depends on the material concerned. In some materials there is no intensity minimum, while in others, the minimum persists for a range of δ roughly between $1.95 < \delta < 2.05$. As an illustration of these two cases, the results for molybdenum and copper obtained from the standard, sub-matrix, and exact theories are discussed in this section. In the sub-matrix approach, only mixing between Bloch waves two and three was included. Furthermore, high atomic number materials were not considered. The reason for this was that any observed effects of Bloch wave mixing could be associated with quasi-degenerate diffraction conditions and not with atomic number (see Section 7.2). Only the results from the standard and sub-matrix approaches will be presented since the intensities obtained from the latter method and from the exact method were in good agreement. Also, only values of $\delta \geq 2.0$ will be considered. It should be noted, however, that the results to be presented are identical to those obtained for $\delta \leq 2.0$.

8.3.1 (a) An examination of the critical voltage intensity minimum in molybdenum

The second order reflection chosen for the first set of calculations was the (220) reflection in molybdenum. Thirteen beam systematic calculations were carried out for various crystal thicknesses and deviation parameters ranging from $\delta = 2.01$ to $\delta = 2.0$. Typical results of the variation of the intensity of a second order reflection with accelerating voltage for small values of the deviation parameter are shown in Fig. 41. The intensity is plotted for a thickness of 3000 Å and a deviation parameter of δ = 2.001. An examination of the curves in Fig. 41 shows that there is a large discrepancy between the results of calculations based on the standard and sub-matrix theories. The calculation based on the standard method for taking absorption into account shows a distinct intensity minimum at 74 kV. This minimum lies in the same voltage range as does the critical voltage defined by the symmetry interchange of Bloch waves two and three. Clearly, if only a calculation based on the standard method was performed, there would be a strong temptation to conclude that the intensity minimum in Fig. 41 was the minimum usually associated with the critical voltage. That such a conclusion would be in error can be seen from the intensity versus voltage curve obtained from the sub-matrix theory. This curve shows in fact that no minimum occurs in the voltage range around 74 kV and that the minimum obtained from the standard method is therefore spurious.

It is next of interest to ask how the spurious intensity minimum obtained from the standard approach

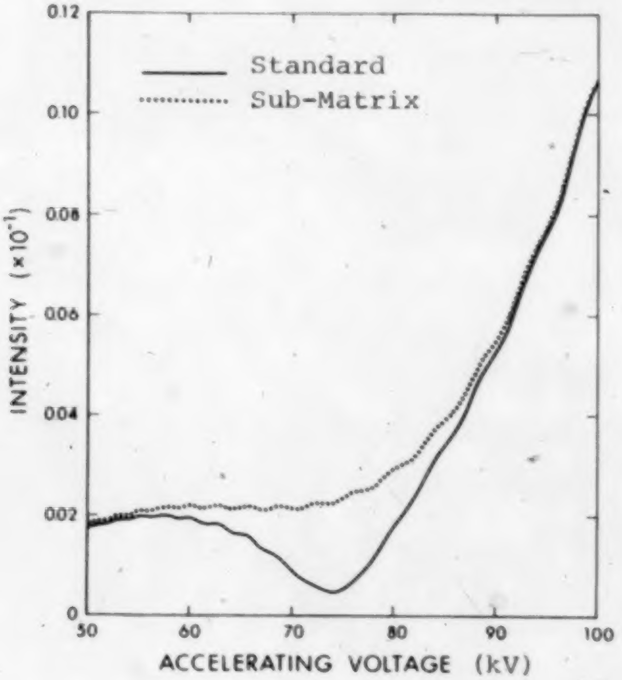

Fig. 41. The variation of the (220) intensity in molybdenum as a function of accelerating voltage for $\delta = 2.001$.

changes as the degeneracy is approached. In order to answer this question, calculations similar to those shown in Fig. 41 have been carried out for deviation parameters decreasing to $\delta = 2.0$. It has been found that the depth of the minimum remains essentially the same as the degeneracy is approached. However, the range of accelerating voltages over which the minimum occurs (i.e., the range of accelerating voltages over which the intensities obtained from the standard and sub-matrix theories are appreciably different) decreased as the degeneracy was approached. For example, for a deviation parameter of $\delta = 2.00007$ the two theories depart significantly over a voltage range of approximately 4 kV, while at $\delta = 2.001$ the corresponding voltage range was 30 kV.

The question then arises as to whether the difference between the standard and sub-matrix theories persists at the exact degeneracy. In order to answer this question, analyses based on both analytical considerations and numerical calculations were carried out. The analytical approach was based on a Bloch wave symmetry argument and showed that for centrosymmetric crystals, $q^{(23)} = 0$ and the sub-matrix theory reduced to the standard theory, i.e., the spurious minimum disappeared. The numerical calculations showed that the spurious minimum persisted even when the deviation parameter was set equal to 2.0, but that the width of the minimum depended on the numerical precision used in calculating the eigenvalues and eigenvectors. For example, the Jacobi method of matrix diagonalization (SSP, 1970) used in an IBM system 360 Fortran IV single precision routine (approximately 7.2 significant decimal digits) produced a spurious minimum whose width was approximately 0.05 kV when the deviation parameter was set exactly equal to 2.0. The same routine in double precision, however, reduced the width of the spurious minimum to 1×10^{-9} kV. These results indicate that the spurious minimum will always remain in numerical calculations based on perturbation theory for the non-degenerate state, but for high precision it will become very narrow. It is clear in comparing the numerical results with the conclusions based on an analytical approach to the problem, that even though the deviation parameter can be set equal to 2.0 in numerical calculations, the effective value of the deviation parameter is not exactly 2.0. Accordingly, the standard theory should not be used in numerical calculations close to the critical voltage even when the exact Bragg condition of the second order reflection is satisfied.

8.3.1 (b) An examination of the critical voltage intensity minimum in copper

Calculations were also carried out for the (222) intensity in copper at small departures from the exact second order Bragg condition. The critical voltage minima obtained with the standard and sub-matrix theories for a crystal thickness of 5000 Å are shown in Fig. 42. Thirteen reflections of the (111) row were included in this calculation and the deviation parameter δ was taken to be 2.002. It can be seen from this figure that a critical voltage intensity minimum is obtained from both theories but that the minimum is more pronounced for the standard theory. The range of voltages over which the standard and sub-matrix theories differed significantly was found to decrease as values closer to $\delta = 2.0$ were considered. (However, it should be noted that the numerical results obtained using the standard and sub-matrix theories again differed for a very small voltage range when the deviation parameter was set equal to 2.0. The range of voltages over which the differences occurred were similar to those discussed for molybdenum in the previous section and were found to depend on the numerical precision of the matrix diagonalization routines.)

When examining the critical voltage intensity minimum at small deviations from the exact Bragg condition of the second order reflection, the question arises

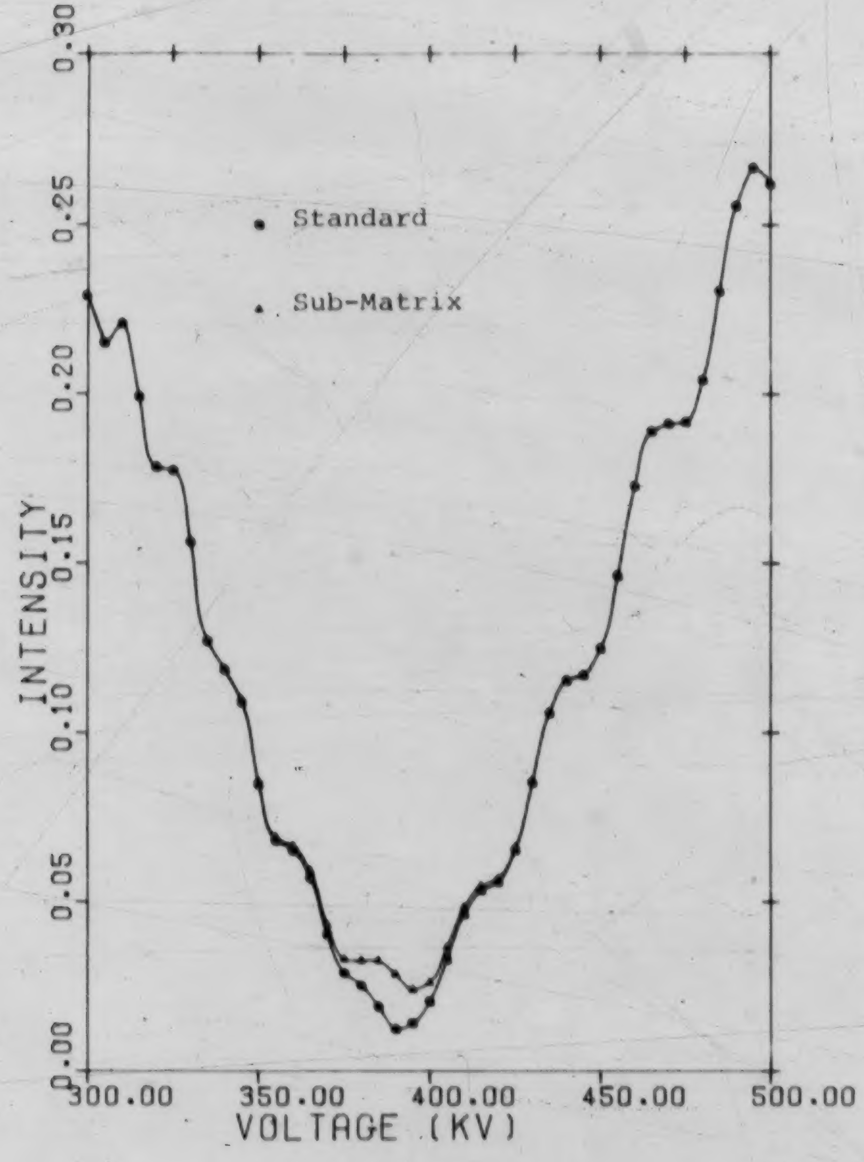

Fig. 42. The variation of the (222) intensity in copper as a function of accelerating voltage for $\delta = 2.002$.

of the range of values of δ over which the critical voltage intensity minimum is obtained. It has already been seen that a minimum is obtained for the (222) intensity in copper for $2.0 \leq \delta \leq 2.002$. The variation in the intensity with accelerating voltage for the standard and sub-matrix theories at $\delta = 2.02$ is shown in Fig. 43. It can be seen from this figure that a distinct intensity minimum is still obtained. Furthermore, the standard and sub-matrix theories differ significantly over a wider voltage range than for $\delta = 2.002$ in Fig. 42. As values of $\delta > 2.02$ were considered, it was found that the agreement between the two theories improves but the intensity minimum becomes less pronounced.

8.3.2 The Standard Theory Mechanism for the Critical Voltage Effect

In the previous section it was found that a critical voltage intensity minimum can occur for small departures from the exact second order Bragg condition. The Bloch wave mechanism which gives rise to this minimum will be examined in this and the following section.

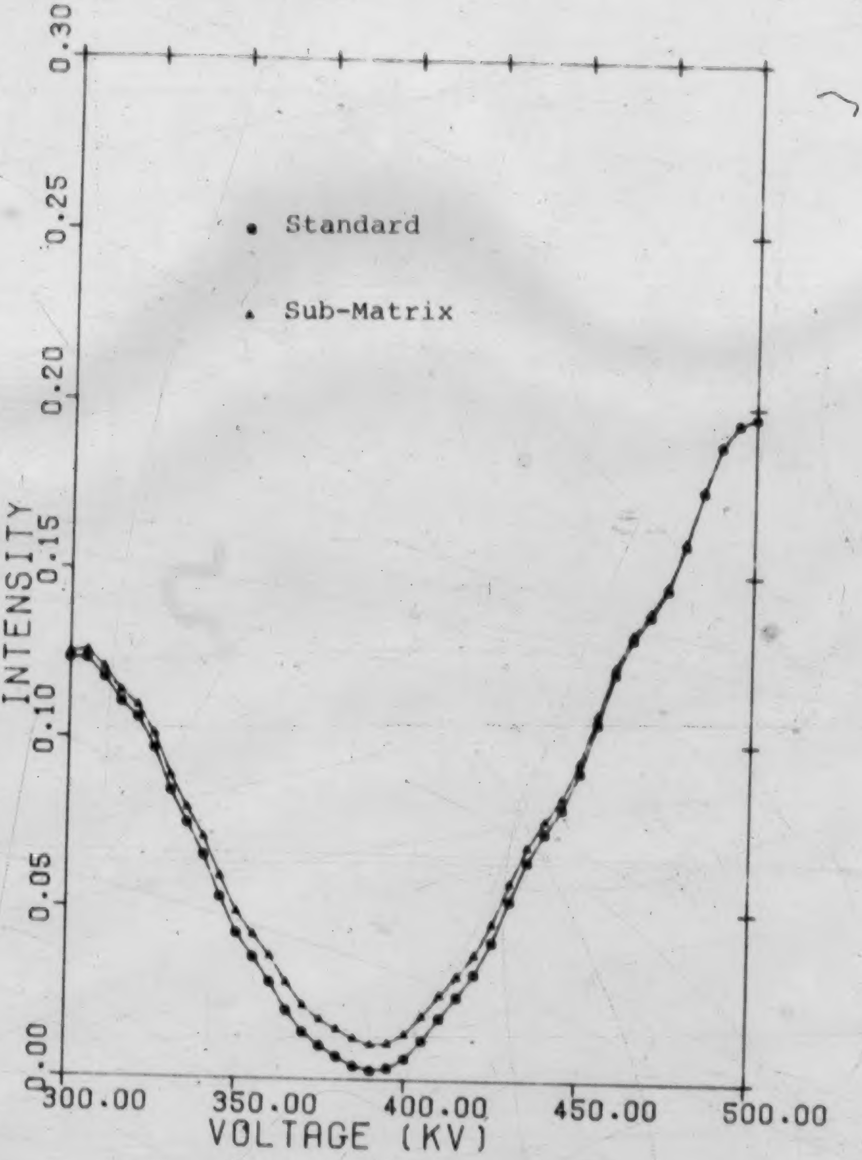

Fig. 43. The variation of the (222) intensity in copper as a function of accelerating voltage for $\delta = 2.02$.

It is first important to illustrate that the Bloch wave mechanism for small departures from the exact second order Bragg condition is in fact different from the mechanism at exactly $\delta = 2.0$. This can be done by examining the excitation amplitudes of Bloch waves two and three obtained by using the standard theory. In order to help visualize the change in symmetry of these Bloch waves at the critical voltage and for δ exactly equal to 2.0, it is useful to plot the values of $C_o^{(2)}C_{2g}^{(2)}$ and $C_o^{(3)}C_{2g}^{(3)}$ as a function of accelerating voltage. Such a plot for the (222) reflection in copper is shown in Fig. 44(a). The change in symmetry and the critical voltage correspond to the vertical line in this figure and occur at about 390 kV. The critical voltage mechanism obtained from the standard theory for δ exactly equal to 2.0 has already been discussed in Section 8.2. (It was noted in Section 8.2 that the intensity minimum arises because $\gamma^{(2)} = \gamma^{(3)}$ at the critical voltage and the excitation amplitudes of these Bloch waves are nearly equal in magnitude and are opposite in sign.)

In order to compare the critical voltage mechanism considered in this section with that to be considered in the following section, it is convenient

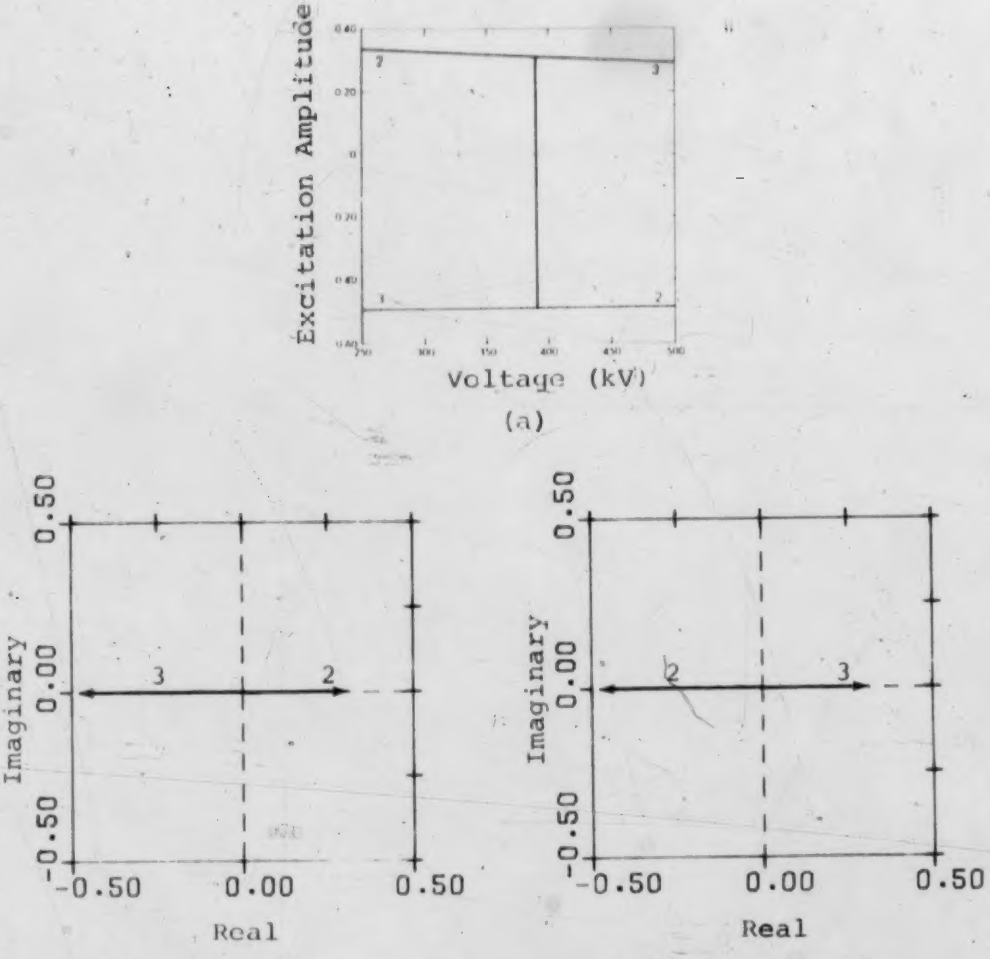

(a)

(b) V = 380 kV

(c) V = 400 kV

Fig. 44. (a): A plot of $C_0^{(i)} C_{2g}^{(i)}$ (i = 2,3) as a function of accelerating voltage at the exact Bragg condition of the reflection 2g; (b) and (c): Plots of $C_0^{(i)} C_{2g}^{(i)}$ (i = 2,3) in the complex plane for voltages below and above the critical voltage.

to plot the values of $C_o^{(2)}C_{2g}^{(2)}$ and $C_o^{(3)}C_{2g}^{(3)}$ in the complex plane. The values of these excitation amplitudes for voltages below and above the critical voltage are shown in Figs. 44(b) and 44(c). It can be seen from Fig. 44(b) that, below the critical voltage, the excitation amplitude of Bloch wave three is negative while that of Bloch wave two is positive (i.e. the two excitation amplitudes are out of phase by 180°). For voltages above the critical voltage, the signs of the excitation amplitudes are reversed. This change in sign occurs when Bloch waves two and three interchange symmetries at precisely the critical voltage.

It is next of interest to ask how the values of $C_o^{(2)}C_{2g}^{(2)}$ and $C_o^{(3)}C_{2g}^{(3)}$ vary with accelerating voltage for a small deviation from the exact Bragg condition. The results obtained for $\delta = 2.002$ are shown in Fig. 45. In Fig. 45(a) the excitation amplitudes have been plotted as a function of accelerating voltage, while in Figs. 45(b), (c) and (d), the excitation amplitudes for 300 kV, 390 kV and 480 kV have again been plotted in the complex plane. It can be seen from this figure that, in contrast to the case for δ exactly equal to 2.0, the interchange of excitation amplitudes of Bloch waves two and three does not occur at a particular accelerating voltage. Rather, this change occurs over a range of accelerating voltages equal to about 50 kV at $\delta = 2.002$.

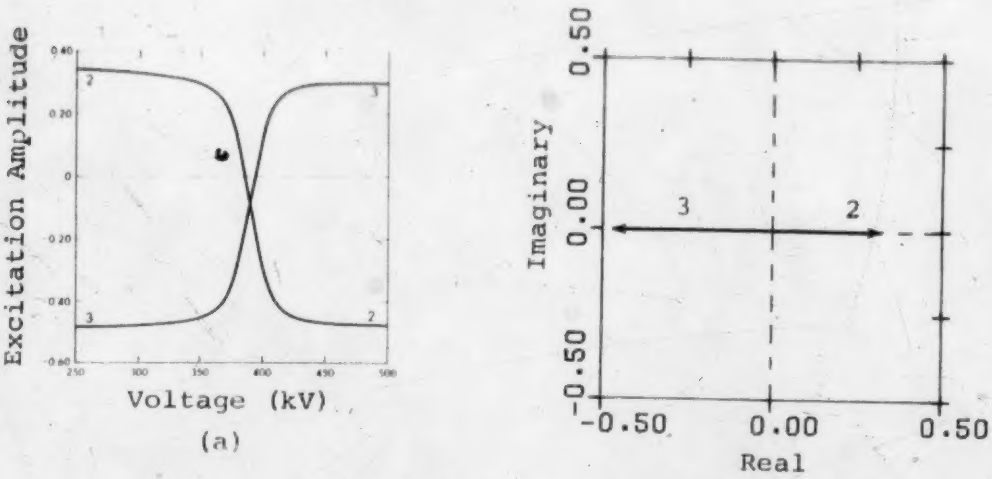

(a)

(b) V = 300 kV

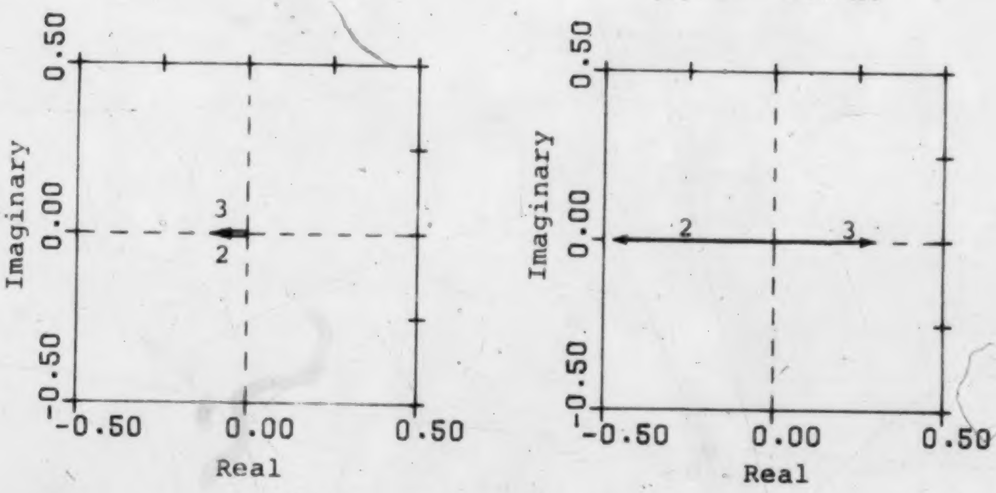

(c) V = 390 kV

(d) V = 480 kV

Fig. 45. (a): A plot of $C_o^{(i)}C_{2g}^{(i)}$ (i = 2,3) as a function of accelerating voltage for $\delta = 2.002$; (b), (c) and (d): Plots of $C_o^{(i)}C_{2g}^{(i)}$ (i = 2,3) in the complex plane for voltages below, at, and above the critical voltage.

As the voltage is increased from about 360 kV to 380 kV, the magnitudes of both excitation amplitudes decrease. However, the excitation amplitude for Bloch wave two changes sign at a lower voltage than that for Bloch wave three and these excitation amplitudes are of the same sign near 390 kV. With a further increase in the voltage, the excitation amplitude of Bloch wave three changes sign and the magnitudes of both excitation amplitudes then increase.

The first problem in analyzing the results shown in Fig. 45 is that of defining a critical voltage since such a definition in terms of Bloch wave symmetry is no longer possible. Under the circumstances, it is reasonable to take the critical voltage to be that voltage which corresponds to the closest separation of branches two and three of the dispersion surface (i.e. the voltage at which Bloch waves two and three are closest to being degenerate). This corresponds to the point in Fig. 44(a) at which the curves for $C_o^{(2)}C_{2g}^{(2)}$ and $C_o^{(3)}C_{2g}^{(3)}$ cross and is again equal to about 390 kV. It can be seen from Figs. 45(a) and 45(c), therefore, that at the critical voltage the excitation amplitudes of Bloch waves two and three are of the same sign. This is in contrast to the situation at $\delta = 2.0$ in Fig. 44 where the excitation amplitudes are of opposite sign. However, the magnitudes of the excitation amplitudes at the critical voltage are very much smaller for $\delta = 2.002$ than for $\delta = 2.0$ (compare Figs. 45 and 44) and as a result a minimum in the intensity is still obtained (see Fig. 42).

The results just presented illustrate that the critical voltage mechanism for small deviations from the exact second order Bragg condition is quite different from the mechanism at δ exactly equal to 2.0. (It is important to emphasize that the same qualitative arguments as those discussed above hold, even for an infinitesimally small deviation from the exact Bragg condition.) However, it was shown in Section 8.3.1 that Bloch wave mixing is important and should be taken into account for small deviations from $\delta = 2.0$. Accordingly, detailed examination of the critical voltage mechanism for these diffraction conditions should be carried out by using the sub-matrix theory. The sub-matrix mechanism for the critical voltage effect will be considered in the next section.

8.3.3 The Sub-Matrix Mechanism for the Critical Voltage Effect

The mechanism for the critical voltage effect at small deviations from the exact second order Bragg condition can be seen by examining the contributions which the perturbed and unperturbed Bloch waves make to the sub-matrix diffracted beam intensity expression of equation 6.45. (In this thesis, the Bloch waves obtained from the standard theory are referred to as unperturbed Bloch waves. On the other hand, Bloch waves formed from a linear combination of the Bloch functions of the unperturbed Bloch waves are referred to as perturbed Bloch waves. In the sub-matrix approach considered here, Bloch waves two and three are perturbed Bloch waves while the remainder are unperturbed Bloch waves.) In this analysis, it is necessary to use a 2 × 2 sub-matrix because the mixing between Bloch waves two and three was found to be important for values of δ close to 2.0 (see Section 8.3.1). However, the exact theory is not required because good agreement was obtained between the sub-matrix and exact theories for the medium atomic number materials.

An analysis of the magnitude of the Bloch wave excitation coefficients in the sub-matrix intensity expression 6.45 showed that, except for very thin crystals, Bloch waves two and three were the only primary Bloch waves. (Thus, in this respect, the situation for small deviations from $\delta = 2.0$ is similar to that for δ exactly equal to 2.0, discussed in Section 8.2.) The intensity expression can therefore be written

$$I_{2g} = \left| \sum_{n=2,3} X^{(n)} C'^{(n)}_{2g} \exp(2\pi i \gamma'^{(n)} z) + \Delta \right|^2 \qquad (8.3)$$

where Δ represents the small contribution made by the unperturbed Bloch waves $n \neq 2,3$. The excitation amplitudes $X^{(n)}C'^{(n)}_{2g}$ in this equation are complex and are obtained by the methods given in Section 6.6.

8.3.3 (a) The sub-matrix mechanism for δ = 2.003

In order to see how the minimum in the second order intensity arises, it is necessary to examine the excitation amplitudes for Bloch waves two and three in equation 8.3. These values are complex and therefore the manner in which they vary with voltage will be plotted in the complex plane. The values of these elements at δ = 2.003 for the (222) reflection in copper are shown in Fig. 46. (This value of δ has been chosen in order to first show a typical example of the sub-matrix mechanism for the critical voltage. Other values of δ will be considered in later sections.) It can be seen from Fig. 46 that, for voltages well below 390 kV, the real part of $X^{(3)}C'^{(3)}_{2g}$ is negative in sign and is considerably greater in magnitude than the imaginary part. With an increase in voltage, the magnitude of the imaginary part increases relative to that of the real part until at 390 kV the imaginary part is large while the real part is small. With a

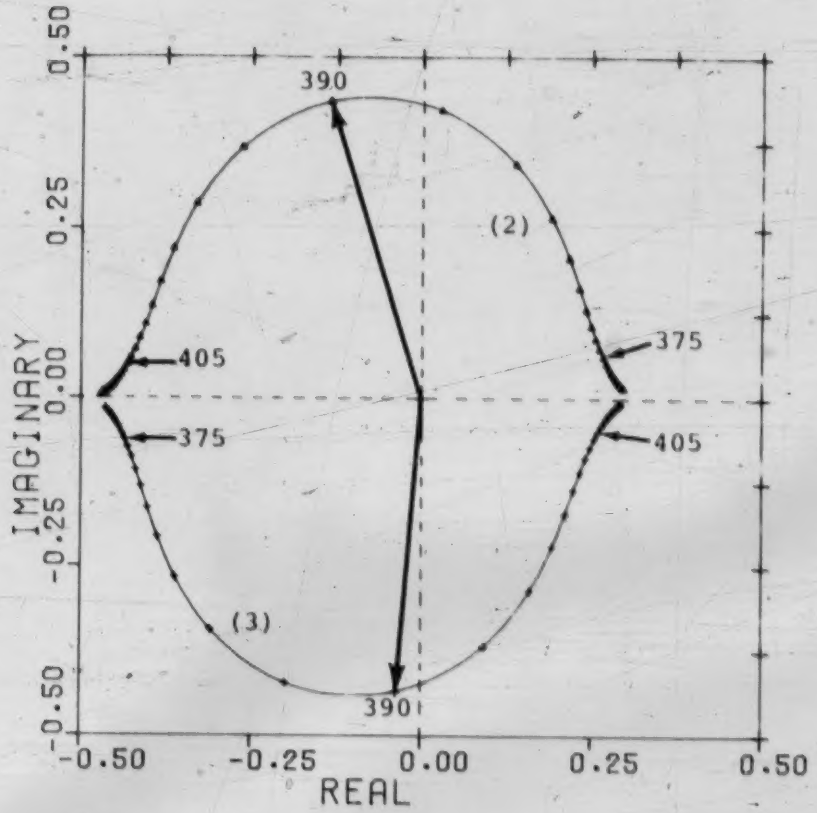

Fig. 46. The excitation amplitudes $X^{(n)}C_{2g}^{\prime(n)}$ of perturbed Bloch waves two and three plotted in the complex plane. The numbers between 375 and 405 indicate the accelerating voltage in kV. The voltage range considered was 360 to 420 kV and the voltage increment was 1.5 kV. Thirteen reflections of the (111) systematic row in copper were taken into account and $\delta = 2.003$.

further increase in the accelerating voltage, the real part of $X^{(3)}C'^{(3)}_{2g}$ again becomes considerably larger in magnitude than the imaginary part, but the real part is now positive. The excitation amplitude of Bloch wave two changes in the opposite manner to that of Bloch wave three as the voltage is increased. As can be seen from Fig. 46 the interchange of the excitation coefficients occurs over a voltage range of about 50 kV. This is approximately the voltage range over which the interchange of the excitation amplitudes of the standard theory occurs, and is also the voltage range over which the intensities obtained from the standard and sub-matrix theories differ significantly.

The minimum in intensity which occurs close to the critical voltage can now be explained by noting firstly that, for all voltages, the excitation amplitudes of Bloch waves two and three are nearly equal in magnitude and nearly out of phase. The phase difference at 390 kV for example is 155°. Furthermore, for voltages close to the critical voltage, $\gamma'^{(2)} \approx \gamma'^{(3)}$. The contributions made by these two perturbed Bloch waves to the diffracted beam intensity will therefore interfere destructively and a minimum in intensity results.

8.3.3 (b) The sub-matrix mechanism for $\delta < 2.003$

In Section 8.3.3(a), the character of the sub-matrix mechanism for the critical voltage has been determined by examining this mechanism at a value of $\delta = 2.003$ for the (111) systematic row in copper. It is next of interest to examine how this mechanism differs for other values of δ. Calculations have therefore been carried out for $2.0 \leq \delta < 2.003$ and for $\delta > 2.003$. For $2.0 \leq \delta < 2.003$ it has been found that the sub-matrix mechanism for the critical effect is similar to that for $\delta = 2.003$ in that the excitation amplitudes are large in magnitude and nearly out of phase for all voltages. However, the shapes of the curves obtained by plotting the excitation amplitudes in the complex plane are found to change. The excitation amplitudes of Bloch waves two and three for $\delta = 2.002$ are shown in Fig. 47. It can be seen from this figure that, for voltages well below the critical voltage, the real part of $X^{(3)}C'^{(3)}_{2g}$ is negative in sign and is considerably greater in magnitude than the imaginary part. With an increase in voltage, the real part increases in magnitude while the imaginary part at first increases and then decreases. At a voltage of approximately 390 kV, the real part then changes sign. With a further increase in voltage, the real part decreases in magnitude while the imaginary part at first

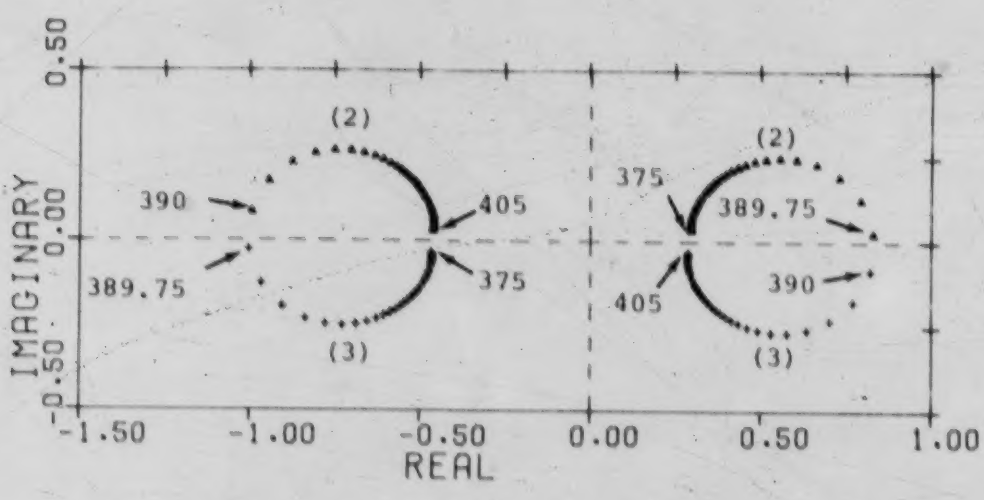

Fig. 47. The excitation amplitudes $X^{(2)}C'^{(2)}_{2g}$ and $X^{(3)}C'^{(3)}_{2g}$ for $\delta = 2.002$. The numbers between 375 and 405 indicate the accelerating voltage in kV. The voltage range considered was 375 to 405 kV and the voltage increment was 0.25 kV.

increases and then decreases. For voltages well above the critical voltage, the real part of $X^{(3)}C'^{(3)}_{2g}$ is positive and considerably greater in magnitude than the imaginary part. The excitation amplitude of Bloch wave two changes in the opposite manner as the voltage is increased. This interchange of the excitation coefficients occurs over a voltage range of approximately 30 kV. It can be seen, however, that for all voltages, the excitation amplitudes of Bloch waves two and three are large in magnitude and nearly out of phase. Since $\gamma'^{(2)} \approx \gamma'^{(3)}$ at the critical voltage, a minimum in the second order diffracted beam intensity is obtained, in a manner similar to that for $\delta = 2.003$ in Section 8.3.3(a).

The sub-matrix mechanism for the critical voltage effect was also examined for $\delta = 2.0017$, 2.001, and 2.0. These results are shown in Fig. 48. It can be seen from this figure that, as values of δ closer to $\delta = 2.0$ are considered, the magnitudes of the imaginary components of the excitation coefficients are reduced. Furthermore, the change in the magnitudes of the real parts is smaller. It is also found that the voltage range over which the interchange in the excitation amplitudes occurs becomes smaller. For example, this voltage range is equal to about 30 kV at $\delta = 2.002$ and 20 kV at $\delta = 2.001$. It can therefore

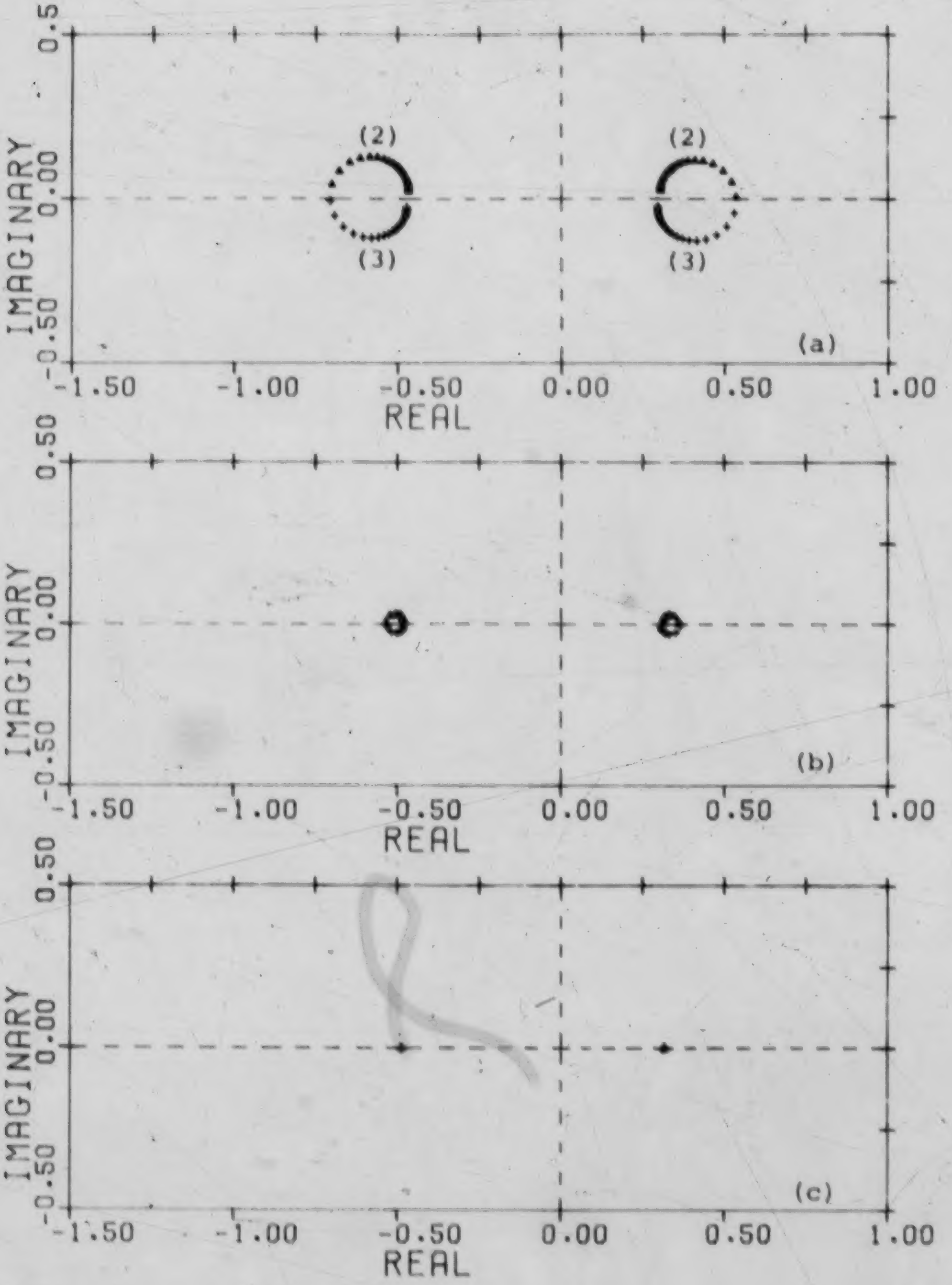

Fig. 48. The excitation amplitudes for Bloch waves two and three for (a) $\delta = 2.0017$; (b) $\delta = 2.001$; and (c) $\delta = 2.0$. The voltage range considered was 375 to 405 kV and the voltage increment was 0.5 kV.

be seen that as the value of δ approaches 2.0, the sub-matrix mechanism for the critical voltage intensity minimum reduces to the standard theory mechanism for δ exactly equal to 2.0 (see Fig. 44). However, it should be noted that, for the sub-matrix theory, the interchange in the excitation coefficients is still found to occur over a very small voltage range even when the value of δ is set exactly equal to 2.0. This range is found to decrease if matrix diagonalization routines of higher precision are used. These voltage ranges are similar to those for which the intensities obtained from the standard and sub-matrix theories were found to differ significantly for δ set exactly equal to zero (see Section 8.3.1(a)). Analytically, however, it can be shown that for δ exactly equal to 2.0, $q^{(23)}$ is zero and the sub-matrix mechanism for the critical voltage effect is equivalent to the mechanism obtained from the standard theory, i.e., the excitation amplitudes remain real and interchange precisely at the critical voltage.

8.3.3 (c) The sub-matrix mechanism for $\delta > 2.003$

It is also of interest to examine the sub-matrix mechanism for the critical voltage at values of δ greater than 2.003. Calculations of the excitation amplitudes for $\delta = 2.02$ have therefore been carried out and the results are shown in Fig. 49. It can be seen from this figure that the interchange of the excitation amplitudes occurs over a voltage range of about 200 kV, which is considerably larger than the 50 kV obtained for $\delta = 2.003$ in Fig. 46. Furthermore, the imaginary components of the excitation coefficients are considerably smaller in magnitude. It can therefore be seen that, as the deviation of the second order reflection from its exact Bragg condition is increased, the sub-matrix mechanism for the critical voltage reduces to the mechanism obtained for the standard theory. (As indicated in Section 8.3.2, a critical voltage intensity minimum is obtained for the standard theory for diffraction conditions where $\gamma^{(2)} \approx \gamma^{(3)}$ and the excitation amplitudes are small in magnitude and are in phase.) As noted in Section 8.3.1(b), however, the critical voltage intensity minimum becomes less pronounced for values of $\delta > 2.02$.

8.4 The Critical Voltage Effect in Materials of Differing Atomic Number

In this section, the critical voltage effect in materials of differing atomic number will be examined. The reason for considering the effects of atomic number is that the off-diagonal elements of the $\underline{B}$ matrix are larger for materials of higher atomic number and the

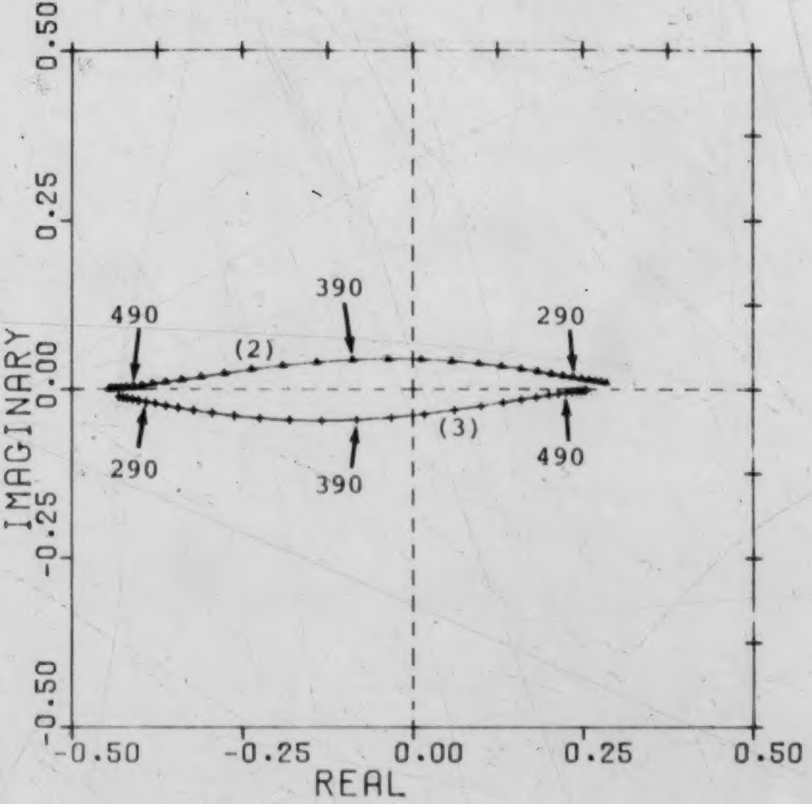

Fig. 49. The excitation amplitudes $X^{(n)}C_{2g}^{\prime(n)}$ of perturbed Bloch waves two and three plotted in the complex plane. The numbers between 290 and 490 indicate the accelerating voltage in kV. The voltage range considered was 240 to 540 kV and the voltage increment was 10 kV. Thirteen reflections of the (111) systematic row in copper were taken into account and $\delta = 2.02$.

effects of Bloch wave mixing are enhanced (see Section 7.2). In order to assess the effects of atomic number, it is important to be able to distinguish between these effects and effects which result from the mixing between the quasi-degenerate Bloch waves two and three. This will be done by carrying out the calculations for δ exactly equal to 2.0 because, for these diffraction conditions, the value of $q^{(23)}$ can analytically be shown to be zero (see Section 6.4). Any differences between the standard and exact theories can then be associated with the other off-diagonal elements of the $\underline{B}$ matrix, i.e., the mixing between other pairs of Bloch waves. As noted previously, these off-diagonal elements are larger for high atomic number materials (see Section 7.2), and therefore differences between the standard and exact theories can be associated with the effects of atomic number. However, it should be noted that for accelerating voltages very close to the critical voltage, the value of $q^{(23)}$ is numerically found to be non-zero for δ exactly equal to 2.0. If the standard and exact theories were compared for this small voltage range, it would not be possible to distinguish between effects associated with atomic number and effects associated with the quasi-degenerate Bloch waves two and three. This problem can be overcome by comparing the exact theory to the sub-matrix theory, which includes mixing between these two Bloch waves. Differences between the results obtained by these two methods can then be associated with the effects of atomic number. The results obtained from the sub-matrix and exact theories will be presented in this section.

In order to examine the critical voltage effect in materials of differing atomic number, the critical voltage intensity minimum was obtained for materials of varying atomic number including silicon, molybdenum and gold. In these calculations, thirteen systematic reflections were considered and δ was set exactly equal to 2.0. The second order reflections considered were the (220) in molybdenum and the (440) in silicon and gold, and the diffracted beam intensity was obtained for a thickness of 5000 Å. These calculations showed that there was good agreement between the sub-matrix and exact theories in the low and medium atomic number materials. This indicates that the effect of the Bloch wave mixing associated with atomic number is not important in these materials. The results for the gold calculation are shown in Fig. 50. It can be seen from this figure that the critical voltage intensity minimum is obtained for the sub-matrix theory at about 740 kV. On the other hand, the minimum is obtained for the exact theory at 755 kV, a difference of about 2%. It therefore can

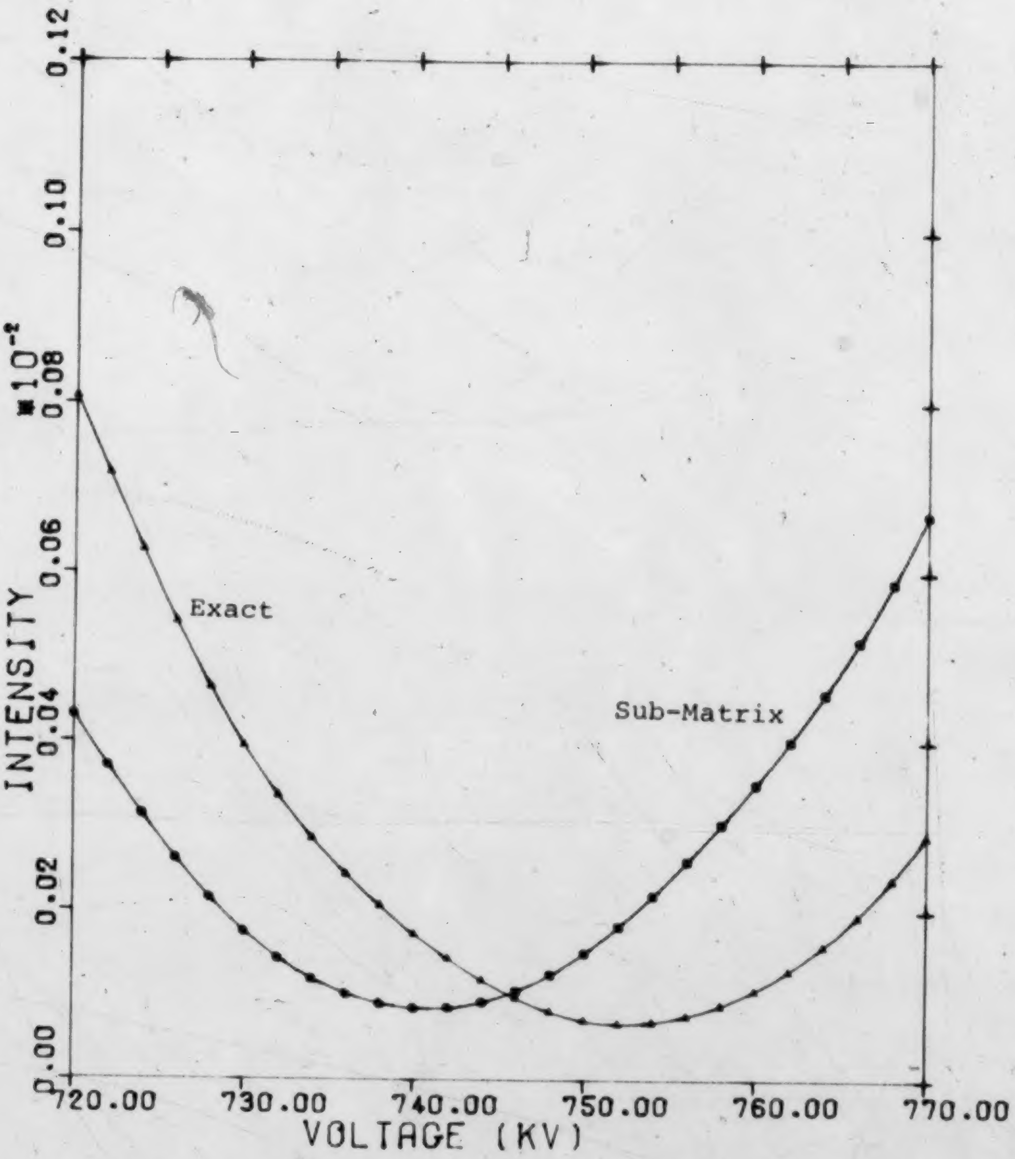

Fig. 50. The critical voltage intensity minima obtained for the sub-matrix and exact theories in gold.

be seen that the effect of Bloch wave mixing can result in a significant change in value of the critical voltage in high atomic number materials. Lally et al. (1972) have previously reported that the critical voltage obtained for gold by using the standard and exact theories differs by 2%. However, these authors did not offer any explanation for this effect. The results presented in this section show that this 2% difference is associated with the effect of atomic number and cannot be attributed to effects associated with the quasi-degenerate Bloch waves.

It is of interest to examine the Bloch wave mechanism which gives rise to this difference between the standard and exact theories. An investigation showed that the 2% difference in the value of the critical voltages obtained from these theories arose because of changes in the real parts of the eigenvalues of Bloch waves two and three. It was also found that as the size of the sub-matrix was increased, better agreement with the exact theory was obtained. For example, the critical voltage minimum for a 6 × 6 sub-matrix including mixing between the first six Bloch waves differed by only 0.07% from the minimum obtained for the exact theory.

8.5 Summary and Conclusions

In this chapter the importance of Bloch wave mixing in the critical voltage effect has been examined. It was noted that the exact Bragg condition of the second order reflection cannot in general be obtained experimentally because of factors such as beam divergence, specimen bending, and the lack of precision which is inherent in determining the crystal orientation. The critical voltage effect was therefore examined for small deviations from the exact Bragg condition of the second order reflection, and it was found that it is necessary to take the mixing between the quasi-degenerate Bloch waves two and three into account. It was also found that it is necessary to take this mixing into account in numerical calculations even when δ is set exactly equal to 2.0. This is because the effective value of δ cannot be set equal to 2.0 with greater precision than that inherent in the matrix diagonalization routines. It was also found that the critical voltage mechanism presented in the literature does not apply at small deviations from $\delta = 2.0$. An alternate mechanism based on the sub-matrix approach was therefore presented.

The effect of atomic number on the minimum in intensity which occurs at the critical voltage was also examined. It was found that Bloch wave mixing can lead to a significant change in the voltage at which this minimum occurs when high atomic number materials are considered.

It can be concluded from these results that the effects of Bloch wave mixing should be taken into account when calculations of the critical voltage effect are carried out. In addition, however, it should be noted that these effects are important over a range of voltages on either side of the critical voltage and over a range of values of δ on either side of $\delta = 2.0$ (see also Section 7.3). The results of this chapter are therefore also of importance in calculations of image contrast. For example, in copper the critical voltage for the (222) reflection is 390 kV, yet significant differences between the standard and exact theories were found at 300 kV for $\delta = 2.1$.

CHAPTER 9

SUMMARY AND SUGGESTIONS FOR FURTHER WORK

9.1 Summary

The purpose of this thesis has been to assess the validity of some of the approximations in the dynamical theory of electron diffraction. The s-value approximation for calculating the diagonal elements of the $\underline{A}$ matrix was considered in Chapter 4. It was found for the diffraction conditions considered that this is a reasonable approximation. This was followed in Chapter 5 by an assessment of the validity of the kinematical theory for large values of δ. These results showed that this theory is not as good an approximation under these conditions as it had previously been considered to be. The approximations which can be used to take absorption into account in the dynamical theory were then considered in Chapter 6. This led to the development of a general formulation of the dynamical theory of electron diffraction including absorption. It was found that the introduction of the imaginary potential leads to a mixing of the unperturbed Bloch waves characteristic of the system without absorption. The assumptions required to reduce the general theory to the low order perturbation theories previously published in the literature were then examined, and a new approach referred to as the sub-matrix approach was developed. Numerical calculations employing this theory were presented in Chapter 7 which showed that it is important to take the mixing of Bloch waves into account in high atomic number materials or when quasi-degeneracy or degeneracy of the kinetic energies of the unperturbed Bloch waves is obtained. A comparison of approximate and exact methods for taking absorption into account showed that the sub-matrix method has a number of advantages over other approximate methods. Firstly, it is applicable under conditions which lead to either non-degenerate, quasi-degenerate or degenerate Bloch waves and secondly, this method can give very close agreement with the exact theory while at the same time providing advantages from a computational point of view. It was then shown in Chapter 8 that it is necessary to take Bloch wave mixing into account in order to obtain a physical understanding of the contrast mechanisms involved in the critical voltage effect.

9.2 Suggestions for Further Work

There are a number of areas in which the work presented in this thesis can be extended. The first of these follows from the assessment of the kinematical theory carried out in Chapter 5. The results of Section

5.4 showed that non-systematic reflections can have an important effect on the weak-beam image of reflection g not only when $s_h \approx 0$ but also when $s_h \approx s_g$. However, it has been assumed in the literature that a non-systematic reflection will only be important if it is close to its Bragg condition (i.e., $s_h \approx 0$). It would therefore be of interest to carry out an experimental investigation of the effect of non-systematic reflections on weak-beam image contrast for diffraction conditions where $s_h \simeq s_g$. Furthermore, it should be noted that in carrying out theoretical calculations of weak-beam contrast, it is necessary to take all reflections into account which have s_h values close to zero or s_g. Since this fact is not reflected in Cann's strong beam criterion of equation 3.2, an improved criterion needs to be developed.

A second possible extension of the work presented in this thesis is concerned with the importance of Bloch wave mixing in determining image contrast obtained under various diffraction conditions. It was shown in Chapters 7 and 8 that Bloch wave mixing can be very important under quasi-degenerate diffraction conditions. Since these conditions can occur when non-systematic reflections are taken into account (Cann and Sheinin, 1974A, 1974B), it would therefore be of interest to examine the effects of these reflections on Bloch wave mixing.

A third extension of this research would be to examine the importance of Bloch wave mixing in noncentrosymmetric crystals. For these materials, the properties of the off-diagonal $\underline{B}$ elements are different (for example, the $\underline{B}$ matrix will not be symmetric). Furthermore, it would be of interest to examine the critical voltage effect in these materials since the value of $q^{(23)}$ will not in general be zero for $\delta = 2.0$. This is in contrast to the case for centrosymmetric crystals where $q^{(23)} = 0$ for $\delta = 2.0$ (see Section 6.4).

REFERENCES

Amelinckx, S., Gevers, R., Remaut, G., and Van Landuyt, J. (Eds.) (1970). Modern Diffraction and Imaging Techniques in Material Science (Amsterdam: North Holland Publ. Co.).

Andrew, J.W., and Sheinin, S.S. (1974A). Proc. 8th Internat. Conf. on Electron Microscopy, Canberra, 1, p. 338.

Andrew, J.W., and Sheinin, S.S. (1974B). Proc. Internat. Crystallographic Conf., Melbourne, p. 302.

Andrew, J.W., and Sheinin, S.S. (1975). phys. stat. sol. (b) 67, 355.

Ayroles, R., Mazel, A., and Ajustron, F. (1973). Phil. Mag. 28, 417.

Bethe, H.A. (1928). Ann. d. Physik 87, 55.

Blackman, M. (1939). Proc. Roy. Soc. A173, 68.

Boersch, H. (1942). Zeit. fur Physik 118, 706.

Boersch, H. (1943). Zeit. fur Physik 121, 746.

von Borries, B., and Ruska, E. (1940). Naturwiss. 28, 366.

Botros, K.Z., and Sheinin, S.S. (1974). phys. stat. sol. (a) 21, 209.

de Broglie, L. (1924). Phil. Mag. 47, 446.

Butler, E.P. (1972). Phil. Mag. 26, 33.

Butler, E.P. (1973). phys. stat. sol. (a) 18, 71.

Cann, C.D. (1973). Ph.D. Thesis, University of Alberta.

Cann, C.D., and Sheinin, S.S. (1972). phys. stat. sol. (a) 14, 663.

Cann, C.D., and Sheinin, S.S. (1974A). phys. stat. sol. (a) 26, 193.

Cann, C.D., and Sheinin, S.S. (1974B). phys. stat. sol. (a) 26, 681.

Cockayne, D.J.H. (1972). Z. Naturforsch. 27a, 452.

Cowley, J.M., and Moodie, A.F. (1957). Acta Cryst. 10, 609.

Darwin, C.G. (1914). Phil. Mag. 27, 315 and 675.

Davisson, C.J., and Germer, L.H. (1927). Nature 119, 558.

Dederichs, P.H. (1972). Adv. Solid State Phys. 27, 135.

Doyle, P.A., and Turner, P.S. (1968). Acta Cryst. A24, 390.

Dupouy, G., Perrier, F., Uyeda, R., Ayroles, R., and Mazel, A. (1965). J. Microscopie 4, 429.

Fujimoto, F. (1959). J. Phys. Soc. Japan 14, 1558.

Fujiwara, K. (1959). J. Phys. Soc. Japan 14, 1513.

Fujiwara, K. (1962). J. Phys. Soc. Japan 17, 118.

Fukuhara, A. (1966). J. Phys. Soc. Japan 21, 2645.

Gevers, R. (1970). In Modern Diffraction and Imaging Techniques in Material Science, edited by S. Amelinckx, R. Gevers, G. Remaut, and J. Van Landuyt (Amsterdam: North Holland Publ. Co.), p. 1.

Gevers, R., Serneels, R., and David, M. (1974). phys. stat. sol. (b) 66, 471.

Gevers, R., Serneels, R., and David,M. (1975). phys. stat. sol. (b) 67, 273.

Gjønnes, J., and Høier, R. (1971). Acta Cryst. A27, 313.

Goodman, P., and Moodie, A.F. (1974). Acta Cryst. A30, 280.

Goringe, M.J., Howie, A., and Whelan, M.J. (1966). Phil. Mag. 14, 217.

Hall, C.R., and Hirsch, P.B. (1965). Proc. Roy. Soc. A286, 158.

Hashimoto, H. (1964). J. Appl. Phys. 35, 277.

Hashimoto, H., Howie, A., and Whelan, M.J. (1962). Proc. Roy. Soc. A269, 80.

Head, A.K., Humble, P., Clarebrough, L.M., Morton, A.J., and Forwood, C.T. (1973). Computed Electron Micrographs and Defect Identification (Amsterdam: North Holland Publ. Co.).

Heidenreich, R.D. (1942). Phys. Rev. 62, 291.

Heidenreich, R.D. (1962). J. Appl. Phys. 33, 2321.

Heidenreich, R.D. (1964). Fundamentals of Transmission Electron Microscopy (New York: Interscience Publishers).

Heidenreich, R.D., and Sturkey, L. (1945). J. Appl. Phys. 16, 97.

Hillier, J., and Baker, R.F. (1942). Phys. Rev. 61, 722.

Hirsch, P.B., Howie, A., Nicholson, R.B., Pashley, D.W., and Whelan, M.J. (1965). Electron Microscopy of Thin Crystals (London: Butterworths).

Hoerni, J.A. (1956). Phys. Rev. 102, 1534.

Howie, A. (1963). Proc. Roy. Soc. A271, 268.

Howie, A. (1966). Phil. Mag. 14, 223.

Howie, A. (1970). In Modern Diffraction and Imaging Techniques in Material Science, edited by S. Amelinckx, R. Gevers, G. Remaut and J. Van Landuyt (Amsterdam: North Holland Publ. Co.), p. 295.

Howie, A., and Valdrè, U. (1964). Proc. Third Eur. Conference on Electron Microscopy, Prague, 1, p. 377.

Howie, A., and Whelan, M.J. (1960). Proc. Eur. Regional Conf. on Electron Microscopy, Delft, p. 181.

Howie, A., and Whelan, M.J. (1961). Proc. Roy. Soc. A263, 217.

Humphreys, C.J., and Fisher, R.M. (1971). Acta Cryst. A27, 42.

Humphreys, C.J., and Hirsch, P.B. (1968). Phil. Mag. 18, 115.

Ibers, J.A., and Vainshtein, B.K. (1962). International Crystallographic Tables, Vol. III (Birmingham: Kynoch Press).

IMSL (1974). International Mathematical and Statistical Libraries, Inc. (Houston, Texas).

Kambe, K., and Molière, K. (1970). In Advances in Structure Research by Diffraction Methods, edited by R. Brill and R. Mason (London: Pergamon Press), p. 53.

Kamiya, Y., and Uyeda, R. (1961). J. Phys. Soc. Japan 16, 1361.

Kato, N. (1952). J. Phys. Soc. Japan 7, 397.

Kinder, E. (1943). Naturwiss. 31, 149.

Knoll, M., and Ruska, E. (1932). Ann. d. Physik 12, 607.

Lally, J.S., Humphreys, C.J., Metherell, A.J.F., and Fisher, R.M. (1972). Phil. Mag. 25, 321.

MacGillavry, C.H. (1940). Physica 7, 329.

Margenau, H., and Murphy, G.M. (1956). The Mathematics of Physics and Chemistry (Princeton, N.J.: Van Nostrand).

Metherell, A.J.F., and Fisher, R.M. (1969). phys. stat. sol. 32, 551.

Miyake, S. (1959). J. Phys. Soc. Japan 14, 1347.

Molière, K. (1939). Ann. d. Physik 34, 461.

Nagata, F., and Fukuhara, A. (1967). Japan J. Appl. Phys. 6, 1233.

Niehrs, H. (1959). Z. Naturforsch. 14a, 504.

Pines, D. (1963). Elementary Excitation in Solids (New York: Benjamin).

Pinsker, Z.G. (1953). Electron Diffraction, translated by J.A. Spink and E. Feigh (London: Butterworths Scientific Publications).

Radi, G. (1970). Acta Cryst. A26, 41.

Raines, S. (1961). The Wave Mechanics of Electrons in Metals (Amsterdam: North Holland Publ. Co.).

Serneels, R., and Gevers, R. (1972). phys. stat. sol. (b) 50, 99.

Serneels, R., and Gevers, R. (1973A). phys. stat. sol. (b) 55, 335.

Serneels, R., and Gevers, R. (1973B). phys. stat. sol. (b) 56, 681.

Serneels, R., and Gevers, R. (1974). In High Voltage Electron Microscopy, edited by P.R. Swann, C.J. Humphreys and M.J. Goringe (London: Academic Press), p. 57.

Sheinin, S.S. (1967). phys. stat. sol. 21, 247.

Sheinin, S.S., and Andrew, J.W. (1974). phys. stat. sol. (b) 61, K13.

Sheinin, S.S., and Botros, K.Z. (1971). phys. stat. sol. (a) 8, 449.

Sheinin, S.S., and Cann, C.D. (1973). phys. stat. sol. (b) 57, 315.

Spencer, J.P., and Humphreys, C.J. (1971). Proc. 25th Anniv. Meeting EMAG (Cambridge: Institute of Physics), p. 310.

SSP (1970). System/360 Scientific Subroutine Package, Version III (New York: IBM Corporation).

Steeds, J.W., and Valdrè, U. (1968). Proc. Eur. Conf. on Electron Microscopy, Rome, 1, p. 43.

Thomas, L.E. (1972). Phil. Mag. 26, 1447.

Thomas, L.E., Shirley, C.G., Lally, J.S., and Fisher, R.M. (1974). In High Voltage Electron Microscopy, edited by P.R. Swann, C.J. Humphreys, and M.J. Goringe (London: Academic Press), p. 38.

Thomson, G.P., and Reid, A. (1927). Nature 119, 890.

Uyeda, R. (1968). Acta Cryst. A24, 175.

Vainshtein, B.K. (1964). Structure Analysis by Electron Diffraction, translated by E. Feigh and J.A. Spink (London: Pergamon Press).

Watanabe, D. and Uyeda, R. (1968). Acta Cryst. A24, 249.

Watanabe, D., Uyeda, R., and Fukuhara, A. (1968). Acta Cryst. A24, 580.

Whelan, M.J. (1965A). J. Appl. Phys. 36, 2099.

Whelan, M.J. (1965B). J. Appl. Phys. 36, 2103.

Whelan, M.J. (1970). In Modern Diffraction and Imaging Techniques in Material Science, edited by S. Amelinckx, R. Gevers, G. Remaut and J. Van Landuyt (Amsterdam: North Holland Publ. Co.), p. 35.

Whelan, M.J., and Hirsch, P.B. (1957). Phil. Mag. 2, 1121, 1303.

Wilkens, M., Katerbau, K.H., and Rühle, M. (1973). Z. Naturforsch. 28a, 681.

Yoshioka, H. (1957). J. Phys. Soc. Japan 12, 618.

APPENDIX A

Approximate Methods for Calculating the Eigenvalues and Normalized Eigenvectors of a Symmetric Matrix

In this appendix, the first and second order approximate methods for calculating the eigenvalues and normalized eigenvectors of a symmetrical matrix will be considered. The approximations used are similar to those outlined in texts such as Margenau and Murphy (1956).

As a first order approximation to be used in diagonalizing the symmetric matrix $\underline{A}$, let it be assumed that all the off-diagonal elements of $\underline{A}$ are small and can be neglected, i.e. that they can be taken to be zero. The matrix $\underline{\Lambda}$ then takes the form

$$\underline{\Lambda} \approx \begin{bmatrix} \Lambda_{11} & 0 & 0 & \cdots \\ 0 & \Lambda_{22} & 0 & \cdots \\ 0 & 0 & \Lambda_{33} & \cdots \\ \cdots & \cdots & \cdots & \cdots \end{bmatrix} . \qquad (\mathrm{A}.1)$$

Since this matrix is already diagonal, the eigenvalues $\gamma^{(i)}$, correct to first order, are simply the elements along the diagonal, i.e.,

$$\gamma^{(i)} = \Lambda_{ii} . \qquad (\mathrm{A}.2)$$

The corresponding eigenvectors can be found by substituting these first order eigenvalues into the first order eigenvalue equation

$$\begin{bmatrix} A_{11}-\gamma^{(i)} & 0 & 0 & \cdots \\ 0 & A_{22}-\gamma^{(i)} & 0 & \cdots \\ 0 & 0 & A_{33}-\gamma^{(i)} & \cdots \\ \cdots & \cdots & \cdots & \cdots \end{bmatrix} \begin{bmatrix} C_1^{(i)} \\ C_2^{(i)} \\ C_3^{(i)} \\ \cdots \end{bmatrix} = 0 \ . \qquad (A.3)$$

For example, when $\gamma^{(1)} = A_{11}$ is substituted into this equation, it can be seen that the elements of the eigenvector $\underline{C}^{(1)}$ are proportional to

$$\begin{bmatrix} C_1^{(1)} \\ 0 \\ 0 \\ \cdots \end{bmatrix}$$

Since the element $C_1^{(1)}$ must be chosen so that the eigenvector $\underline{C}^{(1)}$ is normalized, the eigenvector $\underline{C}^{(1)}$ becomes

$$\underline{C}^{(1)} = \begin{bmatrix} 1 \\ 0 \\ 0 \\ \cdots \end{bmatrix} \ . \qquad (A.4)$$

The remaining eigenvectors can be determined in a similar manner. If the n^{th} eigenvector is written as the n^{th} column of the eigenvector matrix $\underline{C}$, then it can be shown that

$$\underline{C} = \underline{I} \tag{A.5}$$

where $\underline{I}$ is the unity matrix.

In this thesis, when the same approximations are used to calculate both the eigenvalues and the eigenvectors, the eigenvectors will be considered correct to one lower order than the eigenvalues. This terminology has been adopted in order to be consistent with the terminology used in perturbation theory. In perturbation theory, the same approximations which yield the energy to a given order also yield the wave functions to the next lower order. The eigenvectors of equation A.5 will therefore be considered correct to zero order.

In order to calculate the eigenvalues correct to second order and the eigenvectors correct to first order, it is necessary to develop a second order approximation to the $\underline{A}$ matrix. In the second order approximation, the effects of the off-diagonal elements of $\underline{A}$ are taken into account in an approximate manner by assuming that a particular element A_{ij} $(i \neq j)$ will only have an effect on the eigenvalues and eigenvectors i and j. Accordingly, the only off-diagonal elements which are taken into account in calculating the i^{th} eigenvalue and eigenvector are A_{ij} and A_{ji} where $j = 1,N$ and $j \neq i$. As an example of the use of this second order approximation, approximate expressions for $\gamma^{(1)}$ and $\underline{C}^{(1)}$ will first be calculated. These expressions will then be generalized.

In order to calculate $\gamma^{(1)}$ and $\underline{C}^{(1)}$ in the second order approximation, only the diagonal elements and the off-diagonal elements A_{1j} and A_{j1} where $j = 2,N$ are retained in the $\underline{A}$ matrix. The eigenvalue equation then can be written

$$\begin{bmatrix} A_{11}-\gamma^{(1)} & A_{12} & A_{13} & \cdots \\ A_{21} & A_{22}-\gamma^{(1)} & 0 & \cdots \\ A_{31} & 0 & A_{33}-\gamma^{(1)} & \cdots \\ \cdots & \cdots & \cdots & \cdots \end{bmatrix} \begin{bmatrix} C_1^{(1)} \\ C_2^{(1)} \\ C_3^{(1)} \\ \cdots \end{bmatrix} = 0 . \qquad (A.6)$$

If it is now assumed that the first order eigenvalue A_{11} is non-degenerate and the second order correction to A_{11} is small, then, to a good approximation, the diagonal terms $A_{ii}-\gamma^{(1)}$ can be set equal to $A_{ii}-A_{11}$ for $i \neq 1$. Equation A.6 then becomes

$$\begin{bmatrix} A_{11}-\gamma^{(1)} & A_{12} & A_{13} & \cdots \\ A_{21} & A_{22}-A_{11} & 0 & \cdots \\ A_{31} & 0 & A_{33}-A_{11} & \cdots \\ \cdots & \cdots & \cdots & \cdots \end{bmatrix} \begin{bmatrix} C_1^{(1)} \\ C_2^{(1)} \\ C_3^{(1)} \\ \cdots \end{bmatrix} = 0 \; . \qquad (A.7)$$

The first order eigenvector $\underline{C}^{(1)}$ can be obtained by solving all but the first equation in A.7 to give

$$C_j^{(1)} = -\frac{A_{1j}}{A_{jj}-A_{11}} C_1^{(1)} \equiv R_j^{(1)} C_1^{(1)} \qquad (A.8)$$

where

$$R_j^{(n)} \equiv -\frac{A_{nj}}{A_{jj}-A_{nn}} \qquad (j \neq n) \qquad (A.9a)$$

and

$$R_n^{(n)} \equiv 1 \; . \qquad (A.9b)$$

The elements of the eigenvector $\underline{C}^{(1)}$ are therefore proportional to

$$\begin{bmatrix} C_1^{(1)} \\ R_2^{(1)} C_1^{(1)} \\ R_3^{(1)} C_1^{(1)} \\ \cdots \end{bmatrix} \; . \qquad (A.10)$$

The value of the element $C_1^{(1)}$ can be determined by requiring that the eigenvector $\underline{C}^{(1)}$ be normalized. Since it has been assumed that the first order eigenvalue A_{11}

is non-degenerate, the denominator in equation A.8 will be large. If the off-diagonal elements of the $\underset{\sim}{A}$ matrix are small, then $|R_j^{(1)}| << 1$ for $j \neq 1$. To a good approximation, therefore, the eigenvector $\underset{\sim}{C}^{(1)}$ will be normalized if $C_1^{(1)} = 1$. The normalized eigenvector $\underset{\sim}{C}^{(1)}$, correct to first order, then becomes

$$\underset{\sim}{C}^{(1)} = \underset{\sim}{R}^{(1)} \qquad (A.11)$$

where $\underset{\sim}{R}^{(n)}$ is a column vector containing the elements $R_j^{(n)}$ in the j^{th} row. The remaining eigenvectors can be calculated in a similar manner and the first order matrix of eigenvectors $\underset{\sim}{C}$ can be written

$$\underset{\sim}{C} = \underset{\sim}{R} \qquad (A.12)$$

where $\underset{\sim}{R}$ is a matrix containing the column vector $\underset{\sim}{R}^{(n)}$ in the n^{th} column.

An important property of the matrix of first order eigenvectors $\underset{\sim}{R}$ is that it can be assumed to be orthogonal, i.e. the inverse $\underset{\sim}{R}^{-1}$ can be approximated by the transpose $\underset{\sim}{R}^T$. If it is assumed that $|R_j^{(n)}| << 1$ for $j \neq n$, then $\underset{\sim}{R}^{-1} \simeq \underset{\sim}{R}^T$ if terms involving the products of the small off-diagonal elements of $\underset{\sim}{R}$ are neglected in comparison to the elements of $\underset{\sim}{R}$. (This can be seen most easily by multiplying $\underset{\sim}{R}$ by $\underset{\sim}{R}^T$, using the fact that $R_j^{(i)} = -R_i^{(j)}$, and examining the approximations required to make this product equal to the unit matrix.)

The second order expression for the eigenvalue $\gamma^{(i)}$ can be found by substituting the expression for $\underline{\underline{c}}^{(1)}$ in equations A.11 and A.9 into the first equation of the set of equations A.7. The eigenvalue $\gamma^{(1)}$, correct to second order, then becomes

$$\gamma^{(1)} = \Lambda_{11} - \sum_{j=2}^{N} \frac{(\Lambda_{1j})^2}{\Lambda_{jj} - \Lambda_{11}} \; . \tag{A.13}$$

When the other eigenvalues are calculated in a similar manner, the general expression for $\gamma^{(n)}$, correct to second order, is found to be

$$\gamma^{(n)} = \Lambda_{nn} - \sum_{j \neq n}^{N} \frac{(\Lambda_{nj})^2}{\Lambda_{jj} - \Lambda_{nn}} \; . \tag{A.14}$$

APPENDIX B

Typical Values for the Elements in the $\underset{\sim}{C}$ Matrix of Table 2 and for the Bloch Wave Excitation Amplitudes $C_0^{(h)}C_q^{(h)}$

In this appendix it will be shown that the decrease in magnitude of the terms U_h as $|\mathbf{h}|$ increases is the controlling factor in determining the relative magnitudes of the Bloch wave excitation amplitudes

$$C_0^{(h)}C_q^{(h)} = -\frac{U_{-h}U_{q-h}}{2Ks_h(s_q-s_h)}$$

obtained from the $\underset{\sim}{C}$ matrix of Table 2. This will be done by examining the $\underset{\sim}{C}$ matrix and the excitation amplitudes under diffraction conditions typical of those obtained when a high order systematic reflection is not close to its Bragg condition. Typical values for the first two rows of the $\underset{\sim}{C}$ matrix of Table 2 are presented in Table B-1. In obtaining this matrix, the six reflections (000) to (660) of the (110) systematic row in molybdenum were taken into account. The accelerating voltage was 100 kV and $\delta = 5.5$. It can be seen from Table B-1 that the elements $C_0^{(h)}$ $(h \neq 0)$ and $C_q^{(h)}$ $(h \neq q)$ are much less than one and that the numerators U_{-h} and U_{q-h} of these terms decrease in magnitude as $|\mathbf{h}|$ increases. The excitation amplitudes

Table B-1. Typical values for the elements of the $\underline{C}$ matrix of Table 2 and for the Bloch wave excitation amplitudes $C_o^{(h)}C_g^{(h)}$.

Bloch Wave (h)	o	g	2g	3g	4g	5g	6g
$C_o^{(h)}$	1	$\frac{0.116}{0.91}$	$\frac{0.052}{0.41}$	$\frac{0.028}{1.52}$	$\frac{0.017}{1.22}$	$\frac{0.011}{0.51}$	$\frac{-0.008}{0.61}$
$C_g^{(h)}$	$\frac{-0.116}{0.91}$	1	$\frac{0.116}{0.52}$	$\frac{0.052}{0.61}$	$\frac{0.028}{0.30}$	$\frac{-0.017}{0.41}$	$\frac{-0.011}{1.52}$
$C_o^{(h)}C_g^{(h)}$	-0.127	0.127	0.0021	0.0016	0.0012	-0.0009	0.0000

calculated from these terms are also given in Table B-1. It can be seen that the excitation amplitudes tend to decrease in magnitude as $|\vec{h}|$ increases, i.e. the decrease in the magnitude of U_h with increasing $|\vec{h}|$ is in fact the controlling factor in determining the relative magnitudes of the excitation amplitudes $C_{o}^{(h)} C_{g}^{(h)}$.

APPENDIX C

Typical Values for the Second Order Correction Terms in Equation 5.2

In this appendix it will be shown that the decrease in magnitude of the terms U_h as $|\vec{h}|$ increases is the controlling factor in determining the magnitudes of the second order corrections for the eigenvalues $\gamma^{(o)}$ and $\gamma^{(g)}$ of equation 5.2. This will be done by examining these correction terms under diffraction conditions which are typical of those obtained when there are no high order systematic reflections close to the Bragg condition. Typical values for the second order corrections for the eigenvalues $\gamma^{(o)}$ and $\gamma^{(g)}$ of equation 5.2 are given in Table C-1. In obtaining this table, the six reflections (000) to (660) of the (110) systematic row in molybdenum were taken into account. The accelerating voltage was 100 kV and $\delta = 5.5$. It can be seen from Table C-1 that the numerators of the correction terms tend to decrease in magnitude as $|\vec{h}|$ increases and that this is in fact the controlling factor in determining the magnitude of the correction terms.

Table C-1. Typical values for the second order corrections to the eigenvalues $\gamma^{(o)}$ and $\gamma^{(g)}$ of equation 5.2.

Bloch Wave (h)	o	g	2g	3g	4g	5g	6g
$\left\lvert\frac{(U_{-h})^2}{(2K)^2 s_h}\right\rvert$		$\frac{1.3\times10^{-2}}{49.3}$	$\frac{2.7\times10^{-3}}{76.6}$	$\frac{8.0\times10^{-4}}{82.1}$	$\frac{2.7\times10^{-4}}{65.6}$	$\frac{1.2\times10^{-4}}{27.4}$	$\frac{5.6\times10^{-5}}{32.9}$
		5.1×10^{-6}	6.6×10^{-7}	1.8×10^{-7}	7.9×10^{-8}	8.1×10^{-8}	3.2×10^{-8}
$\left\lvert\frac{U_{g-h}}{(2K)^2 (s_g - s_h)}\right\rvert$	$\frac{1.3\times10^{-2}}{49.2}$		$\frac{1.3\times10^{-2}}{27.4}$	$\frac{2.7\times10^{-3}}{32.8}$	$\frac{8.0\times10^{-4}}{16.4}$	$\frac{2.7\times10^{-4}}{21.9}$	$\frac{1.2\times10^{-4}}{82.1}$
	5.1×10^{-6}		9.1×10^{-6}	1.5×10^{-6}	9.1×10^{-7}	2.4×10^{-7}	2.7×10^{-8}